FEHRL Investigation on Longitudinal and Transverse Evenness of Roads

Title: FILTER - Theoretical Study of Indices

Authors: **M . Willett** - TRL Limited, United Kingdom
G. Magnusson - Swedish and National Road and Transportation Research Institute, Sweden
B. W. Ferne - TRL Limited, United Kingdom

Secretariat: R. R. Addis
Belgian Road Research Centre (BRRC)
42, boulevard de la Woluwe
BE-1200 Brussels (Belgium)
Phone : +32 2 775 82 38
Fax: +32 2 775 82 54
E-mail: fehrloffice@compuserve.com

Published by
TRL Limited
Old Wokingham Road
Crowthorne
Berkshire
RG45 6AU
United Kingdom

2000
ISSN 1362-6019

Foreword

The purpose of FEHRL is to encourage collaboration between European National Highway Research Laboratories and Institutes in the field of highway engineering infrastructure so as to provide relevant knowledge to European Governments, the European Commission, the road industry and road users. Collaboration between such laboratories, mainly government funded, will ensure the efficient provision of advice in a cost effective and timely manner. It will reduce duplication of effort and lead to a proper integration of European research resources, whilst at the same time permitting a measure of productive competition. The objective of FEHRL is to encourage collaboration between European National Highway Research Laboratories and Institutes in order:

- to provide input to EU and national government policy on highways infrastructure
- to create and maintain an efficient and safe road network in Europe
- to increase the competitiveness of European road construction and road-using industries
- to improve the energy efficiency of highway construction and maintenance
- to protect the environment and improve quality of life

The FILTER Project

This work is part of FILTER, the FEHRL Investigation on Longitudinal and Transverse Evenness of Roads, which aims at providing European highway research laboratories and standardisation bodies with the knowledge required to harmonise the methods of measuring and assessing road evenness.

Specific objectives

1. To draw up a reliable, comprehensive inventory of all the equipment used in Europe for both transverse and longitudinal measurement, along with their specifications and data processing methods. This information is an absolute prerequisite to any attempt by CEN.

2. By comparing the data collected under objective 1, to discuss the possibility of designing general specifications for both the measurement method and the data processing method which would be an acceptable common denominator to most - hopefully all - currently used systems/methods.

3. To determine the influence of measurement errors on the various evenness quantifiers (indices) with a view to subsequently being able to derive specifications for the profile measurement method in order to obtain the desirable level of accuracy for the indices.

4. To experimentally study the actual performance of the existing measurement devices regarding their repeatability, reproducibility and accuracy with a view to furnishing future CEN standards with reasonable performance statements. The experiment will also provide actual road data as input to the theoretical part of the study. This part of FILTER forms the European part of a world-wide effort initiated by Technical Committee n°1 of the World Road Association (PIARC).

Work programme summary

To meet those four objectives, the following tasks have been identified:

- Task 0: To co-ordinate the project.
- Task 1: To establish an inventory of all measuring devices and assessing methods used in Europe.
- Task 2: To compare the measurement methods.
- Task 3: To compare the data processing methods.
- Task 4: To search for correlations between the different quantifiers used.
- Task 5: To study the influence of measurement errors on the quantifiers.
- Task 6: To conduct an experiment to test the performances of the different systems.
- Task 7: To analyse the results of the experiment.

Financing

The members of the FILTER Working Group thank the following institutions for their contribution to the financing of this research effort :

Belgium :	Ministère fédéral des Affaires Economiques - Division Compétitivité NG III, Belgian Road Research Centre.
Denmark :	Danish Road Institute, Danish Road Directorate.
France :	Ministère de l'Equipement, du Transport et du Logement, Ministère de l'Education Nationale, de la Recherche et de la Technologie.
Germany :	Bundesanstalt für Strassenwesen.
Netherlands :	Directorate-general of Public Works and Water Management.
Slovenia :	Direkcija Republike Slovenije za ceste, Zavod za gradbenistvo Slovenije.
Spain :	Centro de Estudios de Carreteras.
Sweden :	Swedish Transport & Communications Research Board, Swedish National Road Administration.
United Kingdom :	Highways Agency.

Participating laboratories

Laboratory	**Role**
BASt - Bundesanstalt für Strassenwesen (DE)	Organisers and hosts, task 6
CEDEX - Centro de Estudios y Experimentacion de Obras Publicas (ES)	Contributors, task 4 Contributors, task 7
CRR - Belgian Road Research Centre (BE)	General project co-ordinators, task 0 Co-ordinators and contributors, task 1 Co-ordinators and contributors, task 2
DRI – Danish Road Institute (DK)	Secretariat and international liaisons, task 0
DWW – Dienst Weg- en Waterbouwkunde ((NL)	Organisers and hosts, task 6
LCPC – Laboratoire Central des Ponts et Chaussées (FR)	Co-ordinators and contributors, task 7 Co-ordinators and contributors, task 4 Contributors, task 6
TRL – Transport Research Laboratory (GB)	Co-ordinators and contributors, task 3 Contributors, task 5 Contributors, task 7
VTI – Swedish National Road and Transport Research Institute (SE)	Co-ordinators and contributors, task 5 Contributors, task 6 Contributors, task 7
ZAG – Zavod za gradbenistvo Slovenije (SI)	Contributors, task 4 Contributors, task 7

Steering committee

The project has been set up and supervised by the FEHRL Working Group on European Harmonisation of Friction and Evenness Measurement and Assessment Methods the membership of which is the following:

Guy DESCORNET (Convenor)	BRRC	Belgium
Bjarne SCHMIDT (Secretary)	DRI	Denmark
Michel BOULET	LCPC	France
Daniel-Marc DUCROS	LCPC	France
Eckhard KEMPKENS	BASt	Germany
John FATSEAS	KEDE	Greece
Bert de WIT	DWW	Netherlands
Sigmund D∅RUM	NRRL	Norway
Bojan LEBEN	ZAG	Slovenia
Ljubo PETKOVIC	ZAG	Slovenia
Francisco ACHUTEGUI	CEDEX	Spain
Marta ALONSO ANCHUELO	CEDEX	Spain
Georg MAGNUSSON	VTI	Sweden
Leif SJÖGREN	VTI	Sweden
Markus CAPREZ	ETH	Switzerland
Martin HORAT	ETH	Switzerland
Brian FERNE	TRL	United Kingdom
Tony PARRY	TRL	United Kingdom
Martin WILLETT	TRL	United Kingdom

Table of Contents

Summary

This report is concerned with Tasks 3 and 5 of the FILTER project. The aim of Task 3 is "to compare the data processing methods". The task has been subdivided into a comparison of longitudinal processing methods and a comparison of transverse processing methods. TRL have carried out the comparison of longitudinal processing methods; this work is reported in Section 2. The comparison of transverse processing methods has not been done for the reasons given in Section 3. The aim of Task 5 is to "study the effect of measurement errors on the quantifiers". Again, the task has been subdivided into the effect of measurement errors on longitudinal indices and the effect of measurement errors on transverse indices. TRL have carried out the study into the effect of measurement errors on longitudinal errors; this work is reported in Section 4. VTI have carried out the study into the effect of measurement errors on transverse indices; this work is reported in Section 5.

Section 2 compares many of the longitudinal processing methods currently in use in Europe. Twenty longitudinal indices are defined and common elements (and differences) between them are qualitatively identified and discussed. The transfer functions for fourteen of the longitudinal indices are reported. (It was not practicable to determine the transfer functions for the other six indices). A method of quantitative estimating which functional characteristics of a pavement the index actually evaluates is described. Quantitative estimates of which functional characteristics the index evaluates are given for fourteen of the indices.

Section 4 describes a method for creating artificial, but realistic, longitudinal profiles. These profiles are used to estimate the influence of different measurement parameters on the longitudinal indices. The influence of acquisition interval (the distance between each two consecutive measurements of the profile), profile averaging length (the length over which the profile is averaged), and random noise have been determined. It has highlighted which measurement errors and operating conditions are have the most significant effect on longitudinal indices. It has highlighted that, in general, longitudinal indices that attenuate both short and long wavelengths are not only better at isolating wavelengths of interest but also are less sensitive to measurement errors.

Section 5 estimates the influence of different measurement parameters on transverse indices. This has been done by using a set of detailed real transverse profiles. The influence of transverse measurement width, transverse alignment, and the number of sensors have been determined. The study has shown that although increased sampling density and measurement width can increase index accuracy, there are limits beyond which the improvements achieved are small.

Section 6 is a discussion on what is needed from indices and what is possible to be achieved with indices. It concludes that all current longitudinal indices treat the reporting length as if it was homogeneous, and report the general level of longitudinal evenness, in a particular wavelength range, for a section of pavement. However, the currently used indices do not explicitly identify singular irregularities that could be of great importance to the highway engineer and to the user.

1 Introduction

This report is concerned with Tasks 3 and 5 of the FILTER project. The aim of Task 3 is "to compare the data processing methods". The task has been subdivided into a comparison of longitudinal processing methods and a comparison of transverse processing methods. TRL have carried out the comparison of longitudinal processing methods; this work is reported in Section 2. The comparison of transverse processing methods has not been done for the reasons given in Section 3.

The aim of Task 5 is to "study the effect of measurement errors on the quantifiers". Again, the task has been subdivided into the effect of measurement errors on longitudinal indices and the effect of measurement errors on transverse indices. TRL have carried out the study into the effect of measurement errors on longitudinal errors; this work is reported in Section 4. VTI have carried out the study into the effect of measurement errors on transverse indices; this work is reported in Section 5.

2 Comparison of Longitudinal Processing Methods

2.1 Introduction

This report is concerned with Task 3 of the experiment, the comparison of data processing methods. The Forum of European Highway Research Laboratories (FEHRL) working group have defined the objectives of this task as follows:

1. To identify any significant common elements in the various methods of interpreting profiles with a view to a harmonisation that encompasses the majority of methods.

2. To determine the theoretical transfer function associated with each algorithm independently of the transfer function of the measurement process itself.

3. To compare and discuss the significance of each algorithm, with a view to establishing which functional characteristics of the road it actually evaluates by inspecting the wavelength range on which it puts most weight.

A list of 29 longitudinal profile algorithms, which were used in the FILTER experiment itself, has been compiled and is given in Annexe A. Although the list is quite extensive, many of the algorithms are very similar or even identical.

2.2 Definitions

Summaries of the definitions of some of the indices are presented below. It should be stressed that these should not be considered definitive and complete definitions. Only the indices, for which the users have supplied a definition, are discussed.

The term low-pass filter refers to filters that allow low frequencies (long wavelengths) to pass and attenuate high frequencies (short wavelengths). The term high-pass filter refers to filters that allow high frequencies (short wavelengths) to pass and attenuate low frequencies (long wavelengths).

2.2.1 IRI

The International Roughness Index (IRI) is calculated using the following steps:

1. The measured profile is filtered with a 250mm low-pass moving average filter.

2. The filtered profile is then filtered using a quarter-car model.

3. The magnitude of the displacement between the sprung mass (the simulated quarter-car's body) and unsprung mass (the simulated quarter-car's axle) in the quarter-car model is summed.

4. The sum is normalised by the length of the profile.

Values of IRI are usually quoted in mm/m or identically m/km.

2.2.2 HRI

The half-car roughness index (HRI) used the same algorithm as the IRI. However, the profile is the average of the profile from both wheelpaths. The response of the HRI will not therefore be considered separately from the IRI.

2.2.3 RN

The Ride Number (RN) is calculated using the following steps:

1. The measured profile is filtered with a 250mm low-pass moving average filter.

2. The filtered profile is then filtered using a quarter-car model. However, the constants are different from those used for the IRI.

3. The root-mean-square (rms) of the displacement between the sprung mass (the simulated quarter-car's body) and unsprung mass (the simulated quarter-car's axle) in the quarter-car model is calculated to give a unitless quantity Profile Index (PI).

4. PI is transformed into RN using an exponential transform. RN can take values between 0 and 5; 5 is very smooth and 0 is very rough.

2.2.4 3m Variance

In order to obtain 3m variance the following steps are used:

1. A high-pass moving average filter of base length 3m is applied to the measured profile.

2. The filtered points are squared.

3. The squared values are then averaged over the reporting interval.

Values of 3m variance are usually quoted in mm^2.

2.2.5 10m Variance

As for 3m variance but a 10m base length is used.

2.2.6 30m Variance

As for 3m variance but a 30m base length is used.

2.2.7 CP 2.5

In order to obtain the coefficient de planéité 2.5 (CP 2.5) the following steps are used:

1. A low-pass moving average filter of base length 2.5m is applied to the measured profile. This smoothed profile is used as a datum line.

2. The magnitude of the area between the datum line and the original profile are summed and divided by two.

3. The summed value is normalised to unit length. The CP unit has the following dimensions: 1 CP = 10^{-5} m = 10^{4} mm^2 / km.

2.2.8 CP 10

As for CP 2.5 but using a base length of 10m.

2.2.9 CP 40

As for CP 2.5 but using a base length of 40m.

2.2.10 $G(n_0)$ and w to ISO 8608

In order to obtain $G(n_0)$ and w to ISO 8608 the following steps are used:

1. The profile is detrended using a high-pass filter or a low order polynomial best fit.

2. The profile is filtered using an anti-aliasing filter.

3. Profile is converted to a Power Spectral Density (PSD) using a Fast Fourier Transform (FFT).

4. The PSD is smoothed in frequency bands.

5. A function of the form $G(n) = G(n_0)\ (n / n_0)^{-w}$ is fitted to the smoothed PSD, where G(n) is the PSD at spatial frequency n, and n_0 is the spatial frequency corresponding to a wavelength of 2π m.

Values of $G(n_0)$ are normally quoted in m^3. w is unitless.

2.2.11 AUN and W

In order to obtain AUN and w to ISO 8608 [1] the following steps are used:

1. The profile is detrended using a high-pass moving average filter.
2. The profile is filtered using a Cosine Digital Tapering window anti-aliasing filter.
3. Profile is converted to a Power Spectral Density (PSD) using a Fast Fourier Transform (FFT).
4. The PSD is smoothed using a three-point smoothing process.
5. The PSD is smoothed in frequency bands.
6. A function of the form $G(\Omega) = G(\Omega_0) (\Omega / \Omega_0)^{-w}$ is fitted to the smoothed PSD. $G(\Omega)$ is the PSD at the angular spatial frequency Ω. Ω_0 is the reference angular frequency corresponding to a wavelength of 2π m. $AUN \equiv G(\Omega_0)$.

Values of AUN are normally quoted in m^3. w is unitless.

2.2.12 Short wavelength energy

In order to obtain the short wavelength energy (SWE) the following steps are used:

1. The measured profile is filtered such that wavelengths less than 0.7m and greater than 2.8m are greatly attenuated. This is achieved using a Chebyshev Type I linear digital bandpass filter.
2. The filtered points are squared.
3. The squared values are summed over the reporting interval (usually 200m).
4. The sum is multiplied by the length of the sampling interval.

Values of SWE are usually quoted in cm^3.

2.2.13 Medium wavelength energy

As for the short wavelength energy but the bandpass filter greatly attenuates wavelengths less than 2.8m and greater than 11.2m.

2.2.14 Long wavelength energy

As for the short wavelength energy but the bandpass filter greatly attenuates wavelengths less than 11.2m and greater than 44.8m.

2.2.15 Short wavelength NBO

In order to obtain the short wavelength NBO the following steps are used:

1. As for the short wavelength energy.

2. The short wavelength energy is converted into a 10-point scale (1 being the roughest, 10 being the smoothest) using a logarithmic transformation.

2.2.16 Medium wavelength NBO

In order to obtain the medium wavelength NBO the following steps are used:

1. As for the medium wavelength energy.

2. The medium wavelength energy is converted into a 10-point scale (1 being the roughest, 10 being the smoothest) using a logarithmic transformation.

2.2.17 Long wavelength NBO

In order to obtain the long wavelength NBO the following steps are used:

1. As for the long wavelength energy.

2. The long wavelength energy is converted into a 10-point scale (1 being the roughest, 10 being the smoothest) using a logarithmic transformation.

2.2.18 Standard deviation from a 3m moving average

In order to obtain standard deviation from a 3m moving average the following steps are used:

1. A high-pass moving average filter of base length 3m is applied to the measured profile.

2. The filtered points are squared.

3. The squared values are then averaged over the reporting interval.

4. The average is then square rooted.

2.2.19 Standard deviation from a 10m moving average

As for standard deviation from a 3m moving average but a 10m base length is used.

2.2.20 Standard deviation from a 30m moving average

As for standard deviation from a 3m moving average but a 30m base length is used.

2.3 Approach

2.3.1 Identification of common elements

The first objective of Task 3 is to identify any significant common elements in the various methods of interpreting profiles. This has been done by analysing the mathematical steps that define the algorithm; common elements and differences can then be identified.

2.3.2 Response of the summary indices

The second objective of Task 3 is to determine the theoretical transfer function associated with each algorithm independently of the transfer function of the measurement process itself. In other words, we want to know how the index responds to different wavelengths. This has been done using a simulative approach.

As any road profile may be exactly modelled as a linear combination of sine waves of different amplitude frequencies and phases, the input profile to the *Index Algorithm* will be considered to be a function of the form:

$$y_i = A \sin(2\pi n x_i + \phi) \qquad (2.1)$$

Where:

y_i is the i^{th} vertical displacement coordinate.

A is the amplitude of the sine wave.

n is the spatial frequency, $n = 1/\lambda$, where λ is the wavelength.

x_i is the i^{th} longitudinal co-ordinate; $x_i = (i-1) \bullet dx$, where dx is the point separation.

ϕ is the phase angle.

The index algorithm will operate on the input profile and a value of the summary index will be obtained. This process will be undertaken for a range of wavelengths from 0.2m ($n = 5\ m^{-1}$, which corresponds to the Nyquist frequency since dx = 0.1m) to 102.4m ($n = 0.00977\ m^{-1}$).

It is not possible to undertake this process for the non-linear indices; i.e. RN, NBO, and the PSD based indices. However, RN and NBO are both based on linear indices; Profile Index (PI) is the precursor to RN (cf. 2.2.3.); and Energy is the precursor to NBO (cf. 2.2.15 –

2.2.17). It is possible to use these precursor indices to estimate the transfer functions of RN and NBO. The PSD based indices have been omitted from this analysis.

2.3.3 Estimation of the realistic response of the summary indices

The third objective of Task 3 is to compare and discuss the significance of each algorithm with a view to establishing which functional characteristics of the road it actually evaluates, by inspecting the wavelength range on which it puts most significance. In order to meet this objective, it is necessary to understand which wavelengths of a road profile have the greatest effect on the summary index.

As has been mentioned earlier, a road profile can be considered as a series of sinusoidal waves of different wavelengths. In general, the amplitude of these sine waves increases with wavelength. It is necessary to take this into account in order to assess the relative importance of each wavelength component of a road profile on the value of the summary index. From ISO 8608, the general form of the fitted PSD is:

$$G_d(n) = G_d(n_0) \bullet (n/n_0)^{-w} \qquad (2.2)$$

Where:

G_d is the displacement PSD.

w is the exponent of the fitted PSD and is termed the waviness. In general $1 \leq w \leq 3$. For most roads, w would be approximately equal to 2.

This implies that the amplitude A is related to the spatial frequency n by:

$$A(n) \propto n^{-w/2} \qquad (2.3)$$

Therefore, the input profile to the *Index Algorithm* will be considered to be a function of the form:

$$y_i = A_0 n^{-w/2} \sin(2\pi n x_i + \phi) \qquad (2.4)$$

Where A_0 is an arbitrary constant.

The index algorithm will operate on the input profile and a value of the summary index will be obtained. This process will be undertaken for a range of wavelengths from 0.1m (n = 10.0 m^{-1}) to 102.4m (ω = 0.00977 m^{-1}). The amplitude of the sine wave will vary as defined in equation 2.3.

In effect, the input signals are weighted to replicate the amplitude-wavelength relationship found in typical pavements. The methodology will give an estimate of the relative contributions of the different wavelength components (characteristics) of the road surface.

As before, it is not possible to undertake this process for the non-linear indices; i.e. RN, NBO, and the PSD based indices. Therefore, the precursor indices, Energy and PI, have been used to estimate the transfer functions of RN and NBO.

2.4 Results

2.4.1 Identification of common elements

It can be seen from an analysis of the mathematical steps that define the algorithm that the indices fall into two distinct categories – indices that quantify in some way the energy in a filtered profile and indices that characterise the PSD. As shown in Table 2.1 the first of these categories can be further broken down into two subsets – indices that quantify the actual energy and indices that transform the energy into a unitless scale.

Table 2.1. The categorisation of longitudinal profile indices.

Longitudinal profile indices		
Characterise energy in filtered profile		Characterise PSD
Measure energy	Convert energy to unitless scale	
IRI (A); Variance (C, D & E); Standard deviation from a moving average (Q, R & S); CP (G, H & I); Wavelength energies (W, X & Y)	RN (N); NBO (J, K & L)	$G(n_0)$ and w ( ); AUN and w (P)

( ) = codes used in the list of longitudinal profiles in Annexe A.

It was found that Variance, Standard Deviation from a Moving Average (SDMA) and CP are closely related. All three indices use only a high-pass moving average filter to filter the profile. The SDMA is the square root of the variance calculated using the same moving average base length. CP is calculated using exactly the same mathematical steps as SDMA, the only differences being the choice of moving average base lengths and a normalisation constant.

It was found that $G(n_0)$ and w, and AUN and w are very similar. They both characterise the profile by fitting a function to the smoothed PSD. They differ in terms of the detrending process, the anti-aliasing filters, and the smoothing process that is used.

2.4.2. Response of the summary indices

The results are summarised in Tables 2.2 and 2.3, and displayed graphically in Figures 2.1. and 2.2. For detail responses of each index, please see Annexe B.

It should be noted that the results in Table 2.3 and Figure 2.2 are an *estimate* of the realistic response; they are *not* definitive. Although, in general, this estimate of the realistic response will closely reflect the actuality, it will not be valid in all cases. The estimates are based upon the waviness w being equal to two. On pavements where the waviness is greater than two, the indices will respond more to longer wavelengths and less to shorter wavelengths. Conversely, on pavements where the waviness less than two, the indices will respond less to longer wavelengths and more to shorter wavelengths.

Table 2.2. Summary of the wavelength response of longitudinal indices.

Index	Type	High Frequency Cutoff			Low Frequency Cutoff		FWHM
		λ(20% Max)	λ(50% Max)	λ(Max)	λ(50% Max)	λ(20% Max)	
IRI	Band-pass	0.72	1.3	2.1	3.5	7.8	2.2
PI	Band-pass	0.24	0.29	0.50	1.4	4.4	1.1
3m Variance	High-pass	-	-	2.2	3.6	4.9	-
10m Variance	High-pass	-	-	6.9	11.5	15.9	-
30m Variance	High-pass	-	-	21.1	34.4	47.6	-
CP 2.5	High-pass	-	-	1.7	3.7	6.2	-
CP 10	High-pass	-	-	6.9	14.8	25.2	-
CP 40	High-pass	-	-	29.9	58.3	99.8	-
Std Dev from a 3m MA	High-pass	-	-	2.2	4.5	7.7	-
Std Dev from a 10m MA	High-pass	-	-	6.9	14.8	25.2	-
Std Dev from a 30m MA	High-pass	-	-	21.1	44.0	75.9	-
Short Wavelength Energy	Band-pass	0.66	0.68	(2.5)*	2.9	3.0	2.2
Medium Wavelength Energy	Band-pass	2.7	2.7	(3.2)*	11.7	12.1	9.0
Long Wavelength Energy	Band-pass	10.6	10.9	(36.2)*	43.2	47.5	32.3

*The response of Short, Medium, and Long Wavelength Energy is almost flat over a range of approximately two octaves. The value of the peak quoted is therefore academic.

Notes on Table 2.2. and Table 2.3.: High cutoff relates to the high spatial frequency (short wavelength) cutoff. Low cutoff relates to the low spatial frequency (long wavelength) cutoff.

The Type field describes the general form of the response. There are two basic forms of indices – the bandpass type that cutoff at both high and low frequencies and the high-pass type that only cutoff at low frequencies.

λ(Max) is the wavelength at which the response of the index is greatest. λ(20% Max) and λ(50% Max) are the wavelengths at which the response is 20% and 50% of the maximum response respectively.

Full Width Half Max (FWHM) is the width of the response at half the maximum response, i.e. FWHM = $\lambda(50\%\ Max)_{Low\ Cutoff}$ - $\lambda(50\%\ Max)_{High\ Cutoff}$. It is a measure of the width of the response.

Table 2.3. Summary of the weighted *wavelength response of longitudinal indices.*

Index	Type	High Frequency Cutoff			Low Frequency Cutoff		FWHM
		λ(20% Max)	λ(50% Max)	λ(Max)	λ(50% Max)	λ(20% Max)	
IRI	Band-pass	1.1	1.6	2.3	23.8	34.7	22.2
PI	Band-pass	0.32	0.48	5.9	10.0	15.0	9.7
3m Variance	Band-pass	1.5	1.9	3.1	6.4	11.0	4.5
10m Variance	Band-pass	4.8	6.2	10.2	20.8	35.6	16.0
30m Variance	Band-pass	14.3	18.3	29.9	62.5	>100	44.2
CP 2.5	Band-pass	0.48	1.3	2.5	7.8	20.3	6.5
CP 10	Band-pass	2.1	5.1	10.2	31.7	82.1	26.6
CP 40	Band-pass	8.6	20.2	39.1	>100	>100	>79.8
Std Dev from a 3m MA	Band-pass	0.61	1.6	3.1	9.7	25.2	8.1
Std Dev from a 10m MA	Band-pass	2.1	5.1	10.2	31.7	82.1	26.6
Std Dev from a 30m MA	Band-pass	6.5	15.1	29.9	94.5	>100	79.4
Short Wavelength Energy	Band-pass	1.2	2.0	2.7	3.0	3.0	1.0
Medium Wavelength Energy	Band-pass	5.0	7.9	11.0	11.8	12.2	3.9
Long Wavelength Energy	Band-pass	17.3	27.8	37.6	45.2	49.6	17.4

Notes: High cutoff relates to the high spatial frequency (short wavelength) cutoff. Low cutoff relates to the low spatial frequency (long wavelength) cutoff. Full Width Half Max (FWHM) is the width of the response at half the maximum response, i.e. FWHM = $\lambda(50\% \text{ Max})_{\text{Low Cutoff}}$ - $\lambda(50\% \text{ Max})_{\text{High Cutoff}}$. It is a measure of the width of the response.

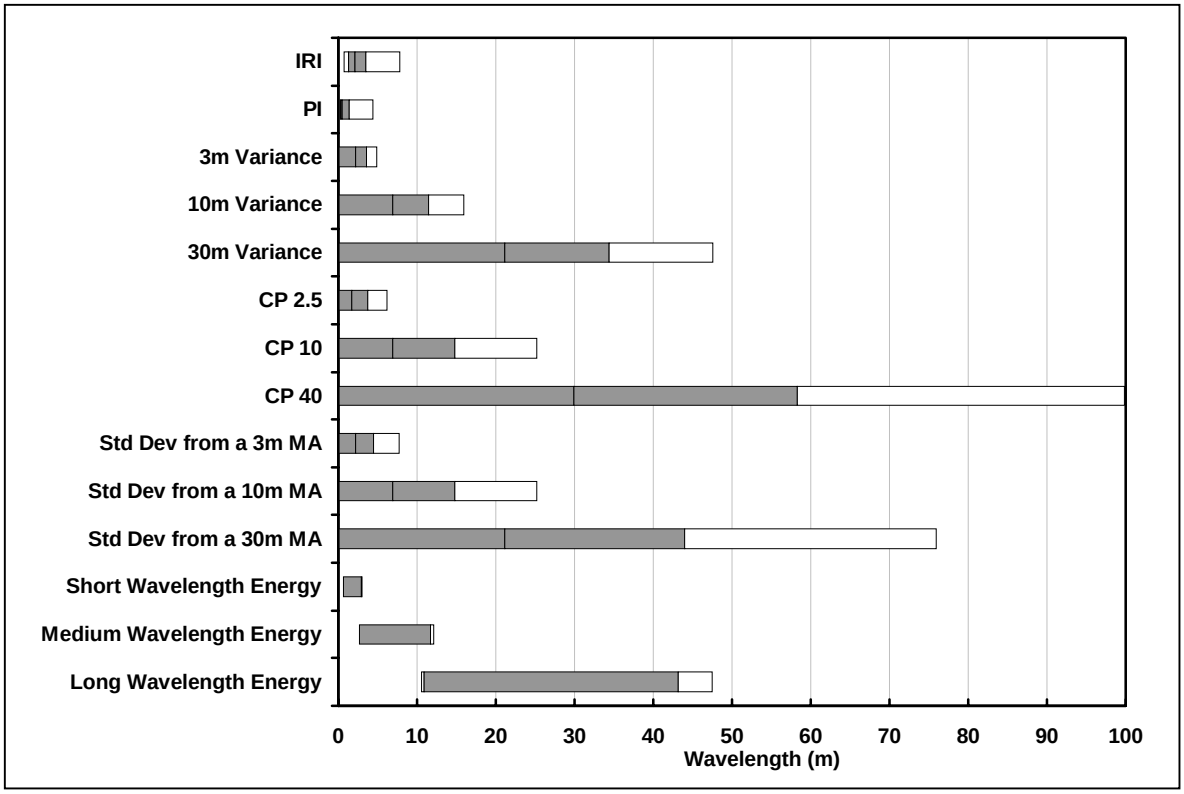

Figure 2.1. Summary of the response of longitudinal indices. The clear box indicates where the response is greater than 20%; the grey box indicates where the response is greater than 50%. The vertical line within the grey area is the location of the peak response.

Notes on Figure 2.1: Because it is not well defined, no peak is given for the Short, Medium and Long Wavelength Energies.

.

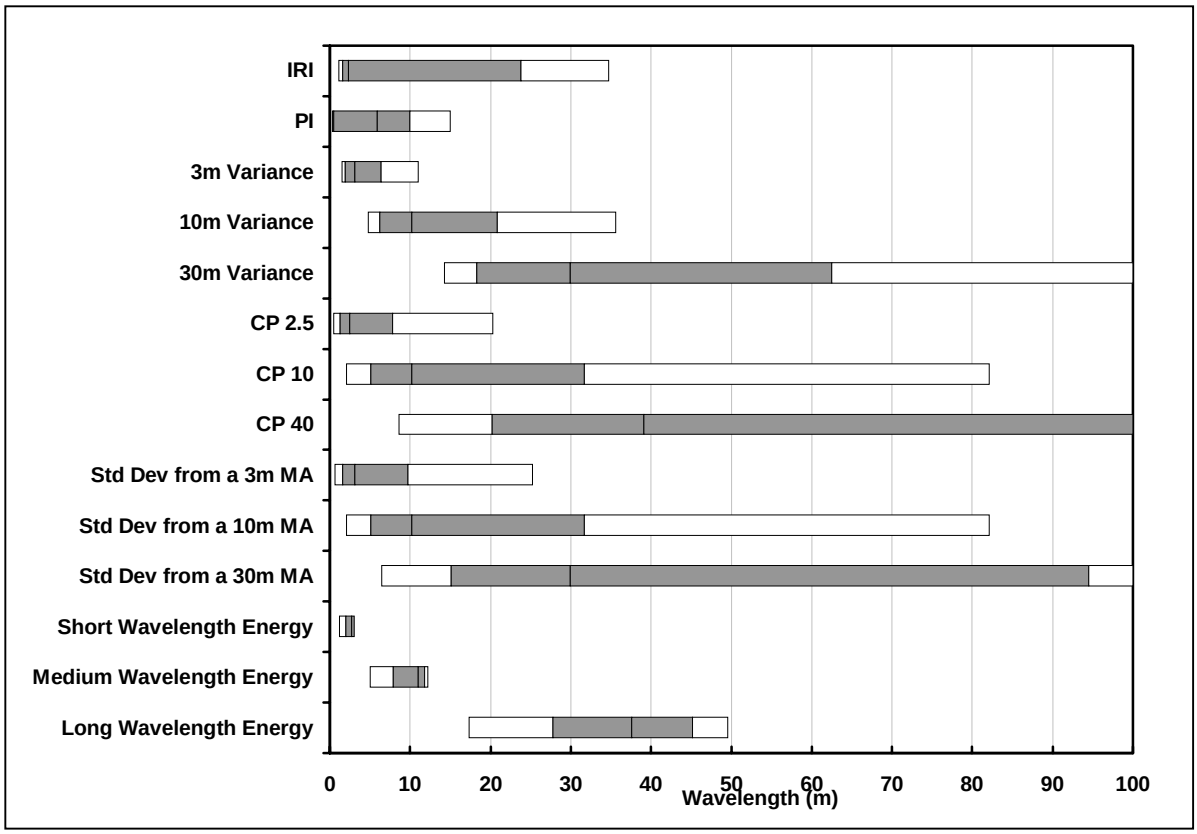

Figure 2.2. Summary of the weighted response of the longitudinal indices. The clear box indicates where the response is greater than 20%; the grey box indicates where the response is greater than 50%. The vertical line within the grey area is the location of the peak response

2.5 Discussion

2.5.1 IRI and PI

Although different in detail, both IRI and PI are based on a model of a quarter car. Therefore, it is not surprising that there are similarities in their responses. Both the unweighted responses of IRI and PI are similar in shape; they both have a single peak and an inflection at a longer wavelength. See Figures B1 and B2 in Annexe B.

The weighted responses of IRI and PI are similar in shape. However, whereas IRI has two distinct peaks, PI has one distinct peak and a large inflection. The width of the weighted responses of IRI and PI is much wider than the width of their unweighted responses. IRI is

significantly influenced by wavelengths up to approximately 35m (i.e. $\lambda(20\%\ peak)_{weighted}$ = 34.7m). PI is significantly influenced by wavelengths up to approximately 15m. However, they will still be influenced by wavelengths greater than this.

2.5.2 Variance, Standard Deviation and CP

Standard Deviation, CP and Variance are all based on a moving average filtered profile. Therefore, their unweighted responses are similar in shape. They are all high-pass filters with ripple in the pass-band. However, Variance has a greater attenuation outside the pass-band, but a greater amount of ripple in the pass-band. See Figures B3 – B8 and B12 – B14 in Annexe B.

The weighted responses of Standard Deviation, CP and Variance are similar in shape; they are band-pass filters with a single peak. Again Variance has a greater amount of attenuation outside the pass-band; in other words, the peak is sharper.

The weighting, which is used to provide an estimate of the realistic response of indices, increases with wavelength. Consequently, the attenuation outside the low frequency end of the pass-band is not very sharp. Therefore, the indices are influenced by much longer wavelengths than their moving average base lengths might suggest.

Each set of three Variance, CP and Standard Deviation indices collectively describe the unevenness of a pavement over a wide range of wavelengths. However, within each set there is considerable overlap among the indices. This overlap is less significant for Variance. The overlap is not a major problem in itself, but it does limit the use of these indices to identify problem wavelengths.

2.5.3 Short, Medium and Long Wavelength Energies

The unweighted response of the Short, Medium, and Long Wavelength Energies are flat in their pass-bands apart from a small amount of ripple. There is a very rapid attenuation outside the pass-band. In total, the three indices continuously cover wavelengths from approximately 0.7m to 40m. See Figures B9 – B11 in Annexe B.

On first examination, it appears that there are gaps in the coverage of the weighted response of the Short, Medium, and Long Wavelength Energies. However, the weighting was based on a particular model; any deviation from that model, for example a peak in PSD at 15m say (a wavelength *apparently* not covered), would invalidate the model.

2.6 Conclusion

Profile indices are required by the road owners to determine if the pavement is providing an acceptable level of serviceability for the user, and if it is not, then these indices can help the owner to identify physical deficiencies of the pavement.

Three broad types of longitudinal profile indices are currently used in Europe: those that measure the energy in a given waveband directly; those that convert the energy to a unitless scale; and those that characterise profile in terms of its power spectral density.

Many of the common indices used are based on deviations from a moving average length. The responses of these indices are similar in form, but of course differ depending on the moving average length used.

The normal method of examining the wavelength response of an index does not take account of the typical mix of amplitudes at different wavelengths present in a normal road profile. When this aspect is taken into account, the indices are, in general, influenced by wavelengths significantly longer than is normally considered to be the case.

2.7 References

[1] INTERNATIONAL STANDARDS ORGANIZATION (1995). Mechanical vibration – Road surface profiles – Reporting of measured data, ISO 8608: 1995.

3 Comparison of Transverse Processing Methods

Comparison between different kinds of transverse indices has not been considered in this study. It is indeed meaningless because there are essentially three kinds of indices that, by definition, cannot be compared. Crossfall is completely independent of rutting and water ponding depends on both rutting and crossfall. Correlation between similar indices reported by different teams would not discriminate the effects of different device performances and different algorithms used to compute the same parameter. An interesting study however would be to compare the outputs of different algorithms applied to the same set of profiles. This has not been possible to do in the course of this project; it is left for a future specific study by the FILTER Group with a view to standardising the definitions and softwares for determining crossfall, rut depth and water ponding.

4 The Influence of Errors on Longitudinal Indices

4.1 Introduction

The aim of this task is to assess quantitatively the influence of errors in the measurement of profile on the summary indices. This quantitative assessment will allow profiler users to assess the level of accuracy in the measurement of profile that they need to achieve a desired level of accuracy in the summary indices.

4.2 Definitions

The following terms, symbols and definitions have been extracted from the definition of terms in Table H1 in Annexe H, and will be used throughout Section 4.

Table 4.1. Definitions of terms used in this section

Term	Symbol	Definition
Profile		A function that describes the geometric properties of a length of road surface in terms of the vertical height and the longitudinal position.
Continuous Profile		A continuous function that describes the geometric properties of a road surface in terms of vertical height and longitudinal position.
Discrete Profile		A discrete function that describes the geometric properties of a road surface in terms of a discrete set of vertical heights and associated longitudinal positions.
True Profile		A continuous profile that exactly describes the geometric properties of a road surface.
Reported Profile		A discrete profile that is the final profile output of a profiler. The Reported Profile will be used to calculate summary indices.
Reporting Interval (Storage sampling interval)	ρ	The linear distance between each consecutive point in the Reported Profile.
Reporting Frequency		The inverse of the reporting interval.
Measured Profile		A discrete profile that is the unprocessed input to a profiler, i.e. it is the profiler's initial measurement of true profile before any processing.

Measurement Interval (Acquisition sampling interval)	Δ	The linear distance between each consecutive point in the Measured Profile.
Measurement Frequency		The inverse of the measurement interval.
Profile Averaging Length	Λ	The length over which a Measured Profile is averaged to produce the Reported Profile.

4.3 Methodology

The term “errors” is slightly misleading. In this context, “errors” are any characteristics of the reported profile (the profile that is used to calculate the summary index) that could result in a value of the summary index that differs from its “true” value. In fact, this task will consider the influence of measurement interval, profile averaging length, as well as the influence of random noise. The term “errors” will be used for all these factors.

How do we define a “true” value for a summary index? An obvious answer is to say that the “true” value of a summary index is the value that is calculated from the true profile. However, it is impossible to numerically calculate a summary index from the true profile as the true profile is a continuous quantity not a set of discrete values. A solution to this problem would be to calculate a “true” value of the summary index from a very detailed profile; i.e. a profile with very small measurement interval. The true value should not be considered a definitive value of the index, but a reference value to which to compare the other values.

To assess the influence of errors, the values of the summary indices calculated from the error inclusive profiles were compared to the true value of the summary index.

Obviously, it is not possible to sample a true profile at any desired frequency with absolute accuracy. Therefore, in this study simulated profiles were used.

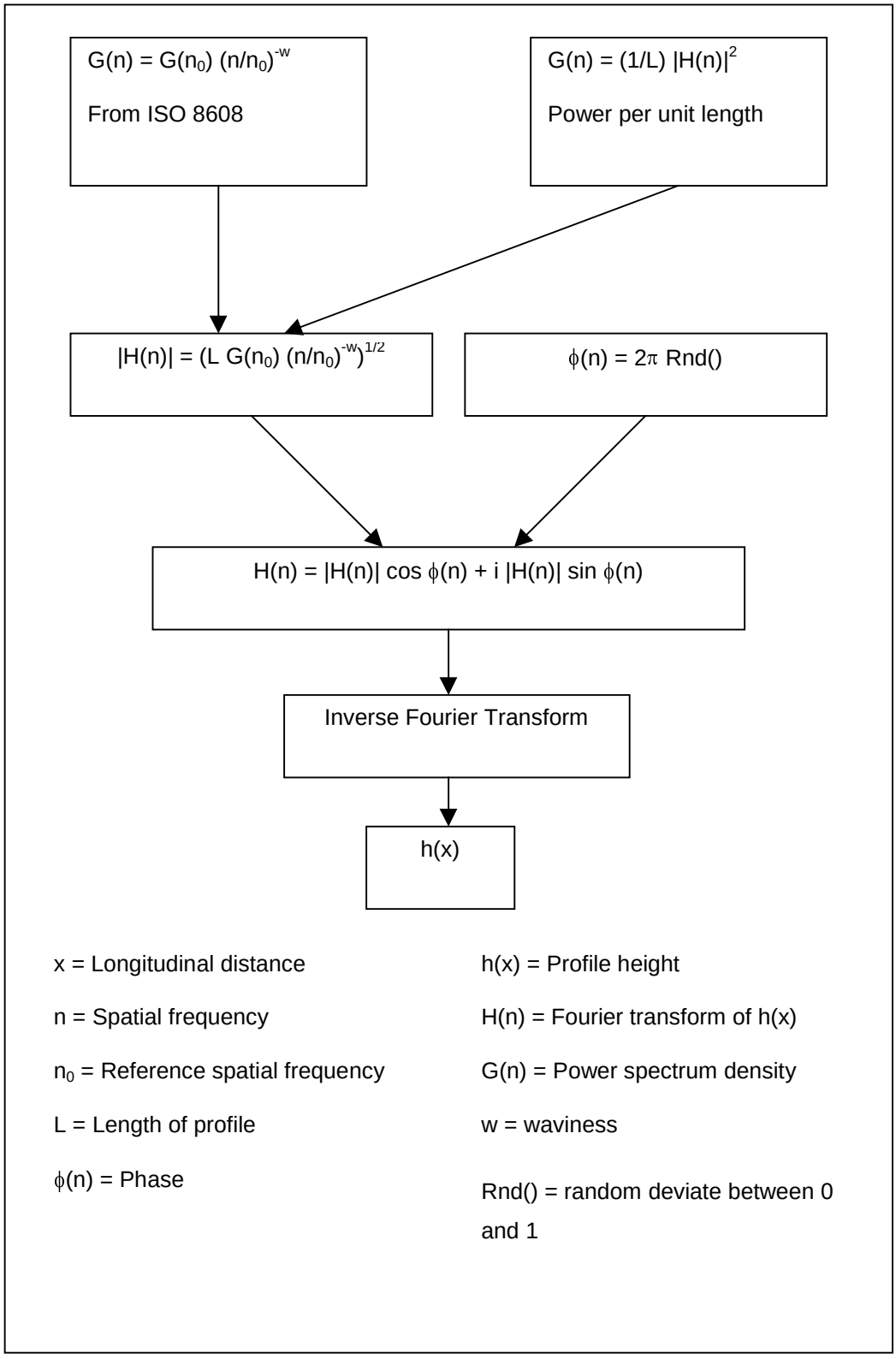

Figure 4.1. The process used to create the artificial profiles.

4.3.1 The Artificial Profile Model

The methodology for creating artificial profiles is given schematically in Figure 4.1. For the vast majority of pavements, there is a simple relationship between the Power Spectrum Density (PSD) and the spatial frequency. From this, it is possible to determine the relationship between the modulus of the Fourier-transformed profile and the spatial frequency. By combining this relationship with a random phase and applying an inverse Fourier-transform, it is possible to create artificial profiles that are indistinguishable from real profiles. See Fig 4.2 for an example of an artificial profile.

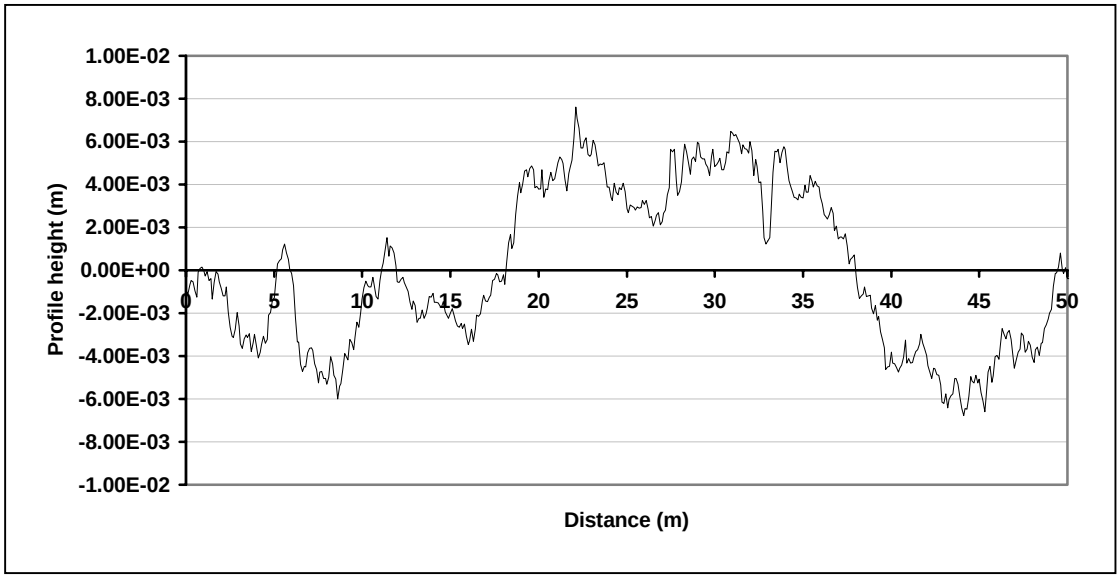

Figure 4.2. An example of an artificial profile.

4.3.2 The Influence of Sampling Interval and Profile Averaging Length

In general, all profilers process the true profile to produce a recorded profile. However, intermediate steps between the true profile and the recorded profile are often different. For example, some profilers may discretely measure the true profile at a fixed spatial sampling rate; others may measure the true profile at a fixed temporal sampling rate. Then the profile may, or may not, be averaged over some length to produce the reported profile. This is a simplification, and in reality, there are often many more intermediate steps. However, it is not possible within the limits of this study to investigate every possible intermediate step. Therefore, this study will limit itself to the investigation of the influence of measurement interval and profile averaging length.

A detailed profile was created using the method described in §4.3.1. The detailed profile had a length of approximately 270m and had a measurement interval of approximately 0.520mm (In fact $\Delta = 3 * 10^{-4} * 3^{1/2}$ and Length $= 2^{19} * \Delta \approx 272.438$m. This value was

chosen for Δ as it is irrational. This removes the possibility of interpolated points coinciding with the original points).

Two different methods were then used to process the detailed profile.

(i) Discrete sampling of the detailed profile.

(ii) Discrete sampling of the detailed profile followed by averaging of the profile over a profile averaging length.

After processing the profile using the above methods, the summary indices were calculated. These values were then compared with an appropriate reference value for the indices.

For the first method (i), the detailed profile was sampled at a measurement interval, Δ = 1.0 mm – 512.0 mm in sixth-octave increments ($\Delta = 1.0 * 2^{n/6}$ mm for n = 0, 1, 2, ..., 54). The profile height at each point was interpolated from the detailed profile using a cubic-spline. For each measurement interval, the summary indices were calculated. This was repeated for 300 different artificial profiles; the same artificial profiles were used for each summary index. The values of the indices were converted into absolute percentage error.

$$E = | (V - V_{Ref}) / V_{Ref}| * 100 \quad (3.1)$$

Where: E is the absolute percentage error.

V is the value of the index.

V_{Ref} is the reference value of the index.

For this method, the reference value of the index is derived from the detailed profile, i.e. Δ = 0.520mm.

Therefore, for each measurement interval there were 300 absolute percentage errors. The 95^{th} percentile of this distribution was calculated. This value, the 95^{th} percentile of the absolute percentage error, was taken as a measurement of the error due to the measurement interval.

For the second method (ii), it was not practical to assess every combination of measurement interval and averaging length. Therefore, this study limited itself to using a single constant averaging length and a range of measurement intervals (method (ii.a)), and a single constant measurement interval and a range of profile averaging lengths (method (ii.b)). The single constant profile averaging length was chosen to be 100mm because it is a common reporting interval / profile averaging length. The single constant measurement interval was chosen to be 1mm, because it is a typical measurement interval, approximately corresponding to a 16kHz laser at 60km/h. The study was limited to the case where the reporting interval was equal to the profile averaging length.

In the first case (ii.a), different measurement intervals and a constant profile averaging length were used. The detailed profile was sampled at a range of measurement intervals, Δ

= 1.0 mm – ~90.5 mm in sixth-octave increments ($\Delta = 1.0 * 2^{n/6}$ mm for n = 0, 1, 2, ..., 39). The profile was then averaged over 100mm (Λ = 100mm) and was reported at 100mm intervals (ρ = 100mm). For each measurement interval, the summary index was calculated. This was repeated for 300 different artificial profiles. The same profiles were used for each summary index. The 95th percentile of absolute percentage error was calculated in a similar manner to that described in method (i). The reference index was calculated from the profile with a measurement interval of 1.0mm (Δ = 1.0mm), and a profile averaging length of 100mm (Λ = 100mm).

In the second case (ii.b), a constant measurement interval and different profile averaging lengths were used. The detailed profile was sampled at the measurement interval, Δ = 1.0 mm. The profile was then averaged over a range of profile averaging lengths Λ = 25mm – 500mm (Λ = n * 25mm, n = 1, 2, …, 20). The reporting interval used was the same as the profile averaging length (ρ = n * 25mm, n = 1, 2, …, 20). For each profile averaging length, the summary index was calculated. This was repeated for 300 different artificial profiles. The same artificial profiles were used for each summary index. The 95th percentile of absolute percentage error was calculated in a similar manner to that described in method (i). The reference index was calculated from the detailed profile ($\Delta \approx 0.520$mm).

This process is summarised in Figure 4.3.

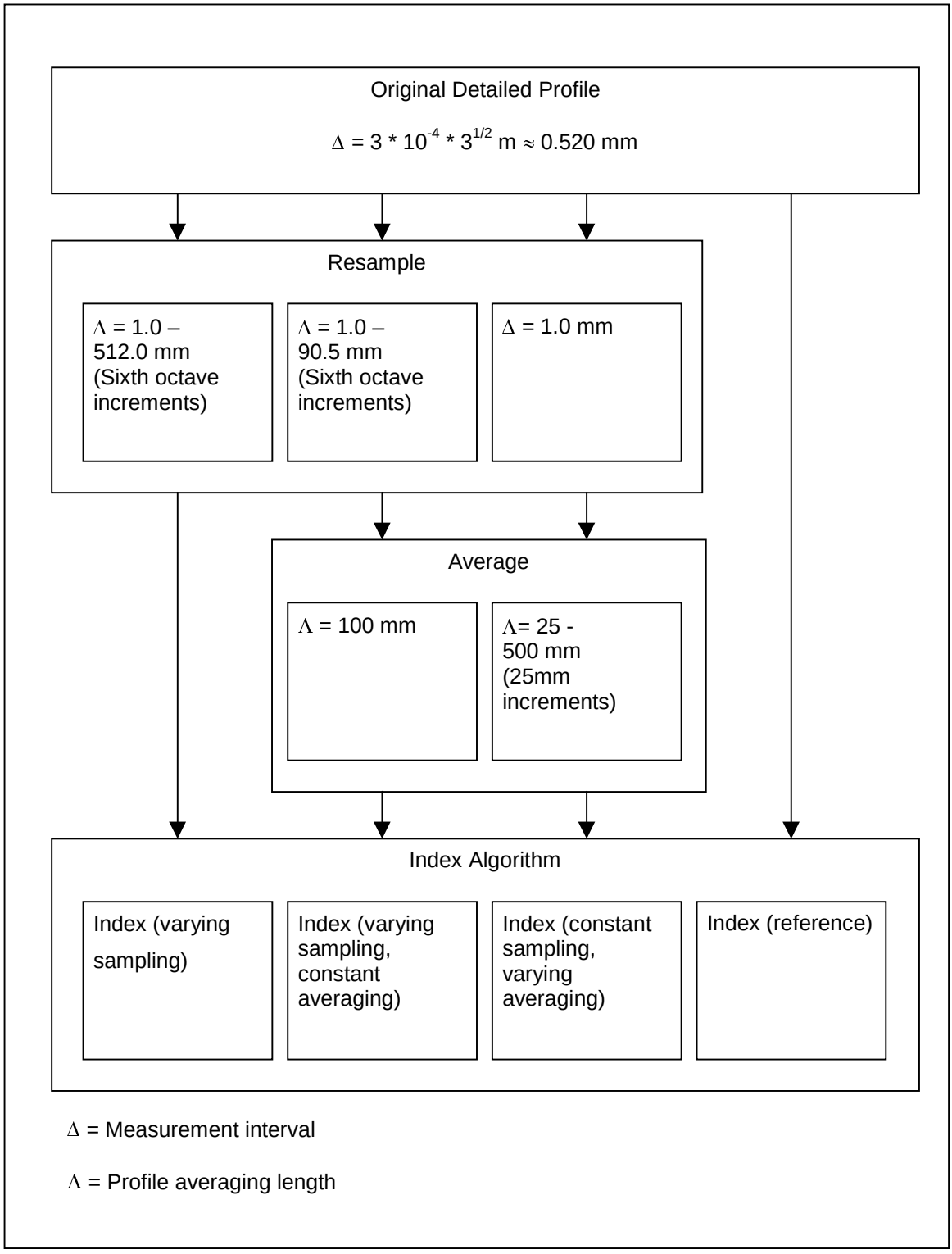

Figure 4.3. Summary of the methodology for the assessment of the influence of measurement interval and profile averaging length.

4.3.3 The Influence of Random Noise

Any measurement of a profile will include some level of noise. This noise could be caused by driver line, vehicle vibration, limitations of the sensors or any other factors that affect the accuracy of the measurements. In reality, it is likely that the noise in the profile measurement will be caused by a combination of many different factors. The form of this total noise is not known. However, for the purposes of this study, the noise was assumed to be Gaussian random noise of a known standard deviation and zero mean.

The detailed profile was sampled at a measurement interval, $\Delta = 1.0$ mm. Gaussian random noise was then added to the measured profile. The profile was then averaged over 100mm ($\Lambda = 100$mm) and was reported at 100mm intervals ($\rho = 100$mm). This was repeated for a range of levels of Gaussian random noise; the standard deviation of the Gaussian random noise, σ, ranged from 0.1mm to 102.4mm ($\sigma = 0.1 * 2^{n/3}$ mm, n = 0, 1, …, 30). For each level of noise the summary index was calculated. This was repeated for 300 different artificial profiles. The same artificial profiles and random noise were used for each summary index. The 95th percentile of the absolute percentage error was calculated for each level of noise.

4.4 Results

4.4.1 The Influence of Measurement Interval and Profile Averaging Length

4.4.1.1 The influence of discrete measurement interval

In general, indices that measure short wavelength unevenness are more sensitive to the discrete measurement interval than indices that measure longer wavelengths. The measurement interval limits the shortest wavelength that may be measured; consequently, the measurement interval affects the high frequency cut-off of the index. This effect is most significant for indices that concentrate on short wavelengths. A summary of the results are shown in Figure 4.4. More detailed results are given for each index in Annexe C.

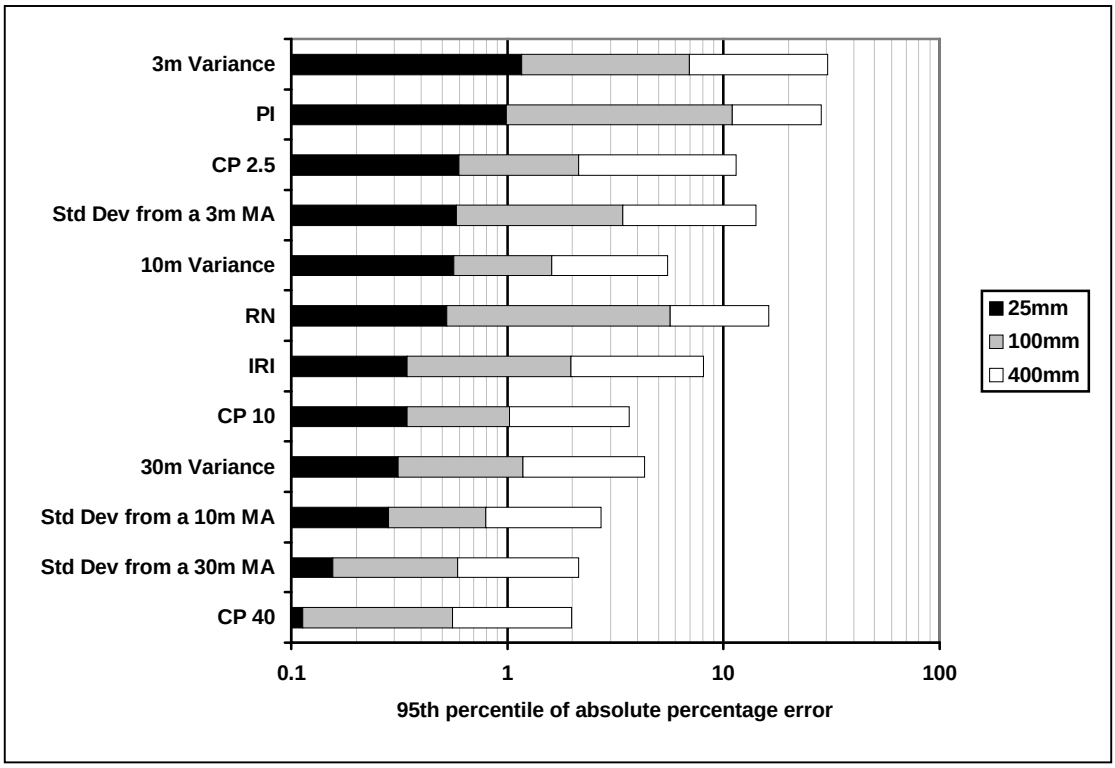

Figure 4.4. The influence of measurement interval. Examples are given for intervals of 25mm, 100mm, and 400mm. The error is calculated relative to a reference index that is derived from the original detailed profile.

4.4.1.2 The influence of measurement interval with constant averaging length

In general, indices that measure short wavelength unevenness are more sensitive to the measurement interval than indices that measure longer wavelengths. The measurement interval limits the shortest wavelength that the profilometer may measure. However, the profile averaging process acts as a low-pass filter and attenuates wavelengths less than 100mm. Consequently, the effect is insignificant. In this analysis, even when sampling the profile at 50mm, 95% of the values of 3m variance are within approximately 3% of their true values. The results are summarised in Figure 4.5. More detailed results are given for each index in Annexe D.

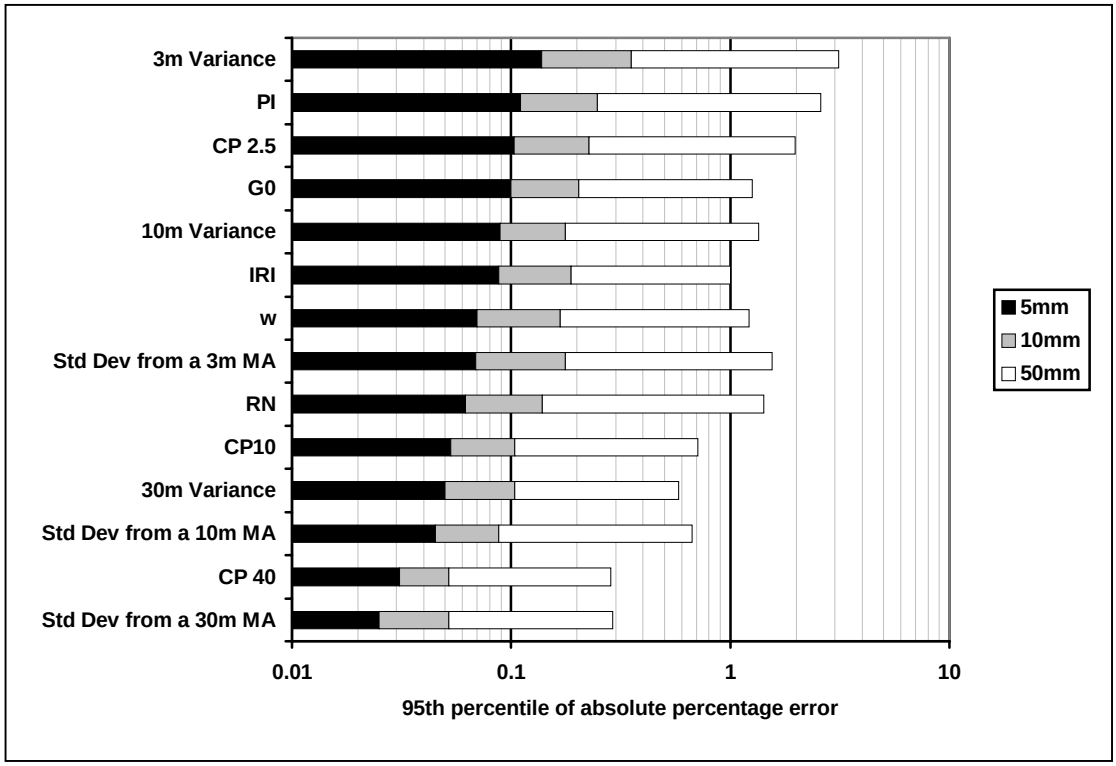

Figure 4.5. Summary of the influence of measurement interval with a constant 100mm averaging length. Examples are given for measurement intervals of 5mm, 10mm, and 50mm. The error is calculated relative to a reference index that was derived using a measurement interval of 1mm and a 100mm averaging length.

Many profilometers sample the true profile with a fixed temporal frequency. Therefore when the profilometers speed varies, the [spatial] measurement interval will vary.

$$\Delta = v / f \tag{4.1}$$

Where Δ is the [spatial] measurement interval; v is the vehicle speed; and f is the temporal sampling frequency. A 16kHz laser on a vehicle travelling at 60km/h will sample the true profile at a measurement interval of approximately 1mm. From this and the above results, it is clear that the influence of the vehicle speed *on the measurement interval* has no significant affect upon an index. However, it should be noted that the vehicle speed might affect the measurement of the true profile in other ways – e.g. accelerometer accuracy in GM principle profilometers.

4.4.1.3 The influence of averaging length with constant measurement interval

More detailed results are given for each index in Annexe E.

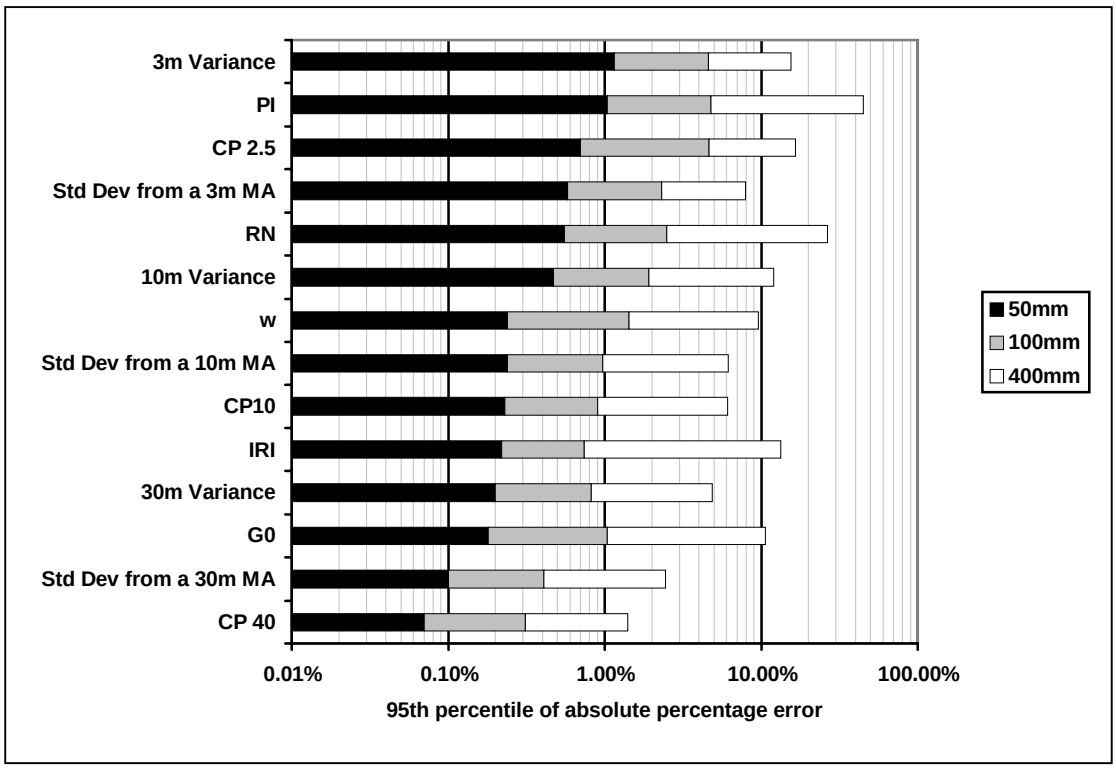

Figure 4.6. Summary of the influence of profile averaging length with a constant 1mm measurement interval. Examples are given for profile averaging lengths of 50mm, 100m, and 400mm. The errors are relative to index calculated from the detailed profile (c.f. Fig 4.3).

4.4.2 The Influence of Random Noise

The absolute level of noise is more significant on smoother pavements than it is on rougher pavements. Therefore, the influence of noise on indices has been assessed on artificial road profiles of four different standards. The evenness of the four different standards of pavement correspond to the centre of the classes A, B, C and D in ISO 8608.

Table 4.2. The four ISO 8608 classes of pavement used to create the artificial profiles for the assessment of the influence of random noise. Approximate equivalent IRI values are also given.

ISO 8608 Class	$G(n_0)$ ($10^{-6}m^3$)	Approximate IRI (mm/m)
A	16	2.2
B	64	4.3
C	256	8.6
D	1024	17.2

Summary results are given for each of the indices for class A and class B pavements are given in Figures 4.7 and 4.8. Detailed results for each index, at each of the four classes are given in Annexe F.

In general, indices that measure short wavelength unevenness are more sensitive to random noise than indices that measure longer wavelengths. One noticeable exception is the SWE.

SWE applies a band-pass filter with very sharp cut-offs. The filter will greatly attenuate the noise at frequencies higher than its high frequency cut-off (as well as frequencies lower than its low frequency cut-off). This is instrumental to SWE being relatively insensitive to noise; at high frequencies, the noise is much more significant relative to the profile. An identical argument will also apply to MWE, and LWE.

Most other indices only apply a high-pass filter, e.g. 3m variance. Consequently, they are much more sensitive to noise than indices that use bandpass filters, e.g. SWE.

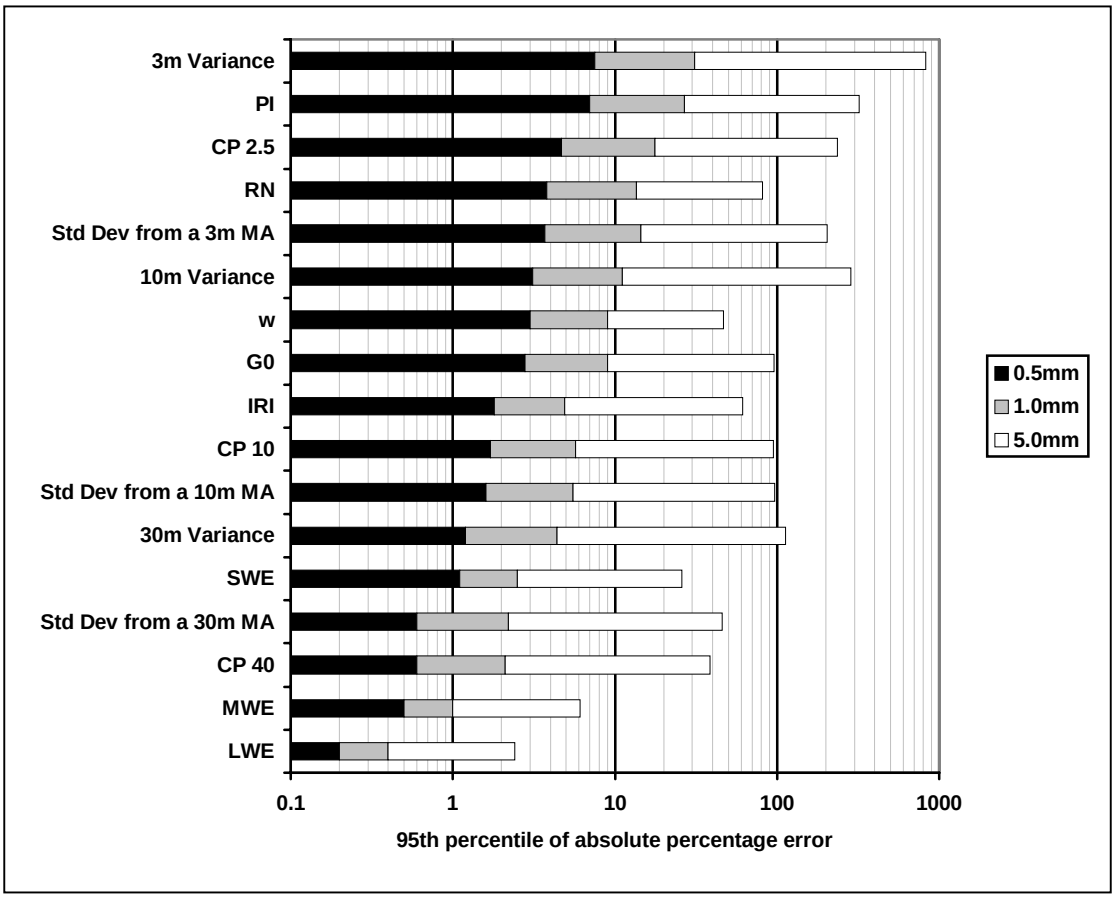

Figure 4.7. Summary of the effect of Gaussian random noise on longitudinal indices for ISO 8608 class A roads. The noise was added to the measured profile (Δ = 1mm) before the profile is averaged (Λ = 100mm). The errors are calculated relative to an error free profile.

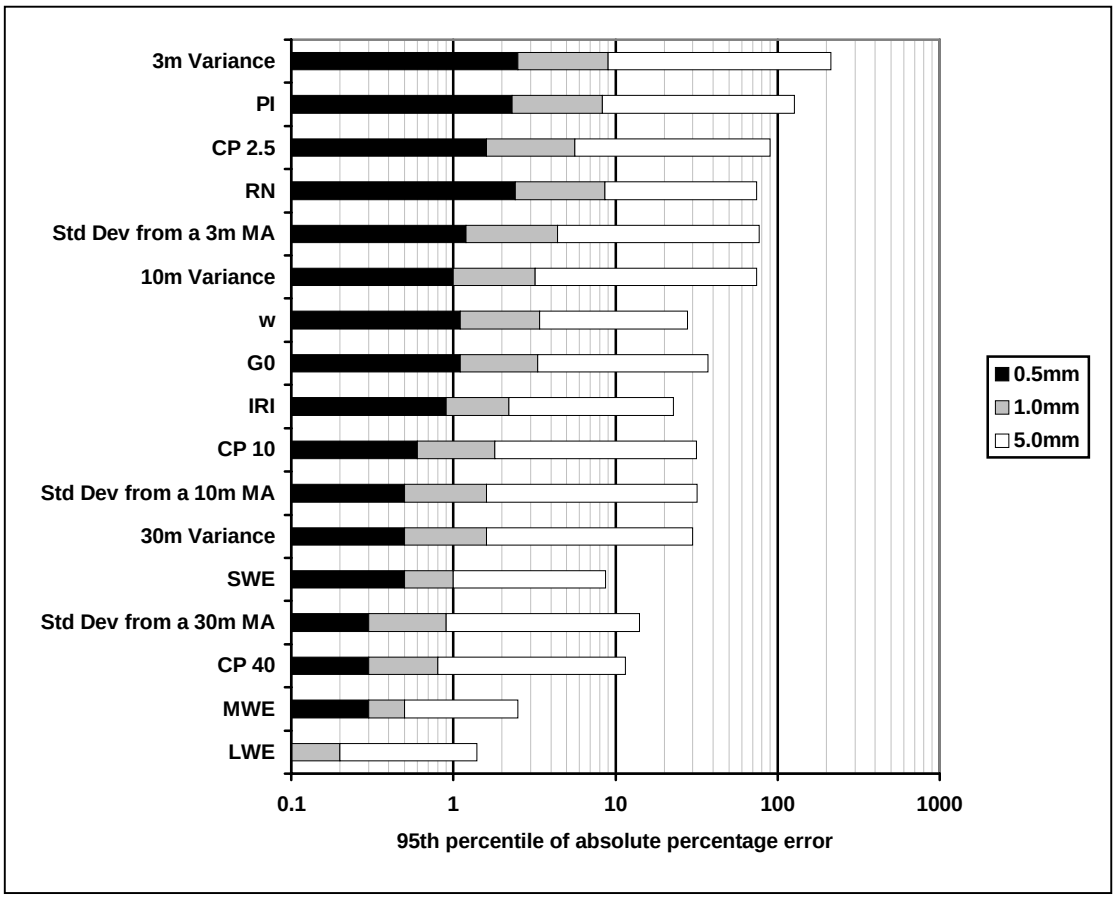

Figure 4.8. Summary of the effect of Gaussian random noise on longitudinal indices for ISO 8608 class B roads.

4.5 Conclusions

In general, indices that measure short wavelength unevenness are more sensitive to the discrete measurement interval than indices that measure longer wavelengths. However, for the range of intervals normally used by current profilometers this has little effect on the index values.

Again, indices that measure short wavelength unevenness are more sensitive to the measurement interval with constant averaging length than indices that measure longer wavelengths. However, for the range of intervals normally used by current profilometers this has little effect on the index values. Consequently, for a profilometer whose measurement interval is speed dependent, there will be little effect on the index values due to variation in speed.

Again, indices that measure short wavelength unevenness are more sensitive to the profile averaging length with constant measurement interval than indices that measure longer wavelengths. For the range of lengths normally used by current profilometers this has little effect on the index values.

Random noise will influence indices that measure short wavelength unevenness. Those most likely to be affected are 3m variance and CP2.5 together with the PI and RN indices. For a given level of noise, the influence will be greater on smoother roads than on rougher roads.

The indices that attenuate short wavelengths as well as long wavelengths (i.e. indices that use a band-pass filter) are in general less susceptible to random noise than indices that only attenuate long wavelengths (i.e. indices that use a high-pass filter). Thus, Short, Medium and Long Wavelength Energies are less likely to be affected by noise than other indices covering the same wavelength range.

4.6 References

[1] INTERNATIONAL STANDARDS ORGANIZATION (1995). Mechanical vibration – Road surface profiles – Reporting of measured data, ISO 8608: 1995

5 The Influence of Errors on Transverse Indices

5.1 Introduction

The transverse profiles of roads are measured for a number of reasons, e.g. research, control of the quality of newly laid road surfaces and for surveying the condition of an existing road net. The transverse profile of the road can be measured stationary or on the run at different speeds. The only way of obtaining an absolutely true picture of the transverse profile is by means of a stationary device with a high accuracy, high resolution sensor traversing the road guided by a straight ruler mounted in a stiff stand. The accuracy of measurement that is provided by such a device is warranted for research and control purposes. For surveying, the stationary device is not only completely unsuitable but its accuracy is also unnecessary high.

High-speed transverse profilometers are basically of two different types, both only sampling the transverse profile, longitudinally or transversally. One type of transverse profilometers is based on photography or video technique. A light line is projected across the road surface and picture is taken of it at an angle to the road surface. This type of profilometer normally covers the entire width of the lane to be measured and often more than that. The picture is stored on photographic film or on videotapes for subsequent evaluation in laboratory. Even if such pictures of the transverse profile can be taken at rather high rate the work involved in the evaluation process requires that the pictures be taken at some distance intervals along the road (longitudinal sampling). The appropriate sampling distance depends on the purpose of the measurement.

The other type of transverse profilometers consists of a beam mounted across the front of a vehicle or underneath it, between the axles. A number of distance measuring sensors are mounted along the beam thus sampling the transverse profile transversely. To allow for measurement in normal traffic without the necessity of a follower car the width of the vehicle including the measuring beam is restricted according to local laws. In the case of laser sensors the measurement width can be increased to some extent using lasers that are mounted at an angle to the vertical. In the case of ultrasonic sensors the measurement width can only be increased by means of adding extensions on both ends of the beam increasing the measurement width to e.g. 4 m. A follower car is then normally required. The measurement resolution and accuracy of the individual laser sensors is with a large margin sufficient for all normal profile measurements. In the case of ultrasonic sensors the accuracy to some extent depends on the shape of the road surface. While the dimensions of the laser light spot are of the order of a few millimetres, the size of the ultrasonic "sound" spot is about 100 mm across. The distance reported by the laser is an average over the small light spot while the ultrasonic sensor reports the distance to the highest point within the "sound" spot. This means that there can be large measurement errors on heavily rutted

roads even if the individual sensors work properly. The distance reported by a laser sensor, on the other hand, is sensitive to the macro texture of the surface, meaning that even if a reported value is correct as such it is not necessary reflecting a true rut depth. In order to overcome this problem the reported distance values normally are the average of all measurements over a certain distance along the road, e.g. 100 mm.

The normal way of evaluating transverse profile measurements is to calculate rut depths and/or theoretical water depths ignoring the effect of longitudinal road slope. In addition to the measurement accuracy of the sensors used in the measurement the rut or theoretical water depths that are the outcome of the calculations will depend on the measurement width and the transverse sampling distance. However, experience has shown that the most influential factor is the lateral position of the measurement vehicle when collecting the profile data. Even a very experienced driver of the measurement vehicle instructed e.g. to keep the right wheels of the vehicle in the middle of the right rut can not avoid a certain amount of lateral wander.

In order to study the effect of lateral wander for different measurement vehicle configurations a simulation exercise has been carried out.

The influence of measurement width and transverse sampling interval on the following indices (defined in Figures 5.1 – 5.3) has been calculated.

maximum theoretical water depth*	(mm)
maximum theoretical water depth in left rut*	(mm)
maximum theoretical water depth in right rut*	(mm)
area of water (sum of both ruts)*	(dm^2)
maximum rut depth	(mm)
maximum depth of left rut	(mm)
maximum depth of right rut	(mm)
area of rut (sum of both ruts)	(dm^2)

* Only in the cases where also the influence of varying the crossfall has been studied.

The calculations are made for seven profiles (labelled A – G) taken from existing roads in Sweden (see Annexe G). The idea behind the selection was to find good a variety of profile shapes as possible from real roads. These measurements have been made by means of the PRIMAL profilometer of VTI. It is described and its performance given in de Wit et. al. [1].

The results are likely to be very dependent on the relationship between the spacing of the wheelpaths and the measuring width of the profilometer. It should be noted from Annexe G that the wheelpath spacing of the sample profiles varies between 1.75 and 2.0m suggesting that in some cases the deformation has been mostly caused by private cars, possibly as a result of studded tyres, and in other cases by commercial vehicles. Thus the results of the investigation and any conclusions drawn should be understood in this context. For other environments different conclusions might have been reached.

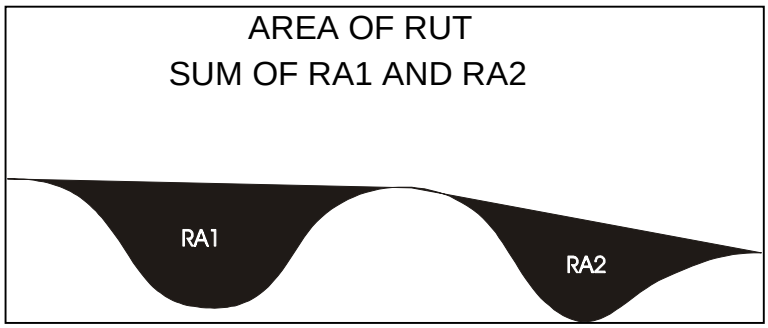

Figure 5.1. Definition of area of rut.

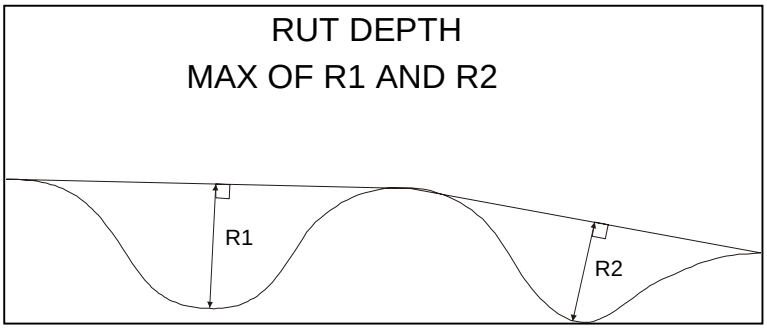

Figure 5.2. Definition of rut depths

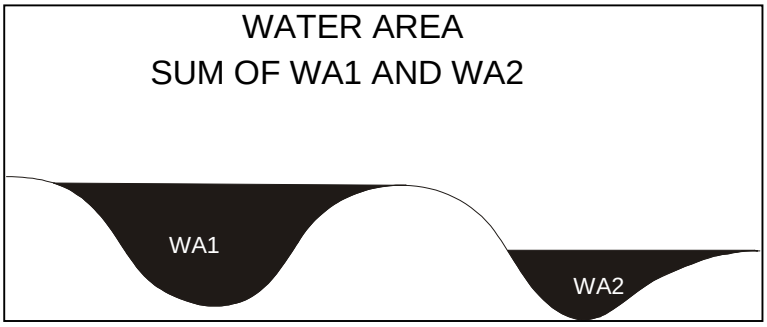

Figure 5.3. Definition of water area.

5.2 Effect on rut depth when varying transverse sampling and lateral position

Five configurations of measurement vehicles have been simulated each with a measurement width of 3 m. One of them provides a continuous transverse profile (transverse sampling = 0) while the other devices have transverse sampling intervals of 0,1; 0,15; 0,25 and 0,3 m respectively. The simulation has been carried out for the following nine lateral positions of the measurement vehicle with respect to the centre line of the lane:

-0,20; -0,15; -0,10; -0,05; 0; +0,05; +0,10; +0,15; +0,20 m.

The idea behind this procedure is to simulate the involuntary but in praxis unavoidable lateral wander by the profilometer when measuring. A ±0,2 m lateral wander is probably a rather realistic figure in survey measurement. For project level measurements the lateral position might be possible to keep within narrower limits.

Table 5.1. shows the "true" values for each profile; i.e. the values that are obtained with continuous sampling and the measurements carried out in the middle of the lane. The average value over all the lateral positions and the standard deviation of the individual values was calculated for all the rut depth indices for each of the seven profiles. Figure 5.4. shows the effect on rut depth and rut area of varying lateral position when measuring with different transverse sampling intervals. Reported data are the average over the seven road profiles. The effects on rut indices of different lateral positions of the measurement vehicle will of course depend on the shape of the transverse profile. The transverse profile is likely to vary along the road and the seven profiles used in this study consist of four variations of what may be considered as "typical" profiles and three non-typical profiles. The reporting of the average values over the seven profiles can be regarded as a case study of survey measurement.

As can be seen all the rut depth indices are decreasing and the rut area increasing with increasing transverse sampling interval. The change is almost linear. Using a 3 m profilometer with a transverse sampling interval of 0,3 m will underestimate the rut depth values by 10 - 14 % and overestimate the rut area by about 18 %.

Table 5.1. Rut data obtained with continuous sampling and the measurements carried out in the middle of the lane. Measurement width 3,0 m.

Index	Profile						
	A	B	C	D	E	F	G
Rut depth right (mm)	2,2	11,0	11,2	9,4	2,8	3,0	2,1
Rut depth left (mm)	9,9	10,4	11,1	10,4	6,2	2,1	2,2
Rut depth max. (mm)	10,6	12,7	11,8	10,4	8,1	3,0	2,3
Rut area (dm^2)	0,89	2,08	1,84	1,36	1,01	0,35	0,32

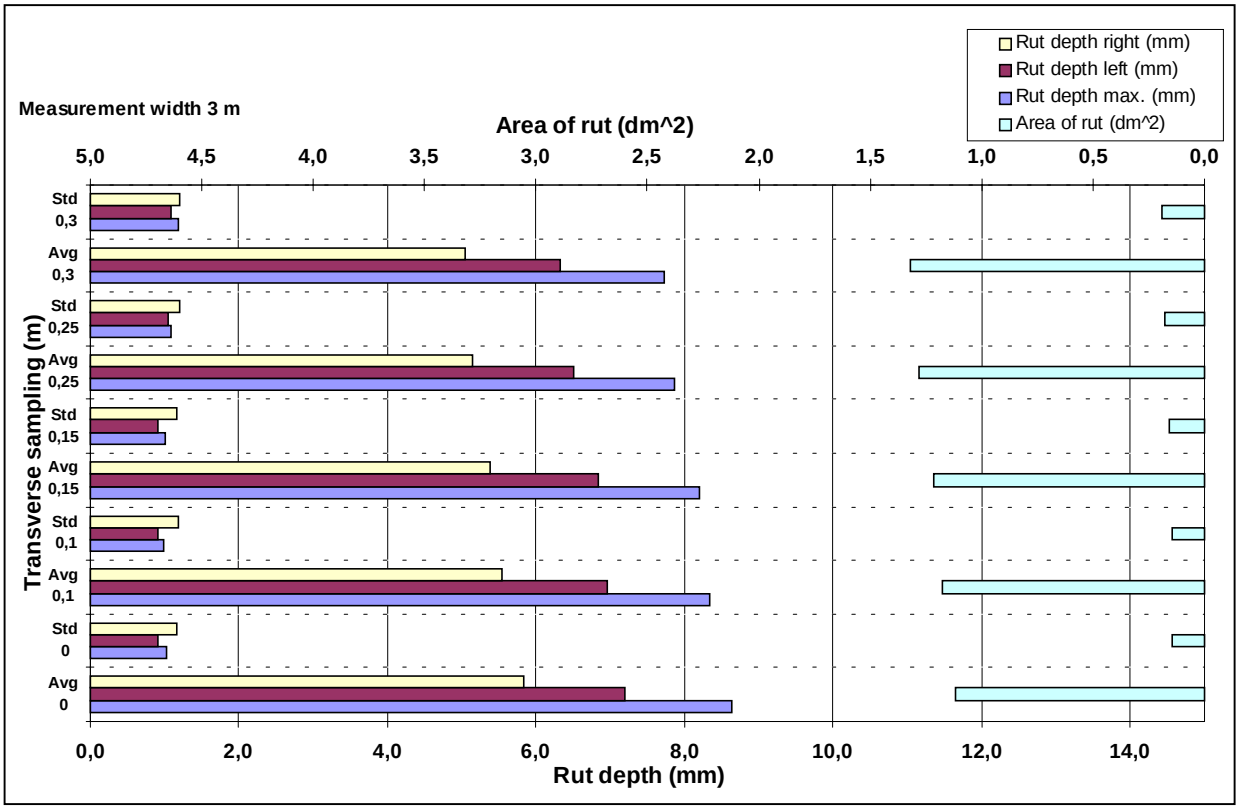

Figure 5.4. The effect on rut depths and rut area of varying lateral position when measuring with different transverse sampling intervals. Average over seven road profiles. (Observe that the scale "Area of rut" is located on top of the diagram and goes from right to the left).

5.3 Effect on rut depth when varying measurement width and lateral position

The same lateral positions as above were simulated for the following five measurement widths: 2,0; 2,6; 3,0; 3,6 and 4,0 m.

Table 5.2. – 5.5. show the effect of measurement width on the rut indices for the different transverse profiles when measured with continuous sampling in the middle of the lane. These values are to be regarded as the "true" values that will be obtained using profilometers with different measurement widths. Figure 5.5. shows the average effect on the rut indices of lateral wander using profilometers with different measurement widths. Reported as averages over the seven profiles.

As can be seen all the rut indices are decreasing with decreasing measurement width. The rut data obtained using the widest profilometer will presumably come closest to the "true" value. Cutting off the 4,0 m profilometer to 3,6 m does not mean any dramatic change in the obtained measurement result. About 5 % reduction on maximum rut depth, 15 % on rut

area and an almost negligible effect on left and right rut depths. Reducing the measurement width to 3,0 m will cause a decrease of obtained maximum rut depth with about 20 % and the rut area with 45 %. Comparing the average values of Table 5.2. – 5.5. with the corresponding values in Figure 5.5. will show that the average values over all seven profiles measured without lateral wander (Table 5.2. – 5.5.) are of the same order of magnitude as those obtained with a lateral wander of ±0,2 m. It thus seems that the influence of lateral wander would have a negligible effect on rut indices, at least for the combination of transverse profiles used in this simulation.

Table 5.2. Rut depths in right rut obtained with continuous sampling and the measurements carried out in the middle of the lane.

Measurement width (m)	Profile							
	A	B	C	D	E	F	G	Average
4,0	10,5	12,8	14,8	11,1	2,8	4,6	2,1	8,4
3,6	7,7	12,1	14,8	10,7	2,8	4,6	2,1	7,8
3,0	2,2	11,0	11,2	9,4	2,8	3,0	2,1	6,0
2,6	1,4	6,5	9,8	5,0	2,8	1,3	2,1	4,1
2,0	1,3	5,9	5,3	0,8	2,8	0,9	2,1	2,7

Table 5.3. Rut depths in left rut obtained with continuous sampling and the measurements carried out in the middle of the lane.

Measurement width (m)	Profile							
	A	B	C	D	E	F	G	Average
4,0	10,1	12,6	12,6	10,7	6,8	2,1	2,2	8,2
3,6	9,9	12,1	12,4	10,7	6,8	2,1	2,2	8,0
3,0	9,9	10,4	11,1	10,4	6,2	2,1	2,2	7,5
2,6	9,9	6,5	8,6	8,9	6,0	2,1	1,6	6,2
2,0	9,7	2,5	2,2	3,9	3,8	1,2	1,1	3,5

Table 5.4. Maximum rut depths obtained with continuous sampling and the measurements carried out in the middle of the lane.

Measurement width (m)	Profile							
	A	B	C	D	E	F	G	Average
4,0	14,0	16,9	17,2	11,1	10,2	4,6	2,3	10,9
3,6	11,3	16,6	17,0	10,7	9,9	4,6	2,3	10,3
3,0	10,6	12,7	11,8	10,4	8,1	3,2	2,3	8,4
2,6	10,6	9,8	10,1	8,9	7,4	2,1	2,1	7,3
2,0	10,2	6,9	5,4	3,9	4,1	1,2	2,1	4,8

Table 5.5. Rut area obtained with continuous sampling and the measurements carried out in the middle of the lane.

Measurement width (m)	Profile							
	A	B	C	D	E	F	G	Average
4,0	2,84	3,57	3,28	1,62	1,72	0,56	0,38	2,00
3,6	1,80	3,28	3,13	1,55	1,54	0,55	0,35	1,74
3,0	0,89	2,08	1,84	1,36	1,01	0,35	0,32	1,12
2,6	0,78	1,30	1,35	0,82	0,80	0,24	0,25	0,79
2,0	0,68	0,51	0,42	0,19	0,35	0,09	0,16	0,34

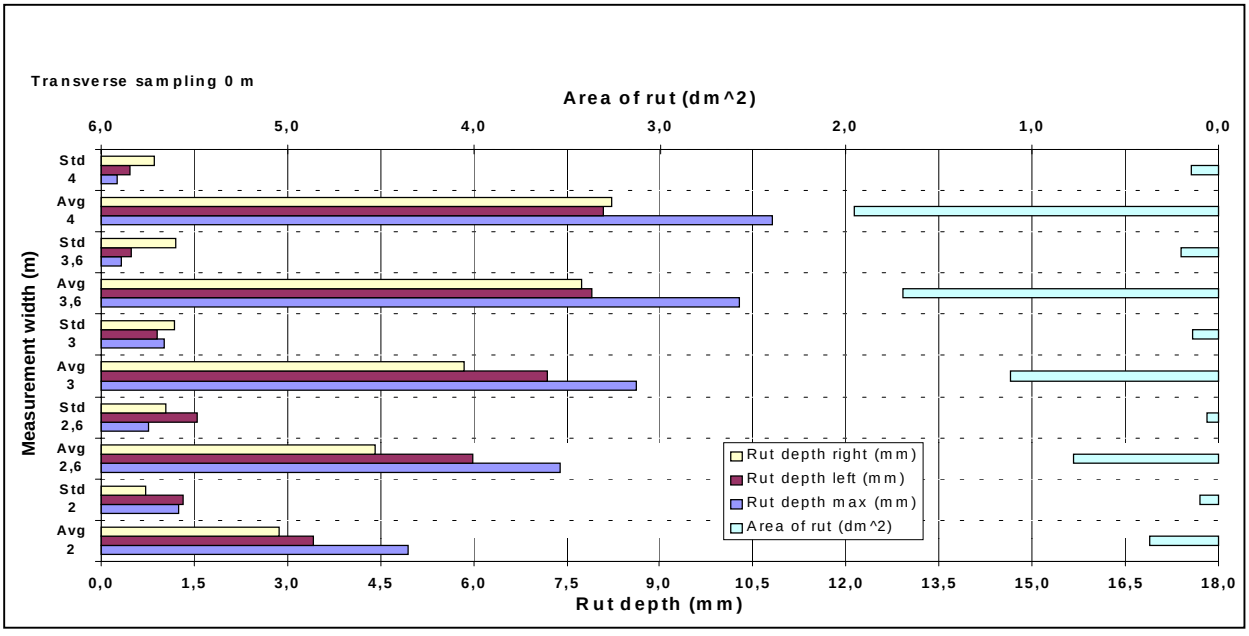

Figure 5.5. The effect on rut depths and rut area of varying lateral position when measuring with continuous sampling and different measurement widths. Average over seven road profiles. (Observe that the scale "Area of rut" is located on top of the diagram and goes from right to the left).

5.4 Effect on water depth when varying transverse sampling and lateral position

The same transverse sampling intervals, lateral positions and measurement width as above were used in this simulation. Table 5.6. shows the "true" values of the water indices, i.e.

the values that are obtained with continuous sampling while measuring in the middle of a lane with crossfall equal to zero. Table 5.7. shows the same but for a lane with a crossfall of 2,5 %. Figure 5.6. shows the effect on water depths and water area of varying lateral position when measuring with different sampling intervals on a lane with crossfall equal to zero. Reported values are the averages over the seven road profiles. Figure 5.7. shows the same type of information but for a lane with a crossfall of 2,5 %.

The effect of varying lateral positions on the water depth on a lane without crossfall is about the same as the effect on rut depth (see Figure 5.4.). The reported water depth decreases about linearly with increasing sampling interval. Using a 3 m profilometer with a sampling interval of 0,3 m will underestimate the water depths by 15 - 22 % as compared to continuous measurements. The reported water area is almost independent of the sampling interval.

The effect on the water depths of varying lateral positions on a lane with a crossfall of 2,5 % is very dramatic. The maximum water depth as an average over the seven profiles decreases from 0,8 mm with continuous sampling to 0,1 mm obtained with the sampling interval of 0,3 m. The standard deviations are very high as compared to the average values. Also the water area shows a steady decrease with increasing sampling interval. However all values are very small. The influence of lateral wander on water indices seems to be the same as for rut indices.

Table 5.6. Water data obtained with continuous sampling and the measurements carried out in the middle of the lane. Measurement width 3,0 m. Crossfall 0 %.

Index	Profile							
	A	B	C	D	E	F	G	Average
Water depth right (mm)	1,7	9,1	8,7	4,3	2,6	1,8	1,4	4,2
Water depth left (mm)	9,1	10,0	10,1	8,9	4,8	2,1	0,6	6,5
Water depth max. (mm)	10,3	12,2	10,1	8,9	7,9	2,1	1,4	7,6
Water area (dm^2)	0,70	1,93	1,32	0,74	0,96	0,22	0,05	0,85

Table 5.7. Water data obtained with continuous sampling and the measurements carried out in the middle of the lane. Measurement width 3,0 m. Crossfall 2,5 %.

Index	Profile							
	A	B	C	D	E	F	G	Average
Water depth right (mm)	0,4	2,8	0,4	0,3	0,4	0	0,4	0,7
Water depth left (mm)	0,8	0,9	0,5	1,2	0,5	0	0,6	0,6
Water depth max. (mm)	0,8	2,8	0,5	1,2	0,5	0	0,6	0,9
Water area (dm^2)	0,01	0,05	0,01	0,02	0,01	0	0,01	0,02

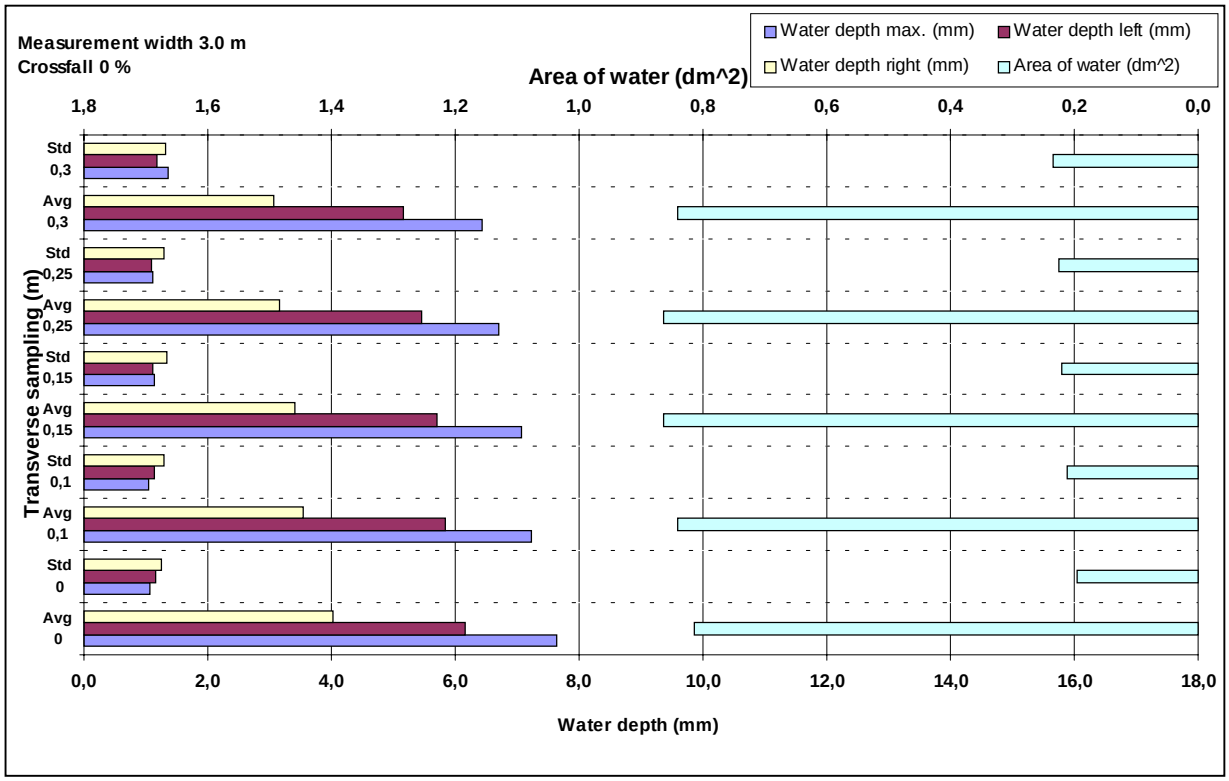

Figure 5.6. The effect on water depths and water area of varying lateral position when measuring with different sampling intervals on a lane with crossfall = 0. Average over seven road profiles. (Observe that the scale "Area of water" is located on top of the diagram and goes from right to the left).

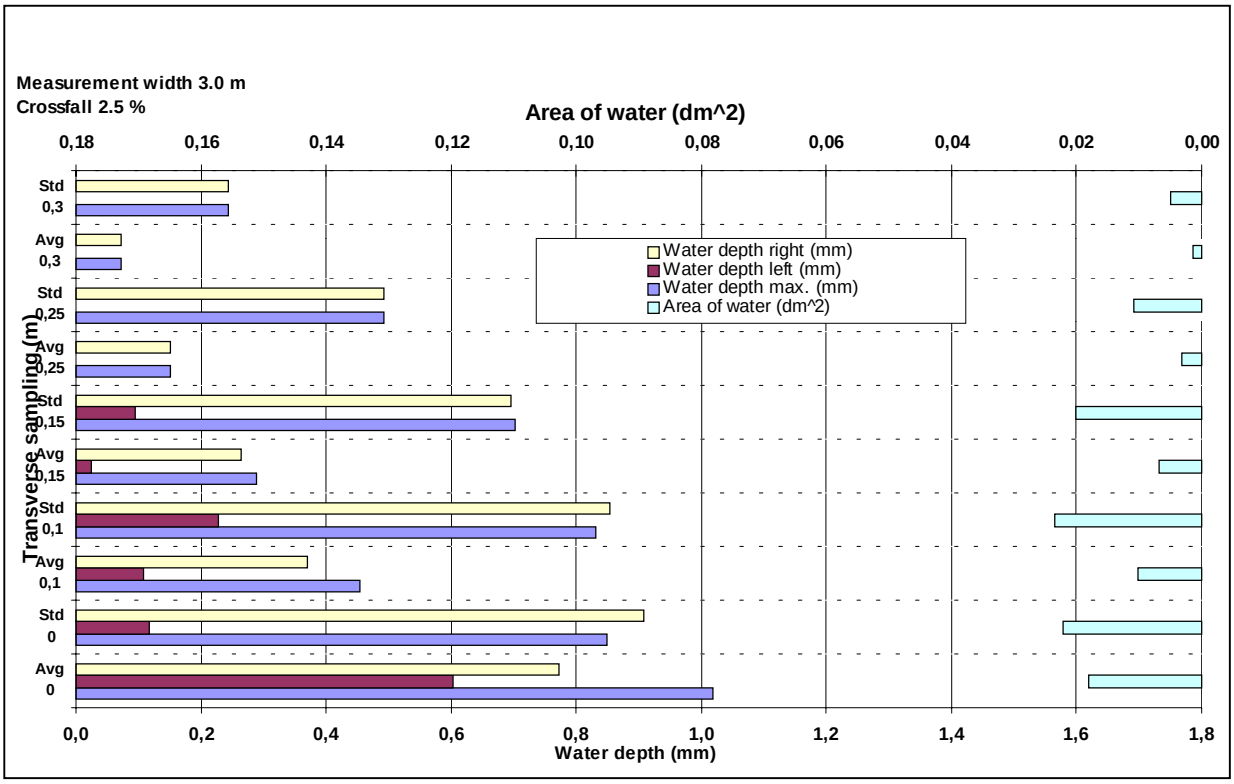

Figure 5.7. The effect on water depths and water area of varying lateral position when measuring with different sampling intervals on a lane with crossfall = 2,5 %. Average over seven road profiles. (Observe that the scale "Area of water" is located on top of the diagram and goes from right to the left).

5.5 Rut depth variation studied in real measurements

Figure 5.8. shows the effect on recorded rut depth of the number of measuring points in the transverse profilometer based on real measurement on 2342 transverse profiles. The measurements have been carried out in three different lateral positions, 0,5; 1,0 and 1,5 m from the road edge. The measurement width was in all cases 3,2 m. The average rut depth over the 2342 transverse profiles was 14,35 mm. As can be seen the rut depth value obtained with a 25-laser device is about 13,7 mm as an average over the three lateral positions. Using 17 lasers will reduce the recorded rut depth value to about 13,4 mm while eleven lasers will give a further rut depth reduction of about 0,7 mm giving a rut depth around 12,7 mm. The required measurement accuracy of course depends on the purpose of the measurement. For surveying purposes a device with eleven measurement points would probably be sufficient, while project level measurements would perhaps require 17 measurement points. Increasing the measurement points to 25 does not seem to be worth the extra expense.

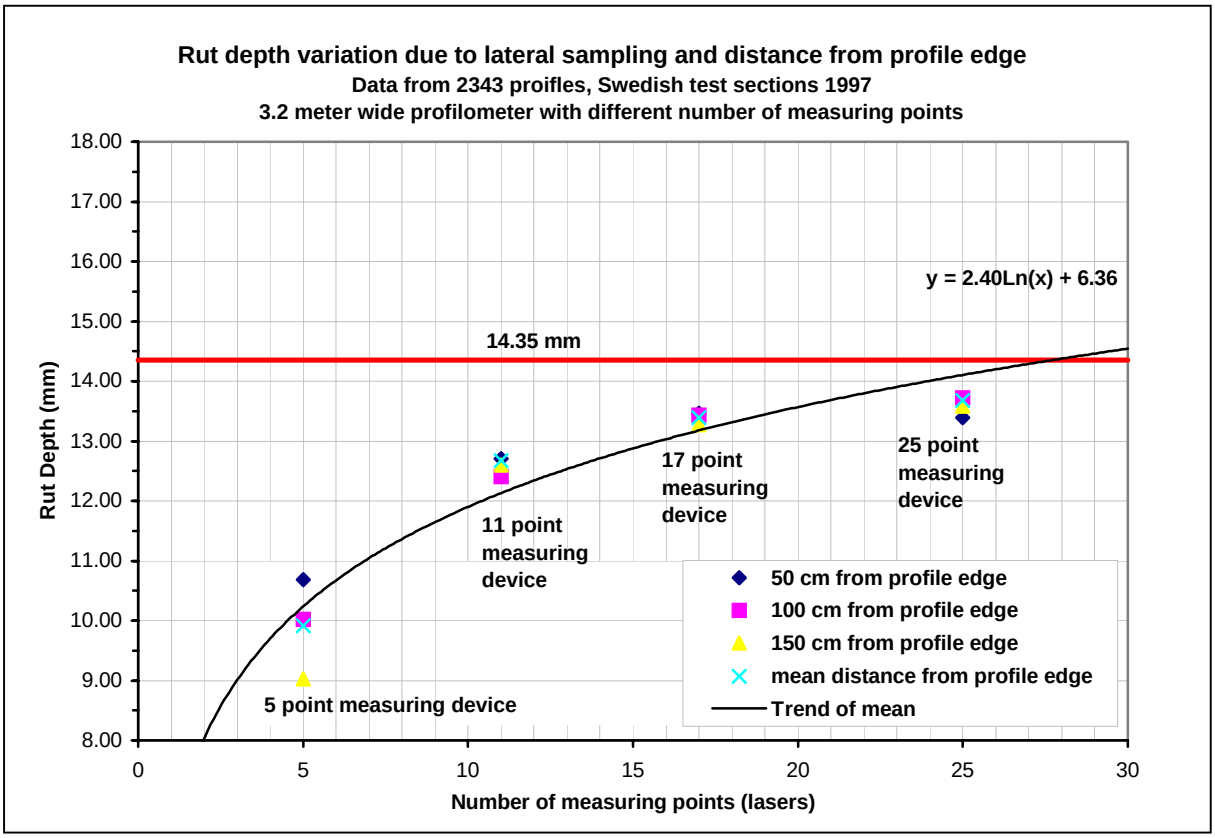

Figure 5.8. The effect of number of measurement points on obtained rut depth.

5.6 Effect on rut depth and rut area of different constant lateral positions for different measurement vehicle configurations.

In contrast to the previous simulations reported in this document the following show the effect on rut depth and rut area of constant lateral positions for different measurement configurations (see Table 5.8.). The presented results are averages over the seven transverse profiles shown in Annexe C.

Table 5.8. Measurement vehicle configurations

Measurement width (m)	Transverse sampling distance (m)
4,0	0,00; 0,10; 0,20; 0,25
3,0	0,00; 0,10; 0,20; 0,25
2,0	0,00; 0,10; 0,20; 0,25

5.6.1 Measurement width 4 m

As can be seen in Figures 5.9. – 5.12. the lateral position of the profilometer has very little influence on rut depths and rut areas for continuous sampling and for the transverse sampling interval of 0,1 m. Increasing the transverse sampling interval above 0,1 m will result in increased sensitivity to lateral position. Increasing the transverse sampling interval will generally reduce the recorded rut depth value and increase the recorded rut area. A deviation to the left will increase the recorded rut depth in the right wheel track and decrease the recorded rut depth in the left wheel track.

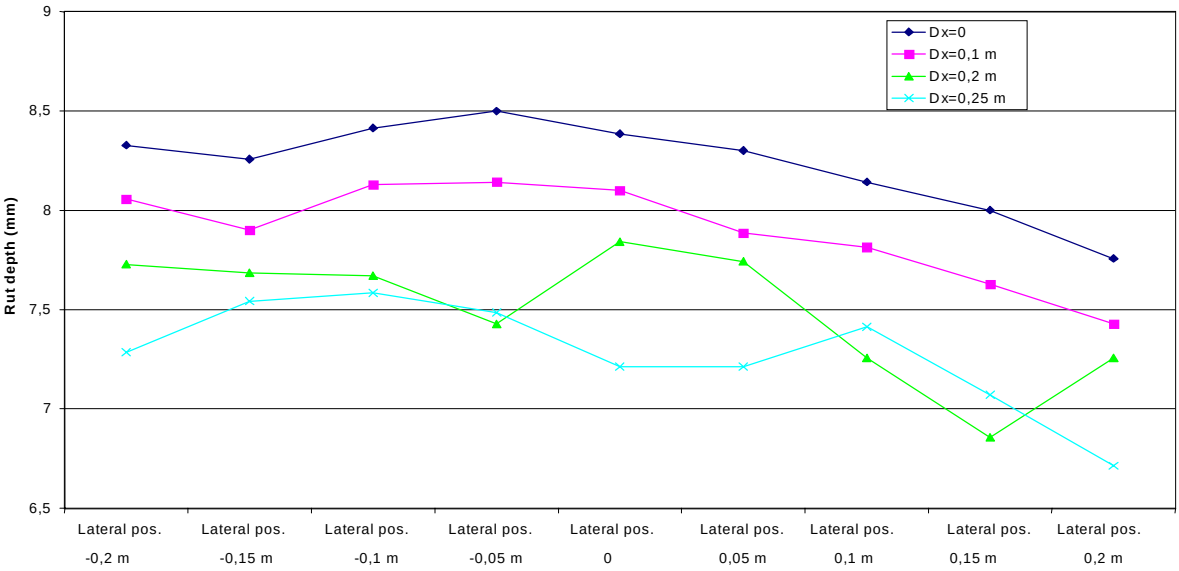

Figure 5.9. Effect of rut depth in right wheel track when varying lateral position and transverse sampling interval Dx. Negative lateral position values mean a deviation to the left. Measurement width 4m.

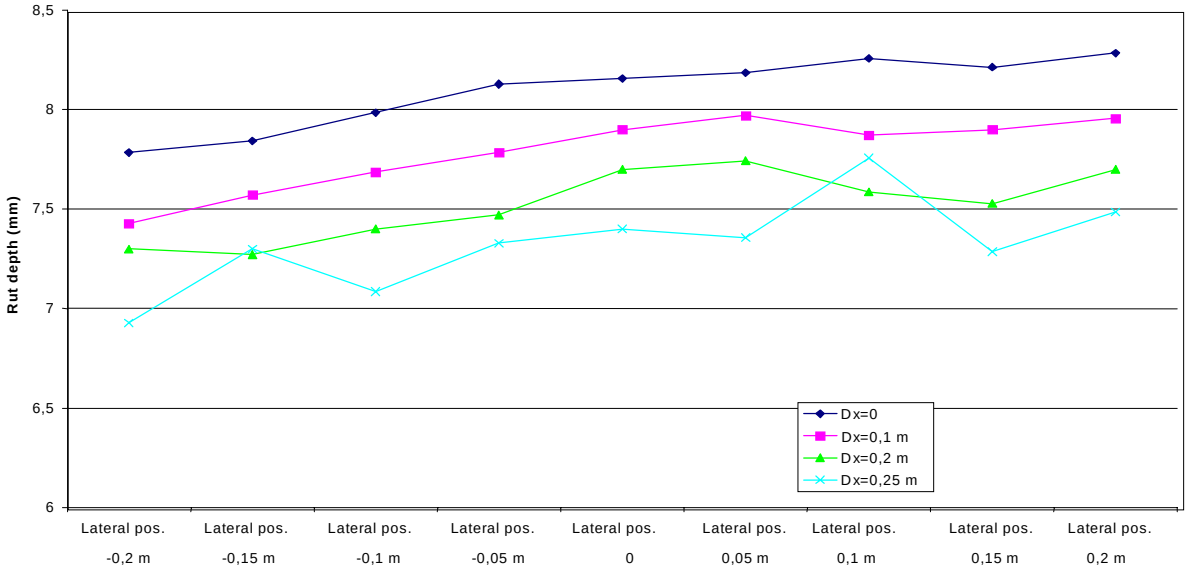

Figure 5.10. Effect of rut depth in left wheel track when varying lateral position and transverse sampling interval Dx. Negative lateral position values mean a deviation to the left. Measurement width 4m.

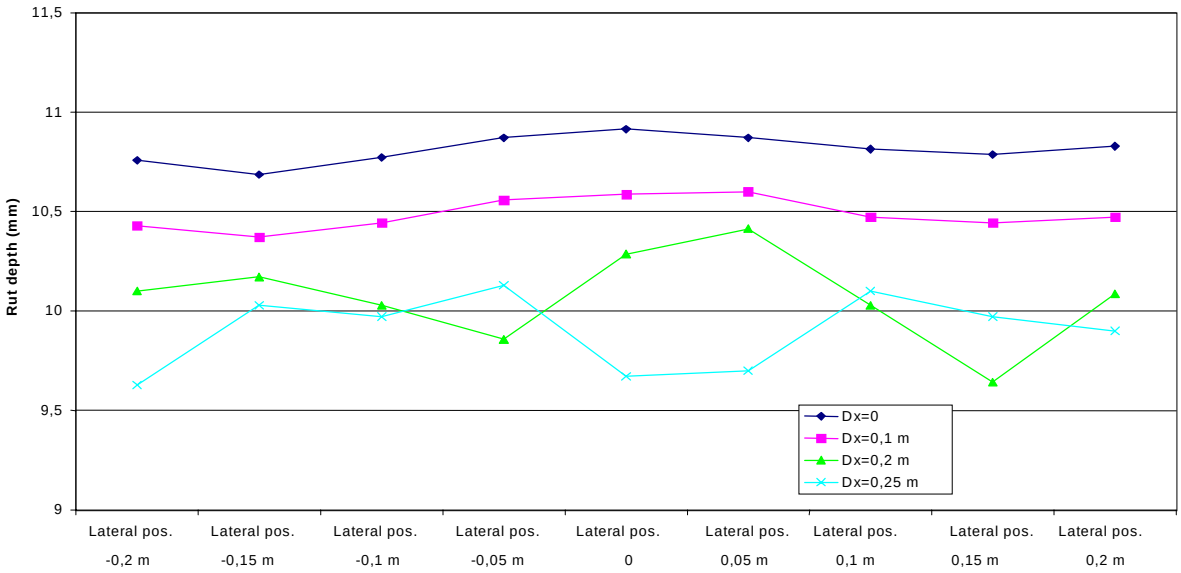

Figure 5.11. Effect on maximum rut depth when varying lateral position and transverse sampling interval Dx. Negative lateral position values mean a deviation to the left. Measurement width 4m.

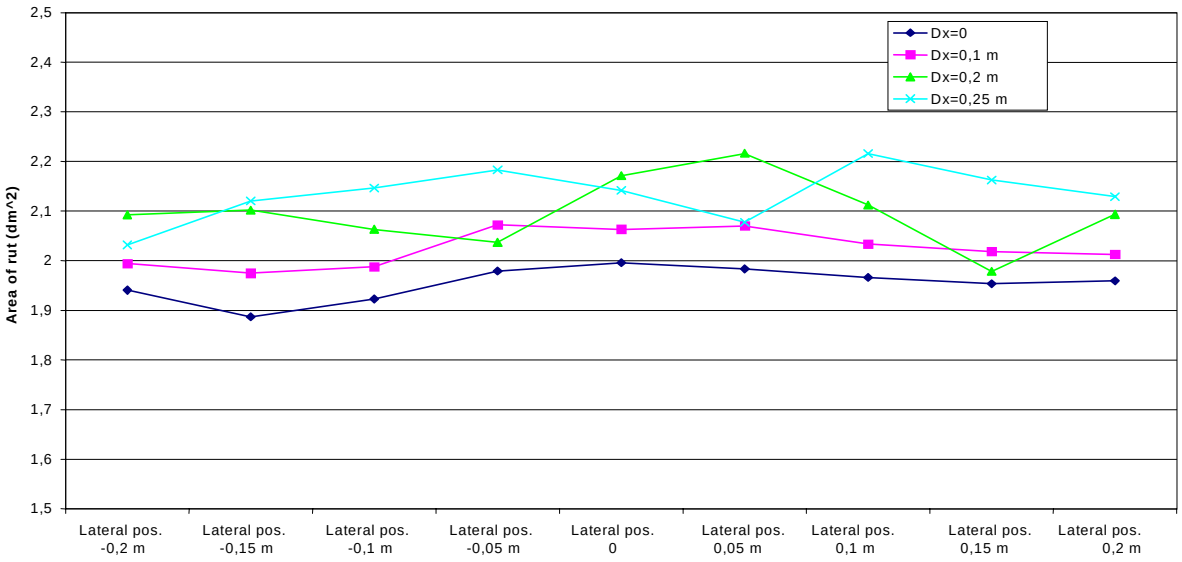

Figure 5.12. Effect on area of rut when varying lateral position and transverse sampling interval Dx. Negative lateral position values mean a deviation to the left. Measurement width 4m.

5.6.2 Measurement width 3 m

Decreasing the measurement width to 3 m will result in a somewhat increased sensitivity to lateral position for right and left rut but not for maximum rut depth and rut area (see Figure 5.13. – 5.14.). In general the recorded rut data are of lower magnitude but qualitatively the results are about the same as for the measurement width 4m. In contrast to the result for the 4m measurement, however, a deviation to the left will increase the recorded rut depth in both right and left wheel track.

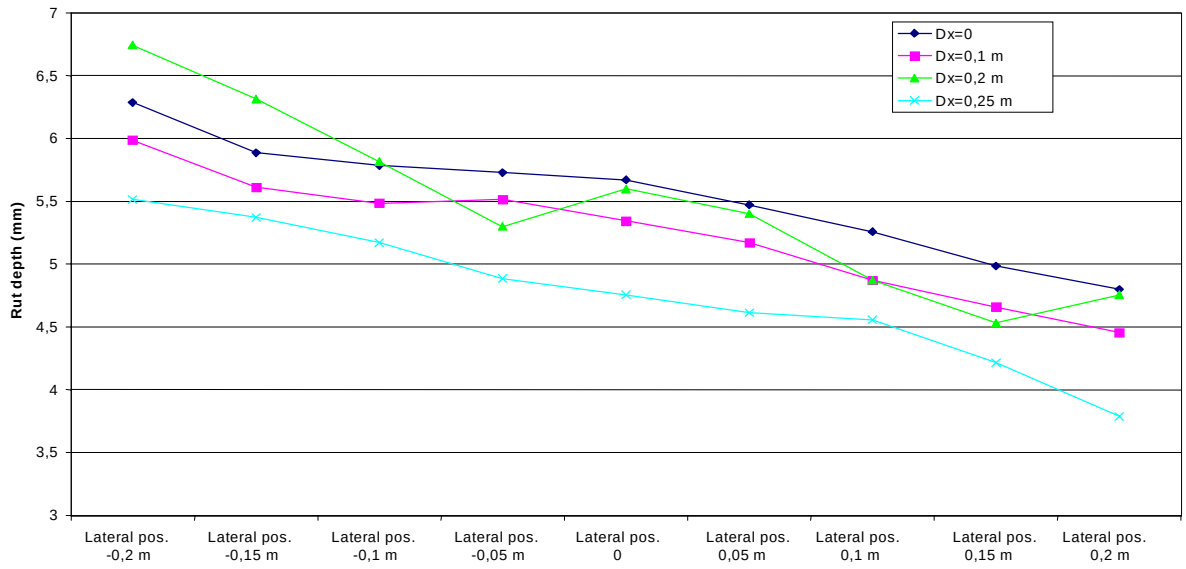

Figure 5.13. Effect on rut depth in right wheel track when varying lateral position and transverse sampling interval Dx. Negative lateral position values means a deviation to the left. Measurement width 3 m.

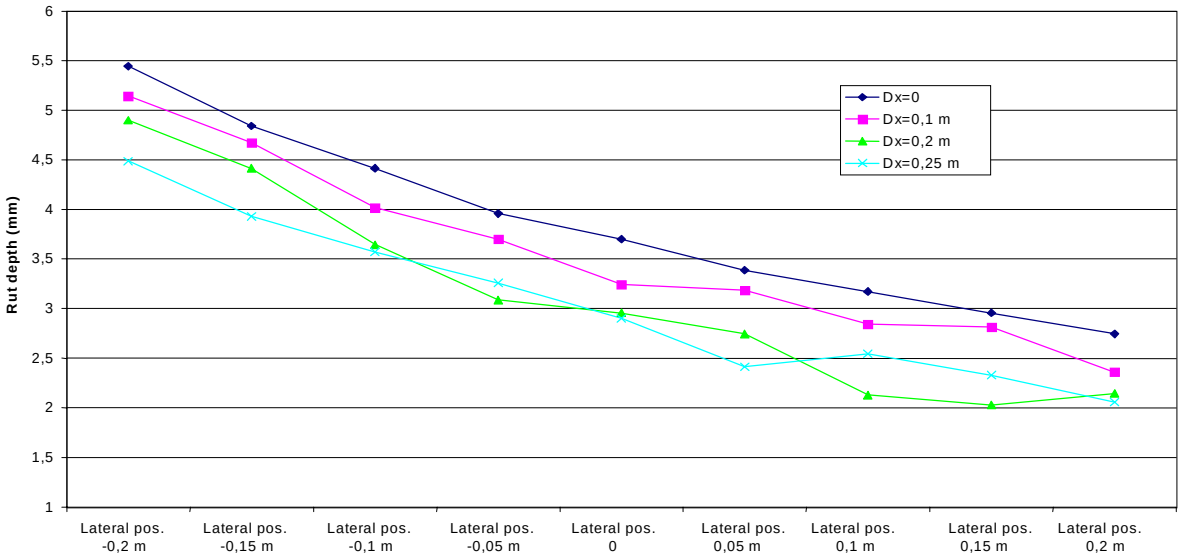

Figure 5.14. Effect on rut depth in left wheel track when varying lateral position and transverse sampling interval Dx. Negative lateral position values means a deviation to the left. Measurement width 3 m.

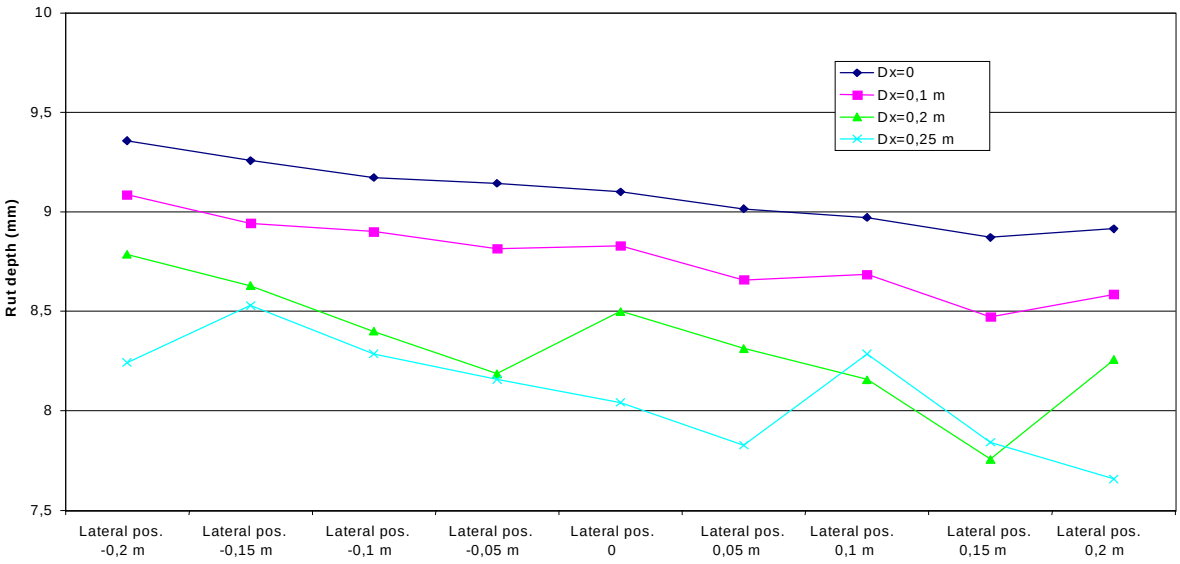

Figure 5.15. Effect on maximum rut depth when varying lateral position and transverse sampling interval Dx. Negative lateral position values means a deviation to the left. Measurement width 3 m.

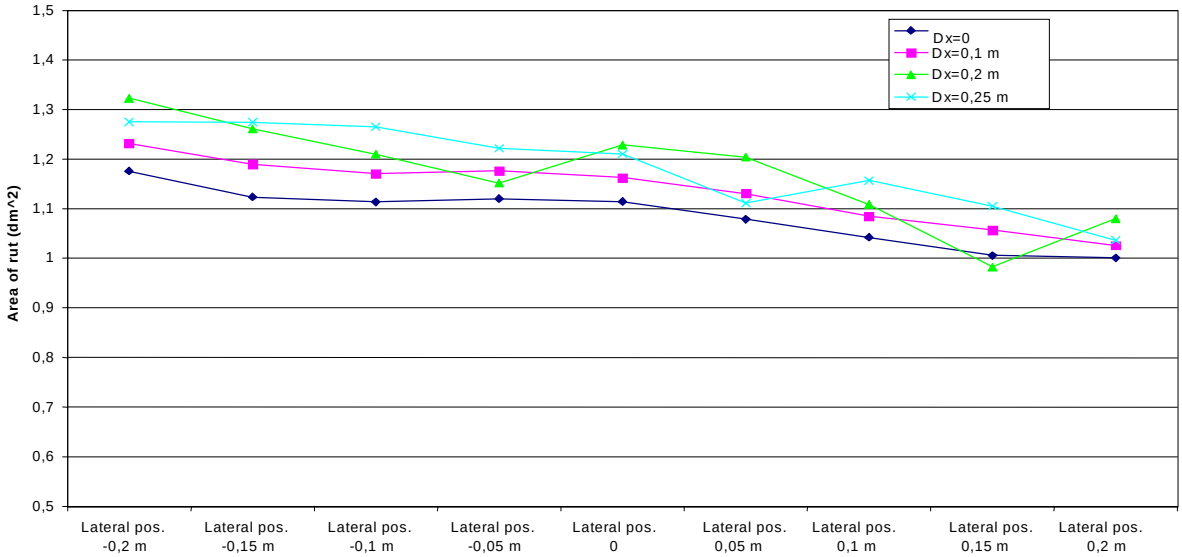

Figure 5.16. Effect on area of rut when varying lateral position and transverse sampling interval Dx. Negative lateral position values means a deviation to the left. Measurement width 3 m.

5.6.3 Measurement width 2 m

Figures 5.17. – 5.20. shows basically the same pattern as the previous figures; i.e. in general the recorded rut data are of lower magnitude than for the wider measurement widths. A deviation to the left will have the same effect as for the measurement width 4 m.

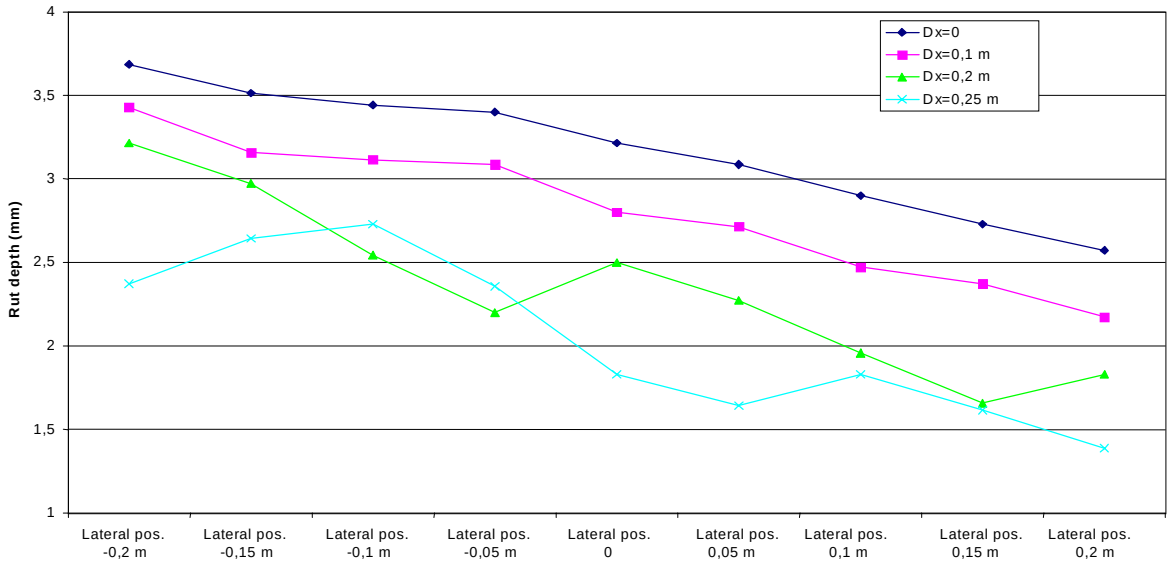

Figure 5.17. Effect on rut depth in right wheel track when varying lateral position and transverse sampling interval Dx. Negative lateral position values means a deviation to the left. Measurement width 2 m.

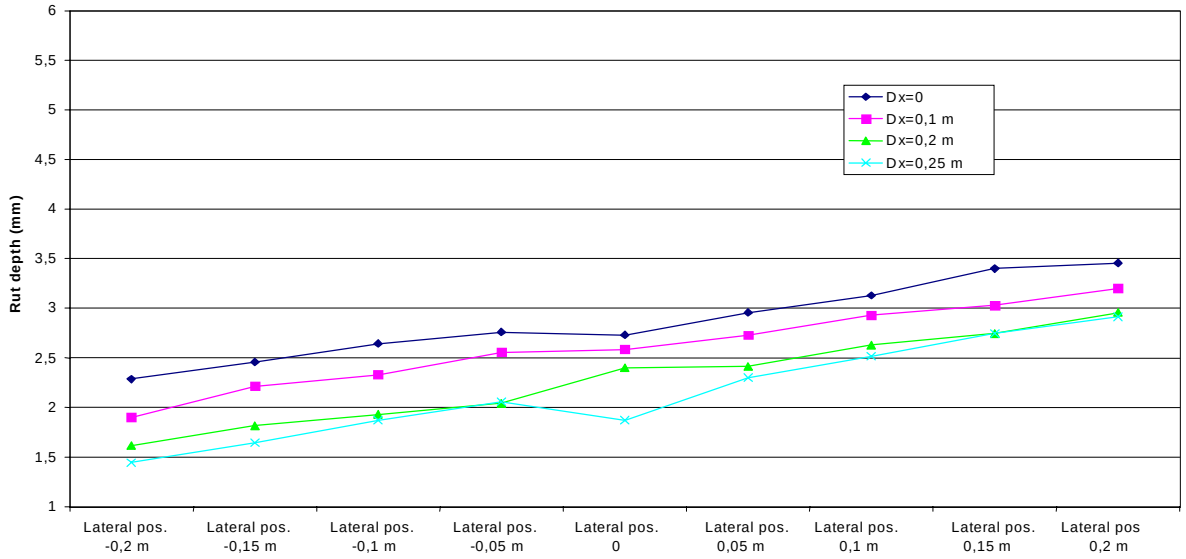

Figure 5.18. Effect on rut depth in left wheel track when varying lateral position and transverse sampling interval Dx. Negative lateral position values means a deviation to the left. Measurement width 2 m.

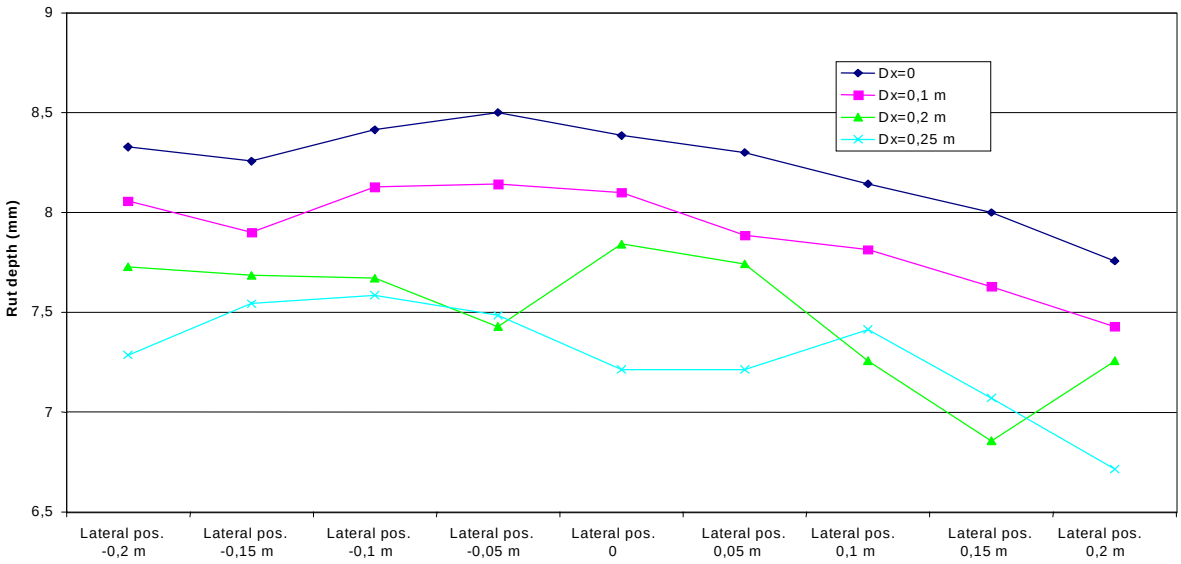

Figure 5.19. Effect on maximum rut depth when varying lateral position and transverse sampling interval Dx. Negative lateral position values means a deviation to the left. Measurement width 2 m.

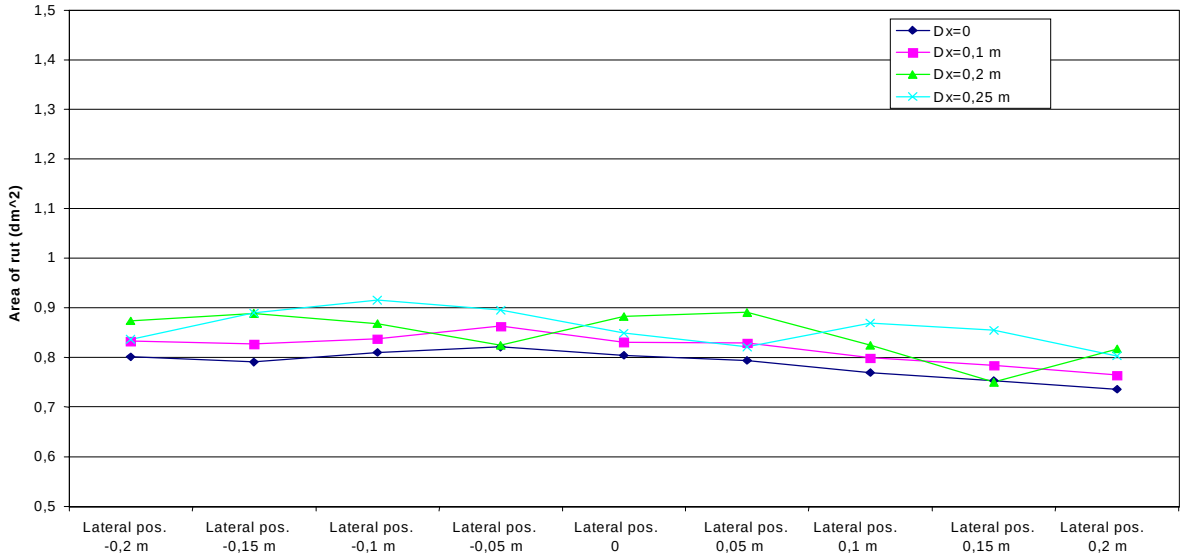

Figure 5.20. Effect on area of rut when varying lateral position and transverse sampling interval Dx. Negative lateral position values means a deviation to the left. Measurement width 2 m.

5.7 References

[1] DE WIT, L., KEMPKENS, E., SJÖGREN, L., DUCROS, D. M. (1999). The FILTER experiment. FEHRL Technical Note 1999/02, DWW, Delft, 1999.

6 The Purpose and Potential of Indices

6.1 What is required from indices?

6.1.1 Introduction

A road owner's aim is to design and maintain a pavement, such that it provides an acceptable level of serviceability to the road user, at a cost that represents value for money. The level of serviceability is defined in terms of the effect the pavement has upon its users. A pavement can affect its users in different ways - namely in terms of ride quality, safety levels, financial cost, and environmental impact. The term "road user" includes, but is not limited to, vehicle users, pedestrians, people that live or work near the road, and indeed the road owner themselves.

To achieve their aim, the owner requires information that meaningfully describes the serviceability of a pavement. If the owner is not providing an acceptable level of serviceability, then they must maintain the pavement. That is, the owner must improve the physical condition of the pavement, because deficiencies in the physical condition have caused an unacceptable reduction in the level of its serviceability. To maintain a pavement, the user must know what is wrong with it. Therefore, the owner also requires information that describes the physical condition of a pavement.

From the above discussion, it is clear that two distinct types of indices are desirable. Firstly indices that describe the effect of the road upon the road user, and secondly indices that describe the physical condition of the road. This information would allow road owners to determine when a pavement is not providing an acceptable level of serviceability, and to determine which physical qualities of the pavement are deficient. However, if the relationship between the physical condition of the pavement and the level of serviceability the pavement provides is known, then one of these type of indices is redundant. The components of a pavement's physical condition that influence the different aspects of its serviceability are known; however, the precise relationship between the two is generally not known.

In general, it is much easier to measure the physical condition of a pavement rather than the effect that it has upon its users.

Therefore, the aim of an index is to quantity the physical condition of a pavement, such that:

- The road owner can determine if the pavement is providing an acceptable level of serviceability.

- If the pavement were not providing an acceptable level of serviceability, the owner could identify the physical deficiency of the pavement.

This statement defines, in general terms, what is ideally required from an index.

6.1.2 Discussion

From the above statement, it is clear what is required from an index in general terms. However, the question, what is *specifically* required from an index of longitudinal profile, needs to be answered. These requirements can be summarised as the ability to:

- Quantify the general level of longitudinal evenness in required wavelength bands, e.g. short, medium and long wavelengths.

- Identify periodic irregularities.

- Identify and locate singular irregularities.

More explicitly, the following factors need to be considered:

- All current longitudinal indices treat the reporting length as if it were homogeneous. They therefore quantify the general level of unevenness for a section of pavement and singular irregularities cannot be explicitly identified. If the reporting length is short and the magnitude of any singular irregularity within the reporting length is very high compared with the background level, then it will have an effect on the index. This effect will be small, depending on the ratio of the point separation to the reporting length.

- Methods that make use of power spectral density allow the identification of periodic irregularities in the surface. Accurate estimates of spectral density estimate require long sample lengths, and give no location information to help identify defects. Power spectral density indices are much more difficult to explain and use than conventional indices.

- There is a need for simple indices capable of identifying large single surface irregularities. It is not possible for an averaging index, such as those in current use, to achieve this objective and therefore alternative forms of index will need to be formulated for these purposes.

- The presence of large singular irregularities could be identified in a given reporting length by considering the range of values, the standard deviation of the averaged values, or the ratio of the maximum value to the mean. However one of the more interesting recent developments in signal processing is a technique known as wavelet analysis [1]. With this technique it is possible to identify singular and periodic irregularities in a pavement surface with one consistent mathematical approach.

- A periodic function will have a large effect on the waveband containing it compared to other wavebands with a range of wavelengths outside that of the periodic function.

- At the network level, it is possible to show the proportion of the network with indices above an acceptable threshold level. Distributions can be used to aid decisions on maintenance budget allocation and trends with time can show the effectiveness of maintenance policies.

- It is also possible to use indices to identify individual lengths of a network that are in need of maintenance. In this case, the reporting length must be sufficiently short to be able to accurately identify lengths of road surface in need of treatment.

6.2 References

[1] DE PONT, J. J. and SCOTT, A (1999). Beyond road roughness: interpreting road profile data. Road & Transport Research, Volume 8, Issue 1, March 1999, 12-28.

7 General Conclusions

This report describes a theoretical study of the current European profile indices, and their response to road surfaces. The possible effect of measurement errors has also been investigated. The objective of the work is to show how each index responds to the measurement of road profiles, highlighting similarities and differences. No judgement is made on the relative merits of the indices, and this is not discussed, but the data will provide a reliable and consensual basis to permit the eventual drafting of European testing standards for measuring the longitudinal and transverse evenness of roads.

This study has shown both the differing and the similar wavelength responses of the various longitudinal profile indices currently used in Europe. The indices investigated can be divided into four different groups, each with a similar, but not identical, form of response:

- The indices IRI, PI and its derivative RN
- Variances or standard deviations from moving averages and the CP indices
- Short, medium and long wavelength energy indices and the corresponding NBO indices
- The indices, G(No), AUN and w, all based on power spectral density analysis.

The study has also highlighted which measurement errors and operating conditions are the most significant for both longitudinal and transverse profile indices. It has highlighted that, in general, longitudinal indices that attenuate both high and low wavelengths are not only better at isolating wavelengths of interest but also are less sensitive to measurement errors.

All current European longitudinal indices treat the reporting length as if it was homogeneous. Currently, no routine longitudinal indices explicitly identify singular irregularities. Such indices could, in addition to the current indices, provide the highway engineer and user with a more useful and complete picture of the condition of the road pavement.

A study of transverse profile indices has shown that although increased sampling density and measurement width can increase index accuracy, there are limits beyond which the improvements achieved are small. For data collected on Swedish roads, theoretical studies show that increasing the measurement width from 3.6m to 4.0m would only improve rut depth measurement accuracy by an estimated five per cent. It is also apparent that increasing the number of measurement points from 11 to 25 would make only 2mm difference to the maximum rut depth measurement. Further analysis suggests that lateral wander of the survey vehicle in the traffic lane has negligible effect on the measurement results.

Annexe A: List of Longitudinal Indices

Table A1. Longitudinal Indices reported in the FILTER experiment.

Code	Index	Definition in §2.2.
A	IRI (International Roughness Index)	Yes
B	HRI (Half-car Roughness Index)	Yes
C	3 m Variance as used in UK	Yes
D	10m Variance as used in UK	Yes
E	30m Variance as used in UK	Yes
F	G(n_0) and w as defined in ISO 8608 Standard	Yes
G	CP 2.5 coefficient as used in Belgium	Yes
H	CP 10 coefficient as used in Belgium	Yes
I	CP 40 coefficient as used in Belgium	Yes
J	Short Wavelength NBO as used in France	Yes
K	Medium Wavelength NBO as used in France	Yes
L	Long Wavelength NBO as used in France	Yes
M	5 meters straight edge	No
N	Ride Number	Yes
P	AUN as used in Germany	Yes
Q	Std. Deviation from 3 m, moving average	Yes
R	Std. Deviation from 10 m, moving average	Yes
S	Std. Deviation from 30 m, moving average	Yes
T	Periodic unevenness height	No
U	Periodic unevenness wavelength	No
V	C as used in Czech republic	No
W	Short wavelength energy as used in France	Yes
X	Medium wavelength energy as used in France	Yes
Y	Long wavelength energy as used in France	Yes
Z	Deviation for 3 m straight edge as used in Russia	No
1	RMS value for waveband .5 - 2.5 m	No
2	RMS value for waveband 2.5 - 10 m	No
3	RMS value for waveband 10 - 50 in	No
4	Slope Variance	No

Annexe B: Wavelength Response of Longitudinal Indices

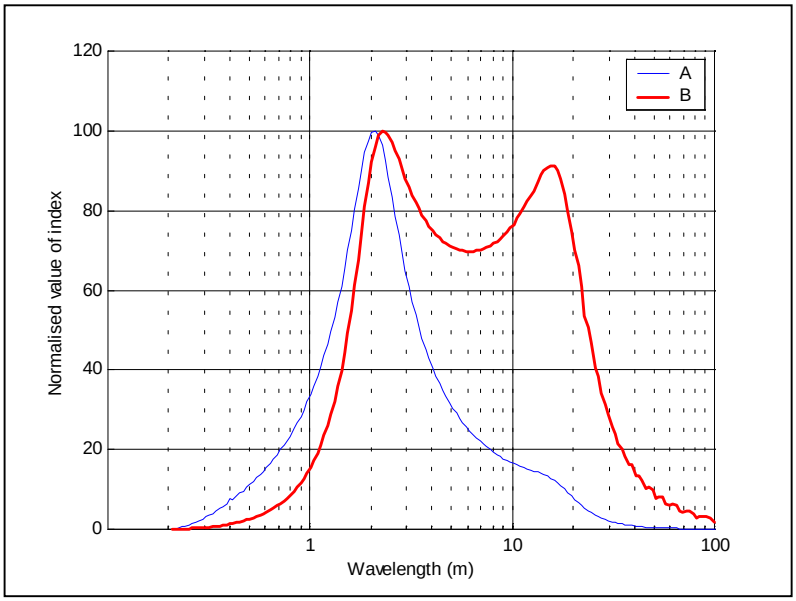

Series A is the wavelength response of IRI. The input profile has a constant amplitude, i.e.
$y = A \sin(2\pi nx + \varphi)$
A = constant
$\varphi = 0$

Series B is the weighted response of IRI. The amplitude of input profile increases with wavelength. It is designed to be typical of the wavelength-amplitude relationship that would be expected on a paved road. The input profile is of the form:
$y = A \sin(2\pi nx + \phi)$
$A = A_0 n^{-w/2}$
w=2

The y-axis is a relative scale and is arbitrary. The plots have been scaled to aid comparison. The input profile point separation is 0.1m. The wavelength is incremented in 1/18th octaves.

Figure B1. The Response of IRI.

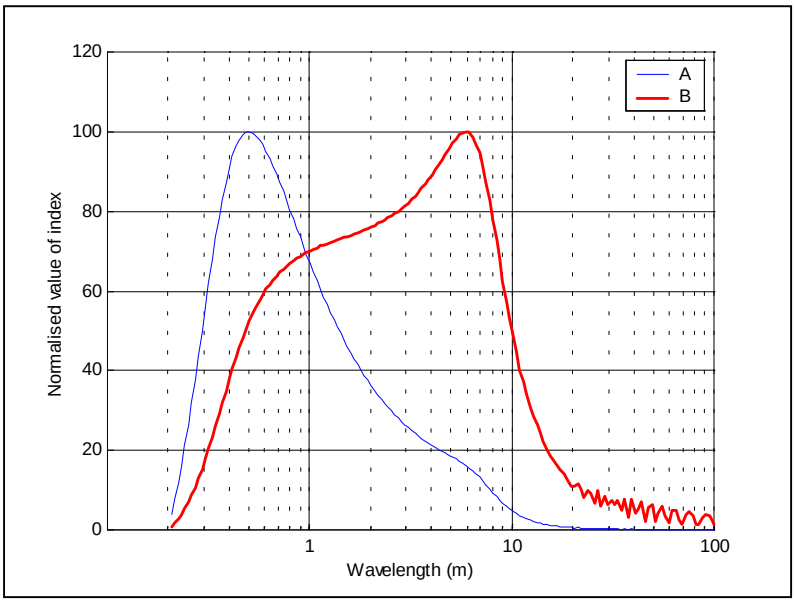

Series A is the wavelength response of PI. The input profile has a constant amplitude, i.e.
$y = A \sin(2\pi nx + \varphi)$
A = constant
$\varphi = 0$

Series B is the weighted response of PI. The amplitude of input profile increases with wavelength. It is designed to be typical of the wavelength-amplitude relationship that would be expected on a paved road. The input profile is of the form:
$y = A \sin(2\pi nx + \phi)$
$A = A_0 n^{-w/2}$
w=2

The y-axis is a relative scale and is arbitrary. The plots have been scaled to aid comparison. The input profile point separation is 0.1m. The wavelength is incremented in 1/18th octaves.

Figure B2. The Response of PI

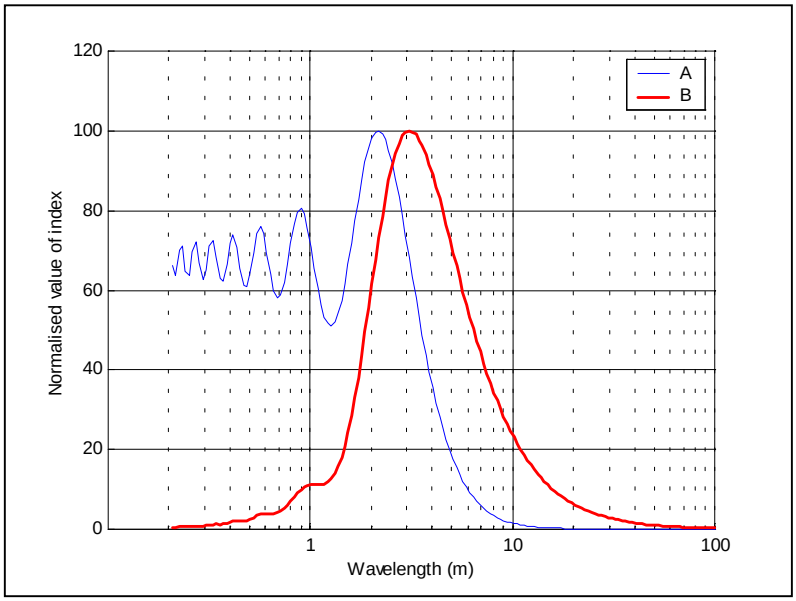

Series A is the wavelength response of 3m Variance. The input profile has a constant amplitude, i.e.
$y = A \sin(2\pi nx + \varphi)$
A = constant
$\varphi = 0$

Series B is the weighted response of 3m Variance. The amplitude of input profile increases with wavelength. It is designed to be typical of the wavelength-amplitude relationship that would be expected on a paved road. The input profile is of the form:
$y = A \sin(2\pi nx + \phi)$
$A = A_0 n^{-w/2}$
w=2

The y-axis is a relative scale and is arbitrary. The plots have been scaled to aid comparison. The input profile point separation is 0.1m. The wavelength is incremented in 1/18th octaves.

Figure B3. The Response of 3m Variance.

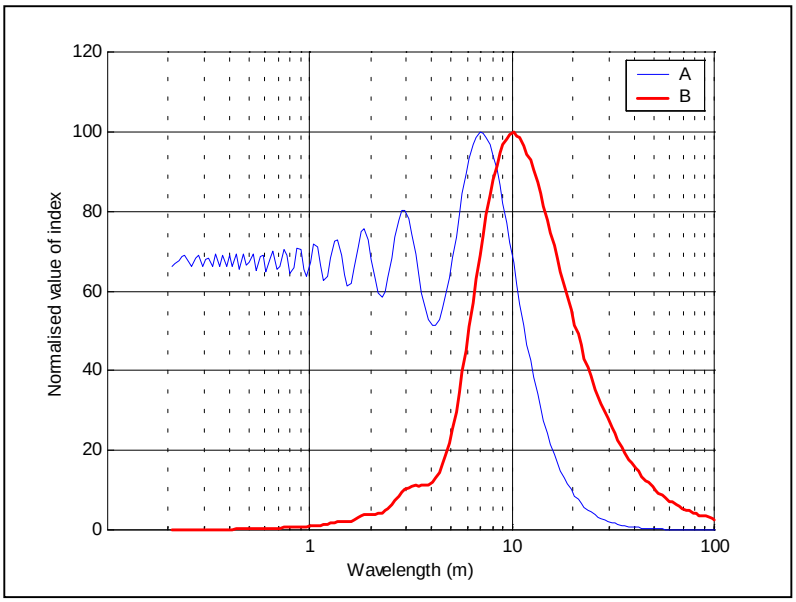

Series A is the wavelength response of 10m Variance. The input profile has a constant amplitude, i.e.
$y = A \sin(2\pi nx + \varphi)$
A = constant
$\varphi = 0$

Series B is the weighted response of 10m Variance. The amplitude of input profile increases with wavelength. It is designed to be typical of the wavelength-amplitude relationship that would be expected on a paved road. The input profile is of the form:
$y = A \sin(2\pi nx + \phi)$
$A = A_0 n^{-w/2}$
w=2

The y-axis is a relative scale and is arbitrary. The plots have been scaled to aid comparison. The input profile point separation is 0.1m. The wavelength is incremented in 1/18th octaves.

Figure B4. The Response of 10m Variance.

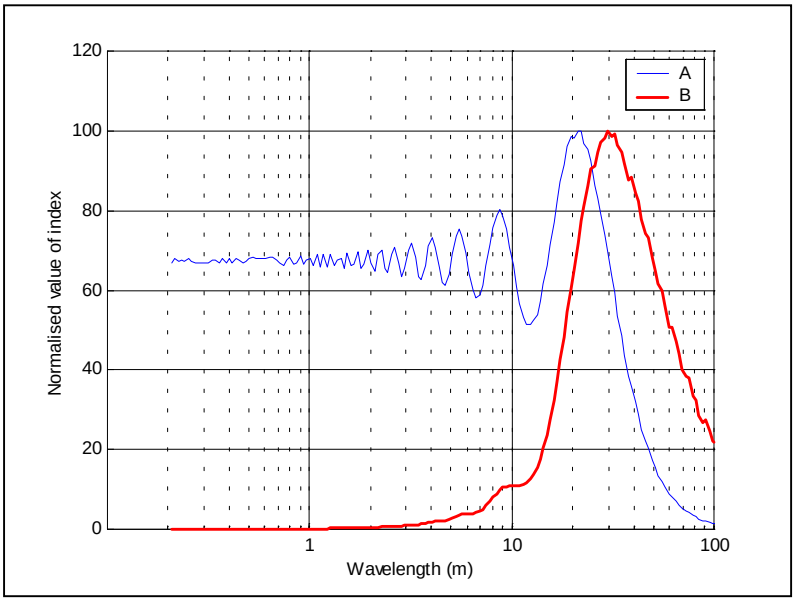

Series A is the wavelength response of 30m Variance. The input profile has a constant amplitude, i.e.
$y = A \sin(2\pi nx + \varphi)$
A = constant
$\varphi = 0$

Series B is the weighted response of 30m Variance. The amplitude of input profile increases with wavelength. It is designed to be typical of the wavelength-amplitude relationship that would be expected on a paved road. The input profile is of the form:
$y = A \sin(2\pi nx + \phi)$
$A = A_0 n^{-w/2}$
w=2

The y-axis is a relative scale and is arbitrary. The plots have been scaled to aid comparison. The input profile point separation is 0.1m. The wavelength is incremented in 1/18th octaves.

Figure B5. The Response of 30m Variance.

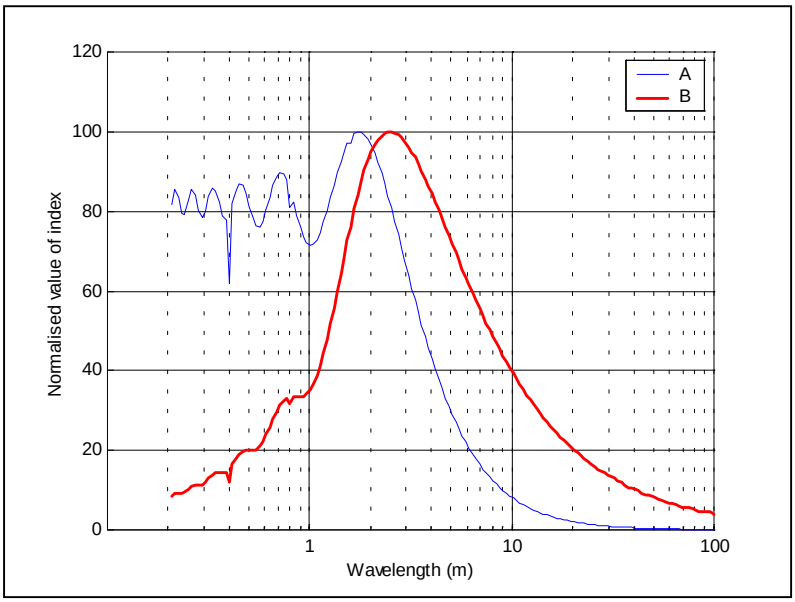

Series A is the wavelength response of CP 2.5. The input profile has a constant amplitude, i.e.
$y = A \sin(2\pi nx + \varphi)$
A = constant
$\varphi = 0$

Series B is the weighted response of CP 2.5. The amplitude of input profile increases with wavelength. It is designed to be typical of the wavelength-amplitude relationship that would be expected on a paved road. The input profile is of the form:
$y = A \sin(2\pi nx + \phi)$
$A = A_0 n^{-w/2}$
w=2

The y-axis is a relative scale and is arbitrary. The plots have been scaled to aid comparison. The input profile point separation is 0.1m. The wavelength is incremented in 1/18th octaves.

Figure B6. The Response of CP 2.5.

The anomaly in series A at 0.4m is a function of the acquisition interval. It would have a negligible effect upon the value of the index because the amplitude of unevenness at this wavelength is relatively small – see series B.

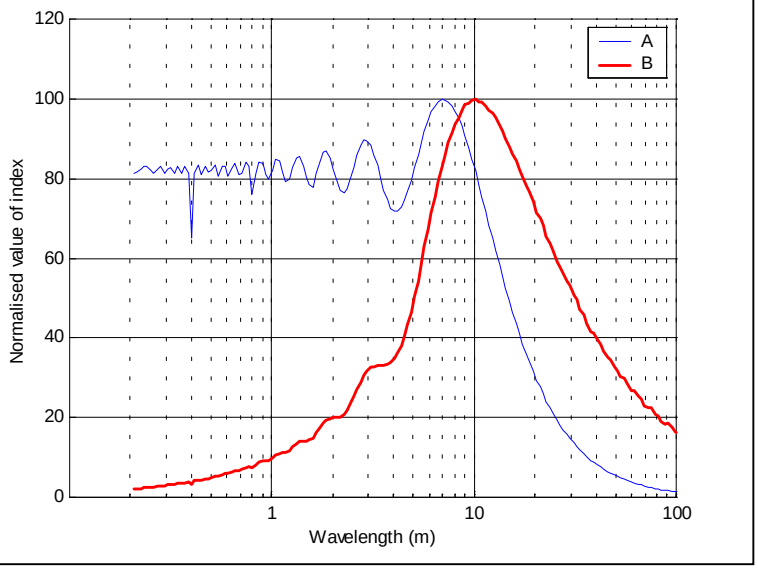

Series A is the wavelength response of CP 10. The input profile has a constant amplitude, i.e.
$y = A \sin(2\pi nx + \varphi)$
A = constant
$\varphi = 0$

Series B is the weighted response of CP 10. The amplitude of input profile increases with wavelength. It is designed to be typical of the wavelength-amplitude relationship that would be expected on a paved road. The input profile is of the form:
$y = A \sin(2\pi nx + \phi)$
$A = A_0 n^{-w/2}$
w=2

The y-axis is a relative scale and is arbitrary. The plots have been scaled to aid comparison. The input profile point separation is 0.1m. The wavelength is incremented in 1/18th octaves.

Figure B7. The Response of CP 10.

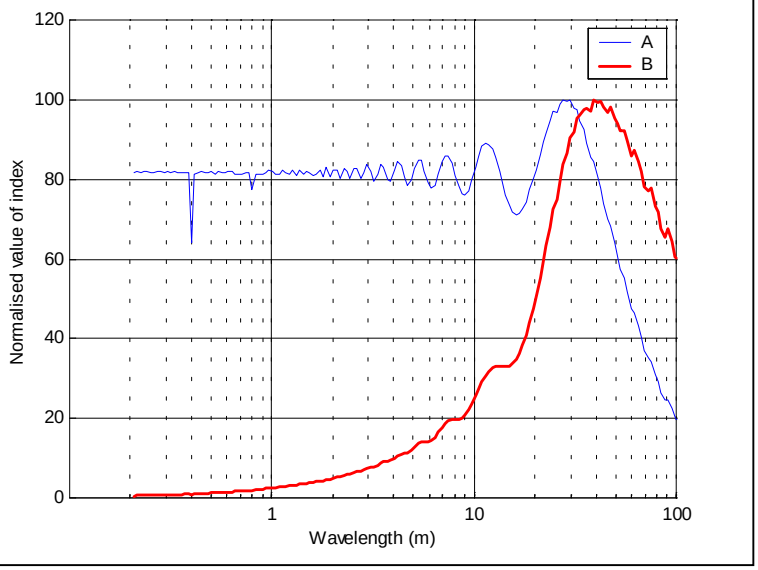

Series A is the wavelength response of CP 40. The input profile has a constant amplitude, i.e.
$y = A \sin(2\pi nx + \varphi)$
A = constant
$\varphi = 0$

Series B is the weighted response of CP 40. The amplitude of input profile increases with wavelength. It is designed to be typical of the wavelength-amplitude relationship that would be expected on a paved road. The input profile is of the form:
$y = A \sin(2\pi nx + \phi)$
$A = A_0 n^{-w/2}$
w=2

The y-axis is a relative scale and is arbitrary. The plots have been scaled to aid comparison. The input profile point separation is 0.1m. The wavelength is incremented in 1/18th octaves.

Figure B8. The Response of CP 40.

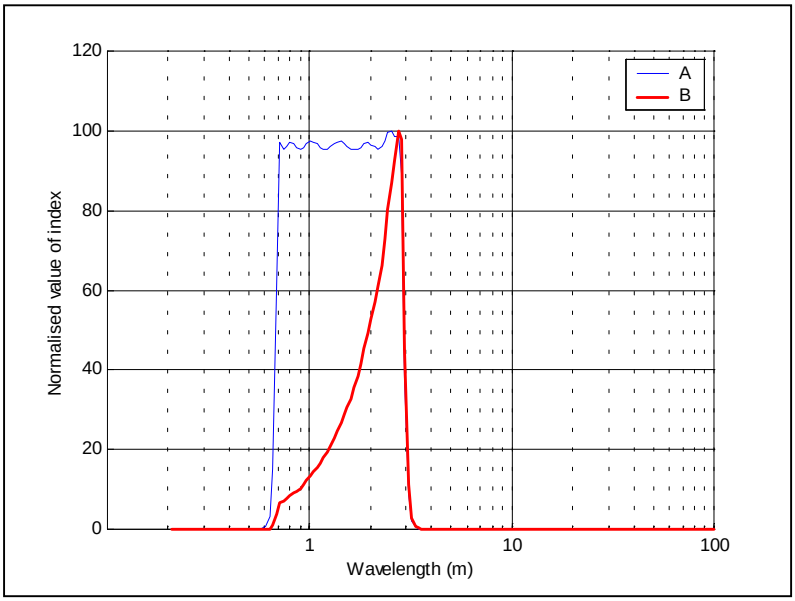

Series A is the wavelength response of SWE. The input profile has a constant amplitude, i.e.
$y = A \sin(2\pi nx + \varphi)$
A = constant
$\varphi = 0$

Series B is the weighted response of SWE. The amplitude of input profile increases with wavelength. It is designed to be typical of the wavelength-amplitude relationship that would be expected on a paved road. The input profile is of the form:
$y = A \sin(2\pi nx + \phi)$
$A = A_0 n^{-w/2}$
w=2

The y-axis is a relative scale and is arbitrary. The plots have been scaled to aid comparison. The input profile point separation is 0.05m. The wavelength is incremented in 1/18th octaves.

Figure B9. The Response of Short Wavelength Energy.

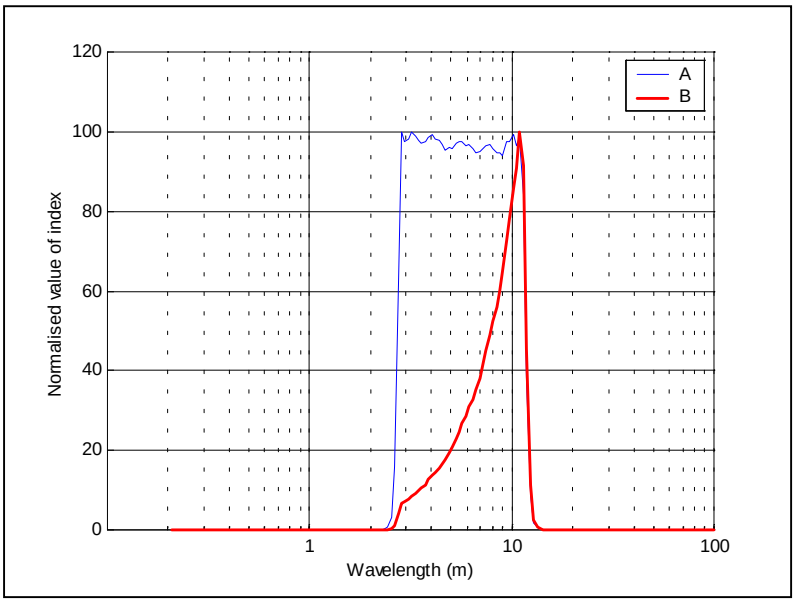

Series A is the wavelength response of MWE. The input profile has a constant amplitude, i.e.
$y = A \sin(2\pi nx + \varphi)$
A = constant
$\varphi = 0$

Series B is the weighted response of MWE. The amplitude of input profile increases with wavelength. It is designed to be typical of the wavelength-amplitude relationship that would be expected on a paved road. The input profile is of the form:
$y = A \sin(2\pi nx + \phi)$
$A = A_0 n^{-w/2}$
w=2

The y-axis is a relative scale and is arbitrary. The plots have been scaled to aid comparison. The input profile point separation is 0.05m. The wavelength is incremented in 1/18th octaves.

Figure B10. The Response of Medium Wavelength Energy.

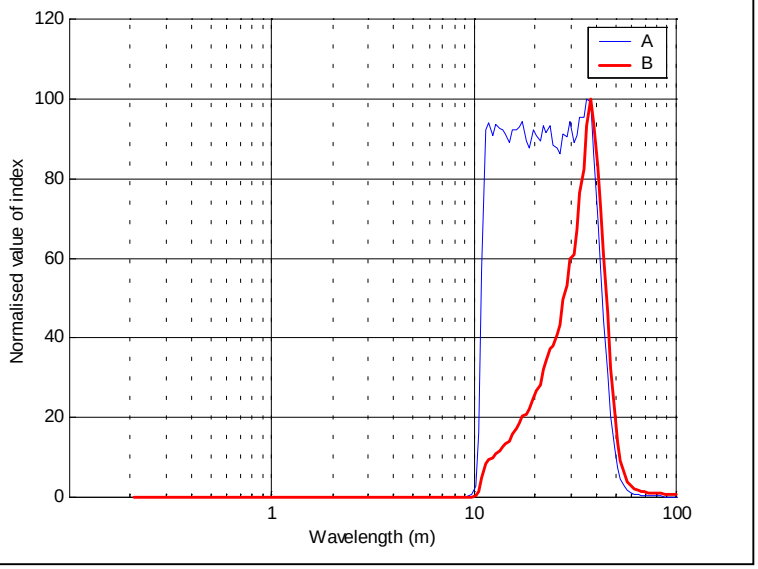

Series A is the wavelength response of LWE. The input profile has a constant amplitude, i.e.
$y = A \sin(2\pi nx + \varphi)$
A = constant
$\varphi = 0$

Series B is the weighted response of LWE. The amplitude of input profile increases with wavelength. It is designed to be typical of the wavelength-amplitude relationship that would be expected on a paved road. The input profile is of the form:
$y = A \sin(2\pi nx + \phi)$
$A = A_0 n^{-w/2}$
w=2

The y-axis is a relative scale and is arbitrary. The plots have been scaled to aid comparison. The input profile point separation is 0.05m. The wavelength is incremented in 1/18th octaves.

Figure B11. The Response of Long Wavelength Energy.

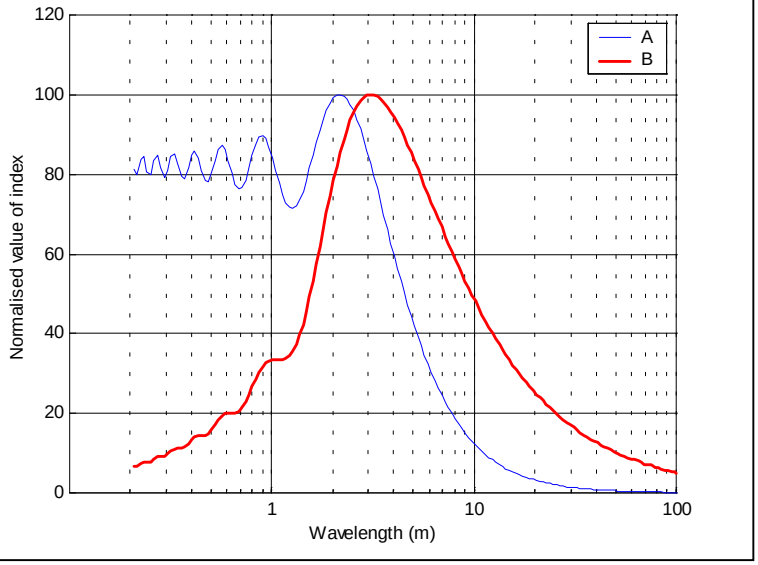

Series A is the wavelength response of Std Dev from a 3m MA. The input profile has a constant amplitude, i.e.
$y = A \sin(2\pi nx + \varphi)$
A = constant
$\varphi = 0$

Series B is the weighted response of Std Dev from a 3m MA. The amplitude of input profile increases with wavelength. It is designed to be typical of the wavelength-amplitude relationship that would be expected on a paved road. The input profile is of the form:
$y = A \sin(2\pi nx + \phi)$
$A = A_0 n^{-w/2}$
w=2
The y-axis is a relative scale and is arbitrary. The plots have been scaled to aid comparison. The input profile point separation is 0.1m. The wavelength is incremented in 1/18th octaves.

Figure B12. The Response of the Standard Deviation from a 3m Moving Average.

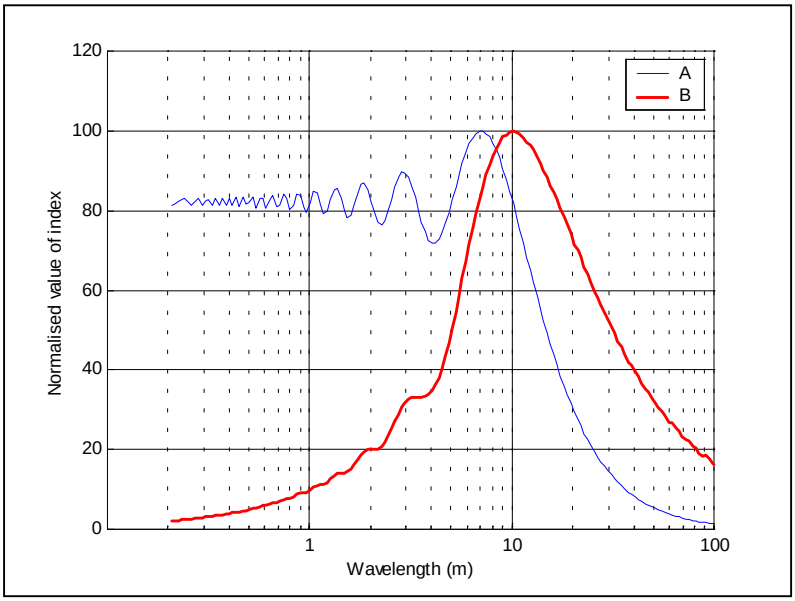

Series A is the wavelength response of Std Dev from a 10m MA. The input profile has a constant amplitude, i.e.
$y = A \sin(2\pi nx + \varphi)$
A = constant
$\varphi = 0$

Series B is the weighted response of Std Dev from a 10m MA. The amplitude of input profile increases with wavelength. It is designed to be typical of the wavelength-amplitude relationship that would be expected on a paved road. The input profile is of the form:
$y = A \sin(2\pi nx + \phi)$
$A = A_0 n^{-w/2}$
w=2
The y-axis is a relative scale and is arbitrary. The plots have been scaled to aid comparison. The input profile point separation is 0.1m. The wavelength is incremented in 1/18th octaves.

B13. The Response of the Standard Deviation from a 10m Moving Average.

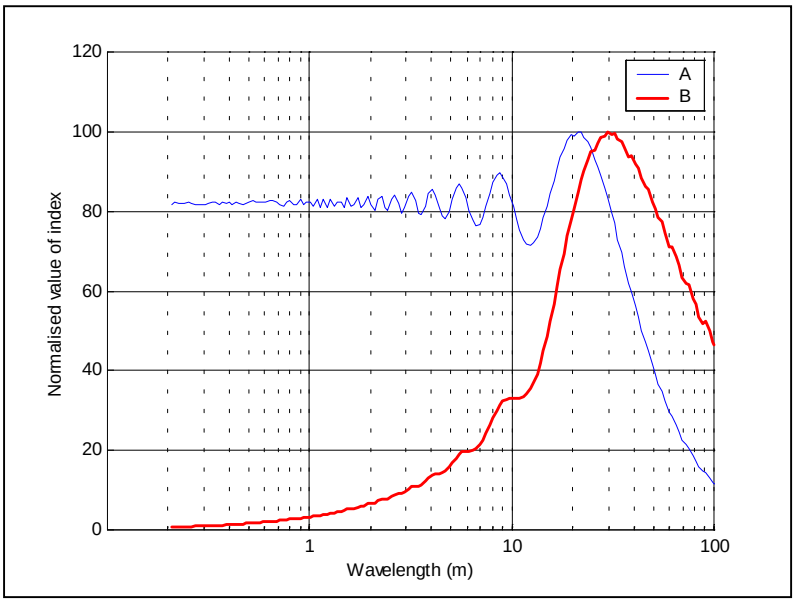

Series A is the wavelength response of Std Dev from a 30m MA. The input profile has a constant amplitude, i.e.
$y = A \sin(2\pi nx + \varphi)$
A = constant
$\varphi = 0$

Series B is the weighted response of Std Dev from a 30m MA. The amplitude of input profile increases with wavelength. It is designed to be typical of the wavelength-amplitude relationship that would be expected on a paved road. The input profile is of the form:
$y = A \sin(2\pi nx + \phi)$
$A = A_0 n^{-w/2}$
w=2
The y-axis is a relative scale and is arbitrary. The plots have been scaled to aid comparison. The input profile point separation is 0.1m. The wavelength is incremented in 1/18th octaves.

B14. The Response of the Standard Deviation from a 30m Moving Average.

Annexe C: The Influence of Discrete Measurement Interval on Longitudinal Indices

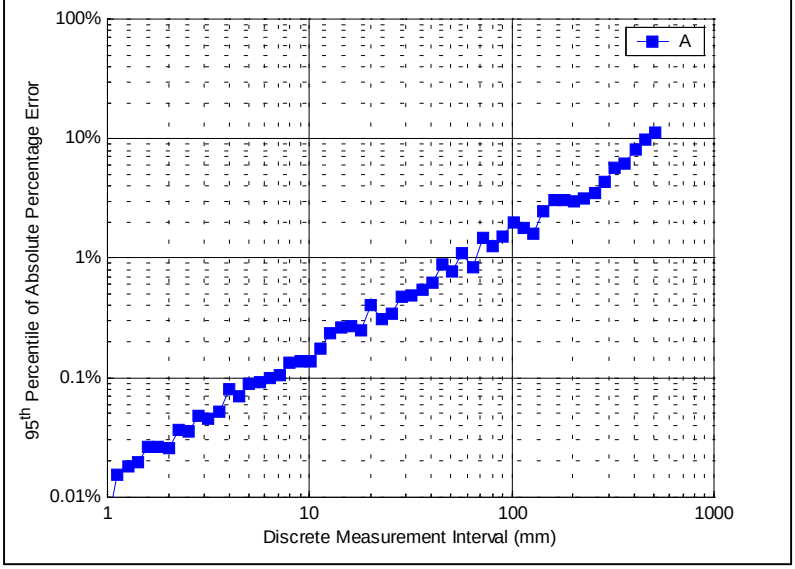

Series A is the Error in IRI resulting from different discrete Measurement Intervals.
A detailed artificial profile, which is indistinguishable from a real profile, was created with a measurement interval of approximately 0.520mm. The evenness of the profile corresponded to the centre of ISO 8608 class A. From this, a reference value of the index was calculated. The detailed profile was then resampled, using a cubic spline interpolation, at measurement intervals between 1.0mm and 512mm. The absolute percentage error was then calculated.

$E_{\%} = | (V - V_{Ref}) / V_{Ref} | * 100$

This was repeated for 300 different artificial profiles. The error is shown in terms of the 95th percentile of the distribution of absolute percentage error

Figure C1. The Influence of Discrete Measurement Interval on IRI.

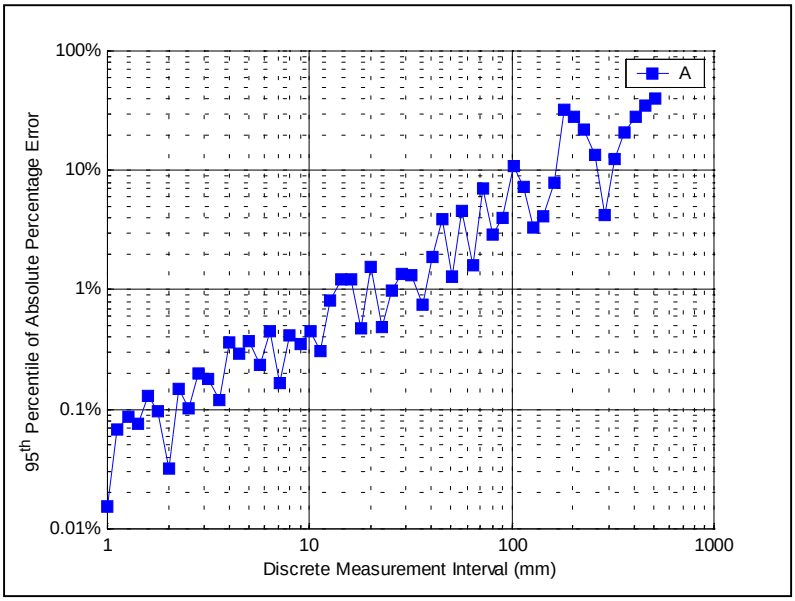

Series A is the Error in PI resulting from different discrete Measurement Intervals.
A detailed artificial profile, which is indistinguishable from a real profile, was created with a measurement interval of approximately 0.520mm. The evenness of the profile corresponded to the centre of ISO 8608 class A. From this, a reference value of the index was calculated. The detailed profile was then resampled, using a cubic spline interpolation, at measurement intervals between 1.0mm and 512mm. The absolute percentage error was then calculated.

$E_{\%} = | (V - V_{Ref}) / V_{Ref} | * 100$

This was repeated for 300 different artificial profiles. The error is shown in terms of the 95th percentile of the distribution of absolute percentage error

Figure C2. The Influence of Discrete Measurement Interval on PI.

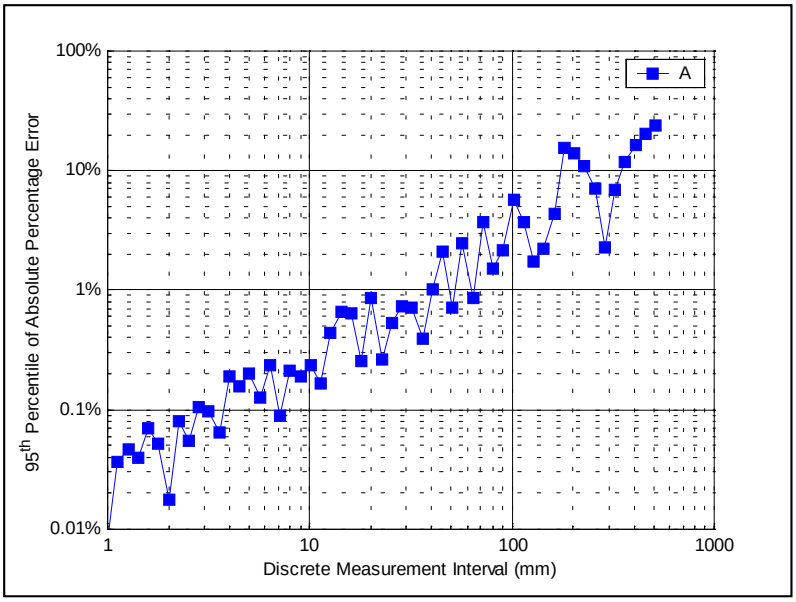

Series A is the Error in RN resulting from different discrete Measurement Intervals.
A detailed artificial profile, which is indistinguishable from a real profile, was created with a measurement interval of approximately 0.520mm. The evenness of the profile corresponded to the centre of ISO 8608 class A. From this, a reference value of the index was calculated. The detailed profile was then resampled, using a cubic spline interpolation, at measurement intervals between 1.0mm and 512mm. The absolute percentage error was then calculated.

$E_{\%} = | (V - V_{Ref}) / V_{Ref} | * 100$

This was repeated for 300 different artificial profiles. The error is shown in terms of the 95th percentile of the distribution of absolute percentage error

Figure C3. The influence of Discrete Measurement Interval on RN.

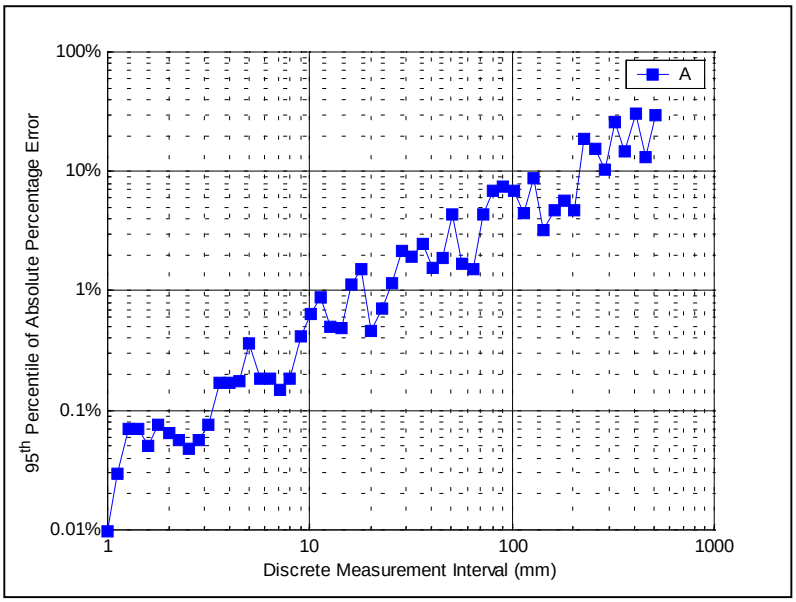

Series A is the Error in 3m Variance resulting from different discrete Measurement Intervals.
A detailed artificial profile, which is indistinguishable from a real profile, was created with a measurement interval of approximately 0.520mm. The evenness of the profile corresponded to the centre of ISO 8608 class A. From this, a reference value of the index was calculated. The detailed profile was then resampled, using a cubic spline interpolation, at measurement intervals between 1.0mm and 512mm. The absolute percentage error was then calculated.

$E_{\%} = | (V - V_{Ref}) / V_{Ref} | * 100$

This was repeated for 300 different artificial profiles. The error is shown in terms of the 95th percentile of the distribution of absolute percentage error

Figure C4. The influence of Discrete Measurement Interval on 3m Variance.

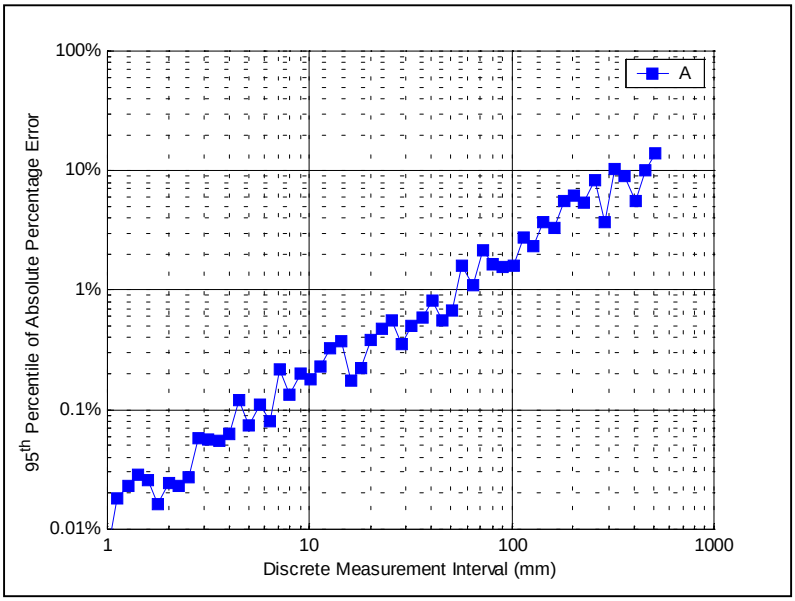

Series A is the Error in 10m Variance resulting from different discrete Measurement Intervals.
A detailed artificial profile, which is indistinguishable from a real profile, was created with a measurement interval of approximately 0.520mm. The evenness of the profile corresponded to the centre of ISO 8608 class A. From this, a reference value of the index was calculated. The detailed profile was then resampled, using a cubic spline interpolation, at measurement intervals between 1.0mm and 512mm. The absolute percentage error was then calculated.

$E_{\%} = | (V - V_{Ref}) / V_{Ref} | * 100$

This was repeated for 300 different artificial profiles. The error is shown in terms of the 95th percentile of the distribution of absolute percentage error

Figure C5. The Influence of Discrete Measurement Interval on 10m Variance.

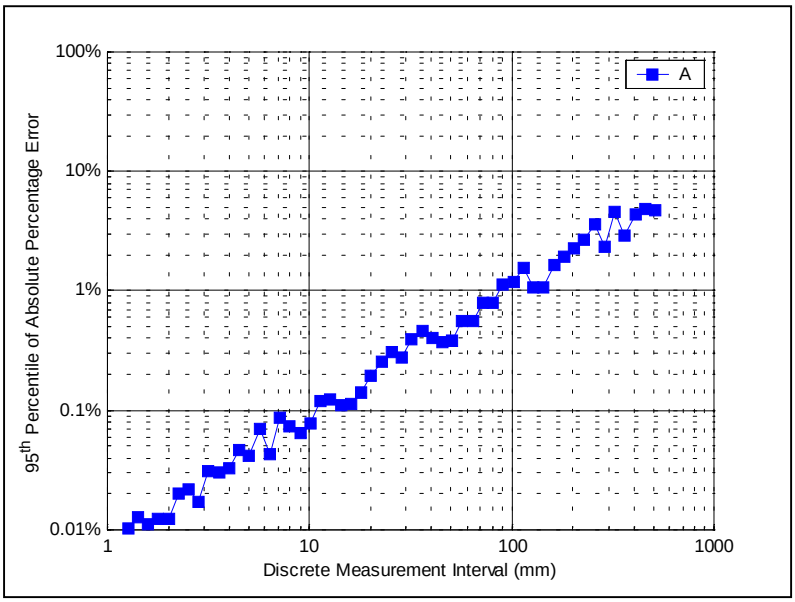

Series A is the Error in 30m Variance resulting from different discrete Measurement Intervals.
A detailed artificial profile, which is indistinguishable from a real profile, was created with a measurement interval of approximately 0.520mm. The evenness of the profile corresponded to the centre of ISO 8608 class A. From this, a reference value of the index was calculated. The detailed profile was then resampled, using a cubic spline interpolation, at measurement intervals between 1.0mm and 512mm. The absolute percentage error was then calculated.

$E_{\%} = | (V - V_{Ref}) / V_{Ref} | * 100$

This was repeated for 300 different artificial profiles. The error is shown in terms of the 95th percentile of the distribution of absolute percentage error

Figure C6. The Influence of Discrete Measurement Interval on 30m Variance.

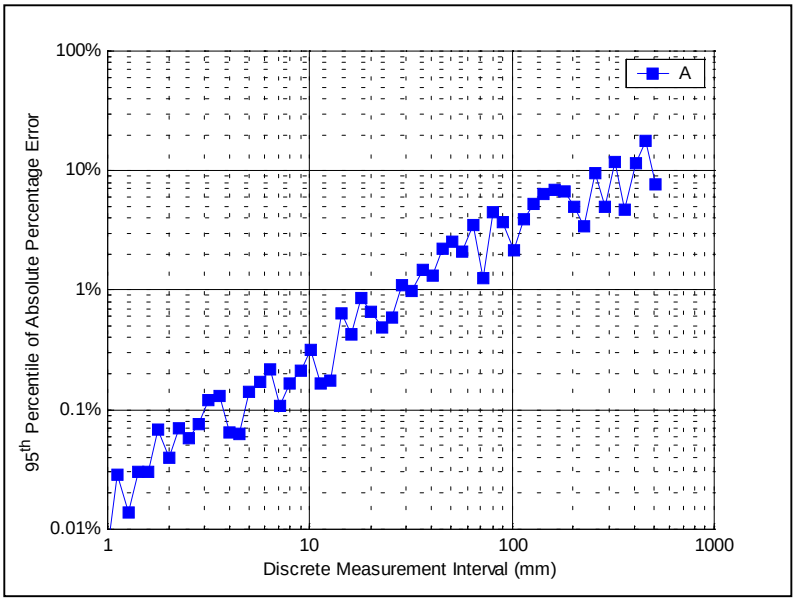

Series A is the Error in CP 2.5 resulting from different discrete Measurement Intervals.
A detailed artificial profile, which is indistinguishable from a real profile, was created with a measurement interval of approximately 0.520mm. The evenness of the profile corresponded to the centre of ISO 8608 class A. From this, a reference value of the index was calculated. The detailed profile was then resampled, using a cubic spline interpolation, at measurement intervals between 1.0mm and 512mm. The absolute percentage error was then calculated.

$E_{\%} = | (V - V_{Ref}) / V_{Ref} | * 100$

This was repeated for 300 different artificial profiles. The error is shown in terms of the 95th percentile of the distribution of absolute percentage error

Figure C7. The Influence of Discrete Measurement Interval on CP 2.5.

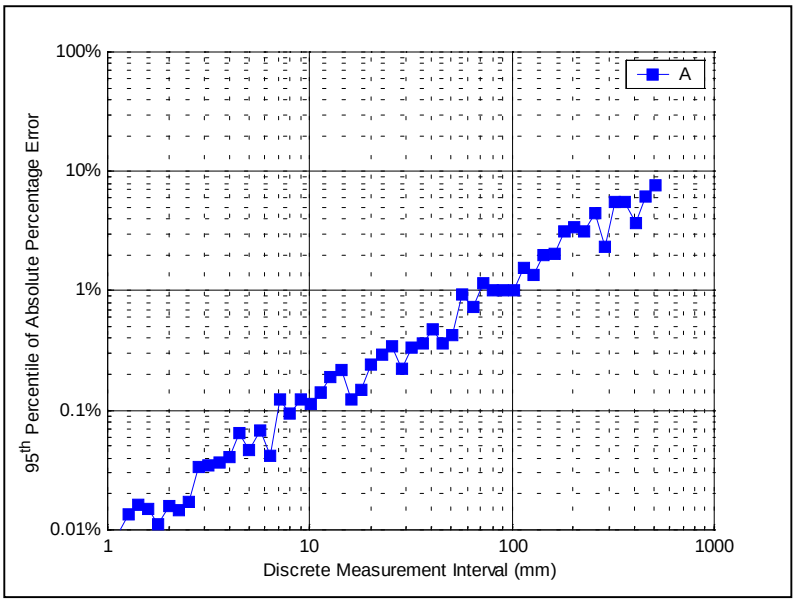

Series A is the Error in CP 10 resulting from different discrete Measurement Intervals.
A detailed artificial profile, which is indistinguishable from a real profile, was created with a measurement interval of approximately 0.520mm. The evenness of the profile corresponded to the centre of ISO 8608 class A. From this, a reference value of the index was calculated. The detailed profile was then resampled, using a cubic spline interpolation, at measurement intervals between 1.0mm and 512mm. The absolute percentage error was then calculated.

$E_{\%} = | (V - V_{Ref}) / V_{Ref} | * 100$

This was repeated for 300 different artificial profiles. The error is shown in terms of the 95th percentile of the distribution of absolute percentage error

Figure C8. The Influence of Discrete Measurement Interval on CP 10.

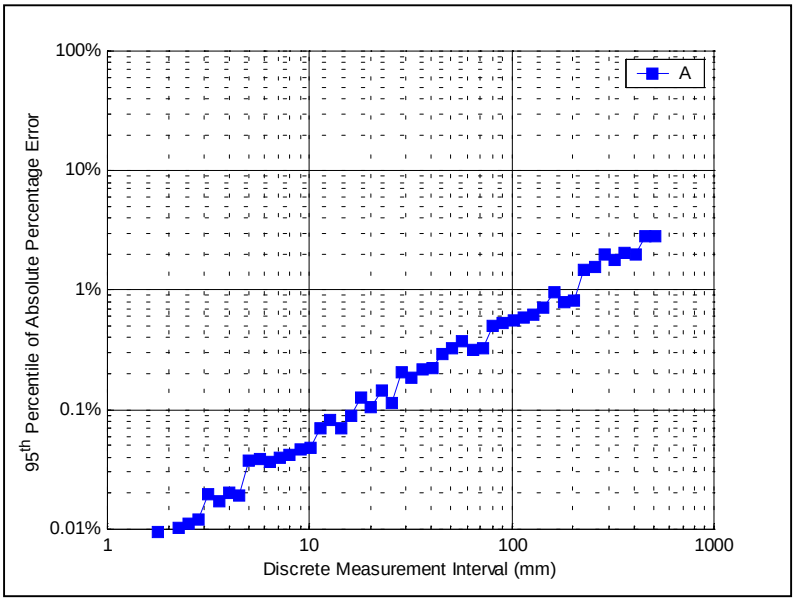

Series A is the Error in CP 40 resulting from different discrete Measurement Intervals.
A detailed artificial profile, which is indistinguishable from a real profile, was created with a measurement interval of approximately 0.520mm. The evenness of the profile corresponded to the centre of ISO 8608 class A. From this, a reference value of the index was calculated. The detailed profile was then resampled, using a cubic spline interpolation, at measurement intervals between 1.0mm and 512mm. The absolute percentage error was then calculated.

$E_{\%} = | (V - V_{Ref}) / V_{Ref} | * 100$

This was repeated for 300 different artificial profiles. The error is shown in terms of the 95th percentile of the distribution of absolute percentage error

Figure C9. The Influence of Measurement Interval on CP 40.

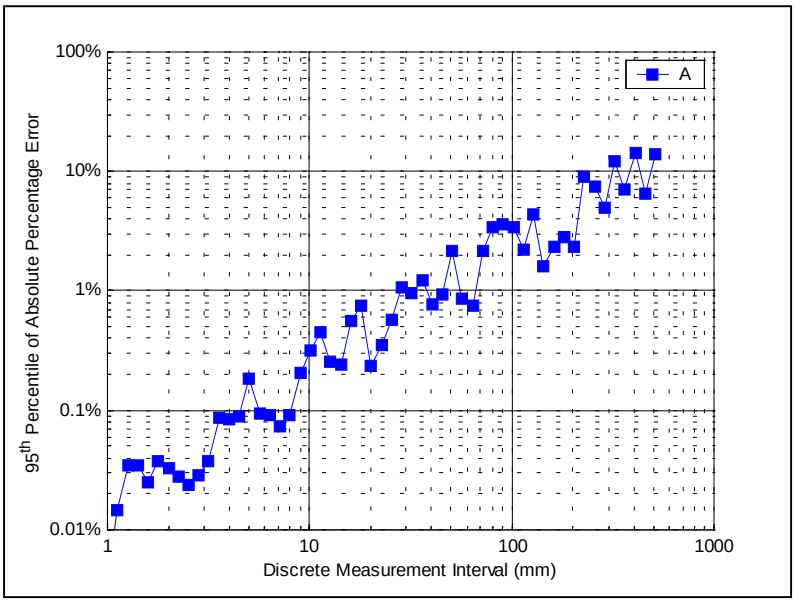

Series A is the Error in Std Dev from a 3m MA resulting from different discrete Measurement Intervals.
A detailed artificial profile, which is indistinguishable from a real profile, was created with a measurement interval of approximately 0.520mm. The evenness of the profile corresponded to the centre of ISO 8608 class A. From this, a reference value of the index was calculated. The detailed profile was then resampled, using a cubic spline interpolation, at measurement intervals between 1.0mm and 512mm. The absolute percentage error was then calculated.

$E_{\%} = | (V - V_{Ref}) / V_{Ref} | * 100$

This was repeated for 300 different artificial profiles. The error is shown in terms of the 95th percentile of the distribution of absolute percentage error

Figure C10. The Influence of Discrete Measurement Interval on the Standard Deviation from a 3m Moving Average.

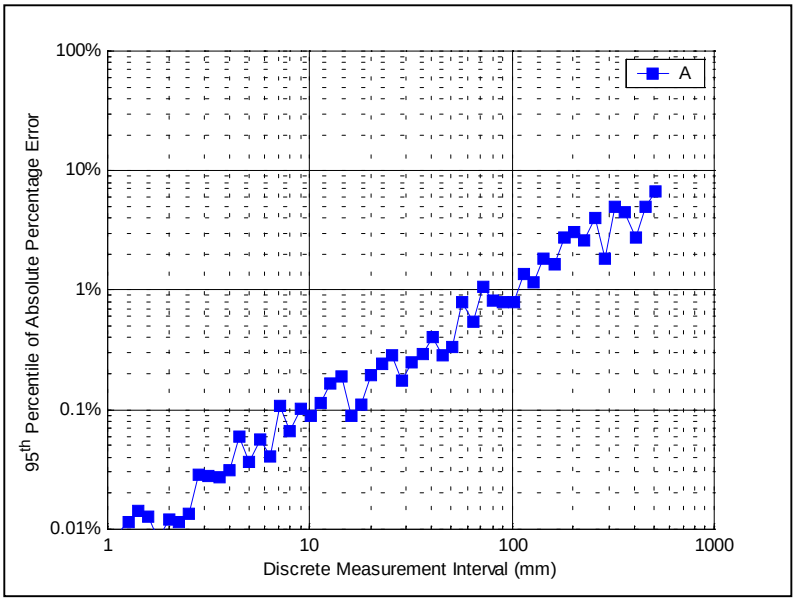

Series A is the Error in the Std Dev formm a 10m MA resulting from different discrete Measurement Intervals.
A detailed artificial profile, which is indistinguishable from a real profile, was created with a measurement interval of approximately 0.520mm. The evenness of the profile corresponded to the centre of ISO 8608 class A. From this, a reference value of the index was calculated. The detailed profile was then resampled, using a cubic spline interpolation, at measurement intervals between 1.0mm and 512mm. The absolute percentage error was then calculated.

$E_{\%} = | (V - V_{Ref}) / V_{Ref} | * 100$

This was repeated for 300 different artificial profiles. The error is shown in terms of the 95th percentile of the distribution of absolute percentage

Figure C11. The Influence of Measurement Interval on the Standard Deviation from a 10m Moving Average.

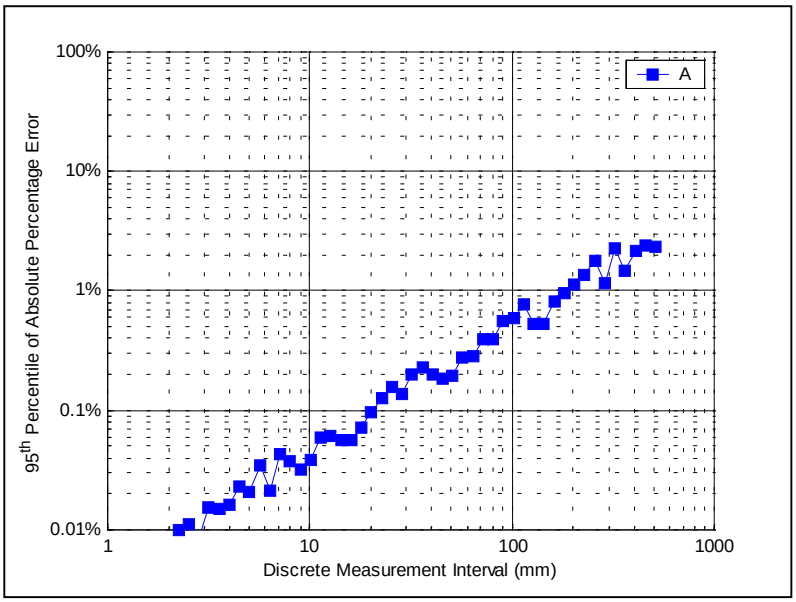

Series A is the Error in the Std Dev from a 30m MA resulting from different discrete Measurement Intervals.
A detailed artificial profile, which is indistinguishable from a real profile, was created with a measurement interval of approximately 0.520mm. The evenness of the profile corresponded to the centre of ISO 8608 class A. From this, a reference value of the index was calculated. The detailed profile was then resampled, using a cubic spline interpolation, at measurement intervals between 1.0mm and 512mm. The absolute percentage error was then calculated.
$E_{\%} = | (V - V_{Ref}) / V_{Ref} | * 100$

This was repeated for 300 different artificial profiles. The error is shown in terms of the 95th percentile of the distribution of absolute percentage error

Figure C12. The Influence of Measurement Interval on the Standard Deviation from a 30m Moving Average.

Annexe D: The Influence of Measurement Interval with Constant Averaging Length on Longitudinal Indices

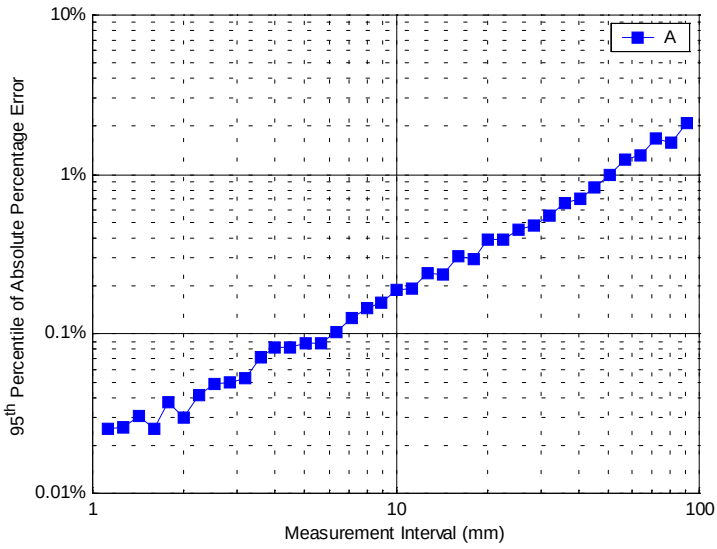

Series A is the error in IRI resulting from different measurement intervals followed by a constant profile averaging length.
A realistic artificial profile, whose evenness corresponded to ISO 8608 class A, was created with a measurement interval of ~0.52mm. This detailed profile was then resampled at measurement intervals of 1.0mm* - 90.5mm, and averaged over 100mm lengths. The absolute percentage error was then calculated.

$E_{\%} = | (V - V_{Ref}) / V_{Ref} | * 100$

This was repeated for 300 different artificial profiles. The error is shown in terms of the 95th percentile of the distribution of absolute percentage error.
* Used to calculate the reference index.

Figure D1. The Influence of Measurement Interval with Constant Averaging Length on IRI.

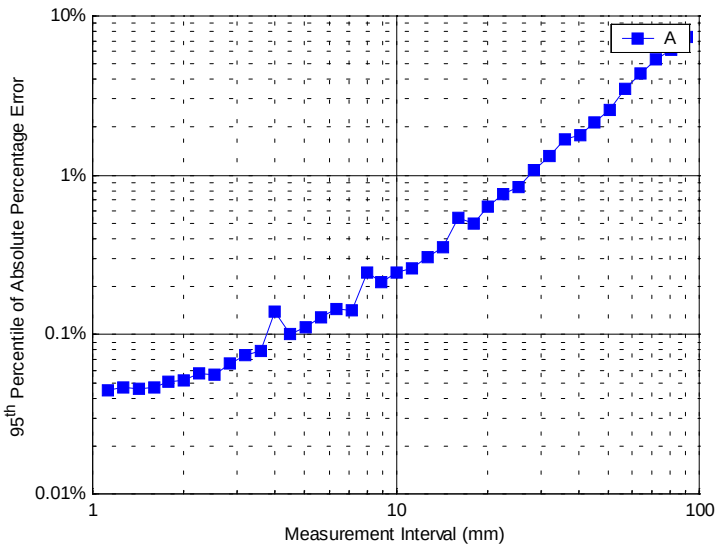

Series A is the error in PI resulting from different measurement intervals followed by a constant profile averaging length.
A realistic artificial profile, whose evenness corresponded to ISO 8608 class A, was created with a measurement interval of ~0.52mm. This detailed profile was then resampled at measurement intervals of 1.0mm* - 90.5mm, and averaged over 100mm lengths. The absolute percentage error was then calculated.

$E_{\%} = | (V - V_{Ref}) / V_{Ref} | * 100$

This was repeated for 300 different artificial profiles. The error is shown in terms of the 95th percentile of the distribution of absolute percentage error.
* Used to calculate the reference index.

Figure D2. The Influence of Measurement Interval with Constant Averaging Length on PI.

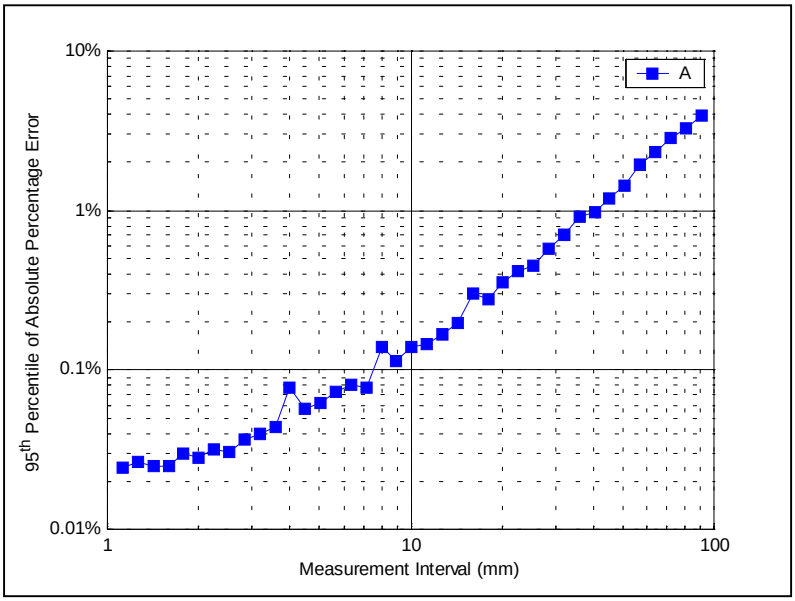

Series A is the error in RN resulting from different measurement intervals followed by a constant profile averaging length.
A realistic artificial profile, whose evenness corresponded to ISO 8608 class A, was created with a measurement interval of ~0.52mm. This detailed profile was then resampled at measurement intervals of 1.0mm* - 90.5mm, and averaged over 100mm lengths. The absolute percentage error was then calculated.

$E_{\%} = | (V - V_{Ref}) / V_{Ref} | * 100$

This was repeated for 300 different artificial profiles. The error is shown in terms of the 95th percentile of the distribution of absolute percentage error.
* Used to calculate the reference index.

Figure D3. The Influence of Measurement Interval with Constant Averaging Length on RN.

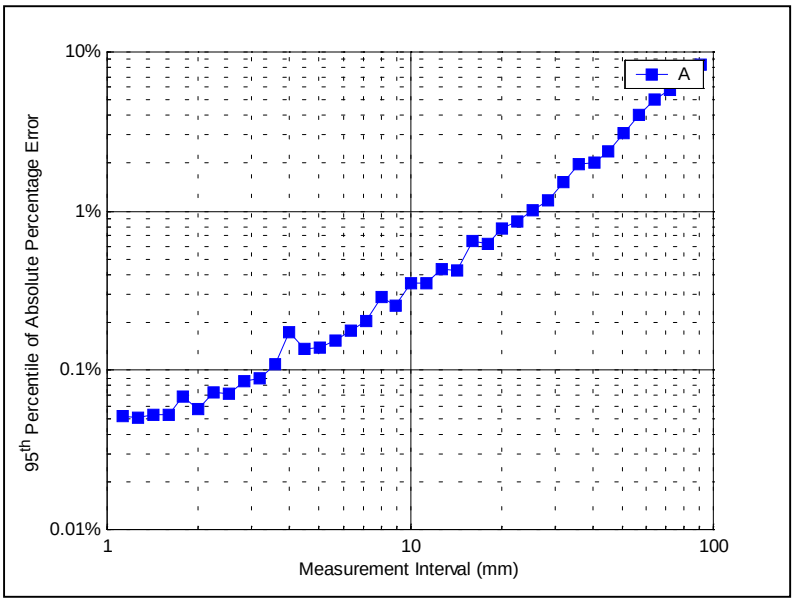

Series A is the error in 3m Variance resulting from different measurement intervals followed by a constant profile averaging length.
A realistic artificial profile, whose evenness corresponded to ISO 8608 class A, was created with a measurement interval of ~0.52mm. This detailed profile was then resampled at measurement intervals of 1.0mm* - 90.5mm, and averaged over 100mm lengths. The absolute percentage error was then calculated.

$E_{\%} = | (V - V_{Ref}) / V_{Ref} | * 100$

This was repeated for 300 different artificial profiles. The error is shown in terms of the 95th percentile of the distribution of absolute percentage error.
* Used to calculate the reference index.

Figure D4. The Influence of Measurement Interval with Constant Averaging Length on 3m Variance.

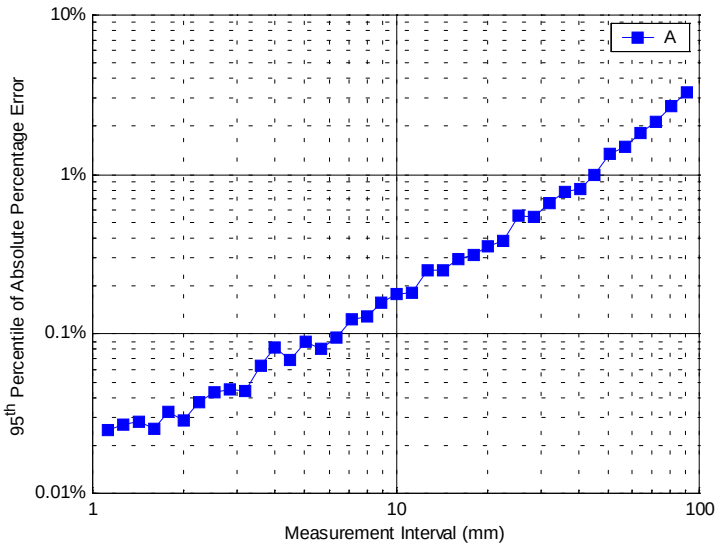

Series A is the error in 10m Variance resulting from different measurement intervals followed by a constant profile averaging length.
A realistic artificial profile, whose evenness corresponded to ISO 8608 class A, was created with a measurement interval of ~0.52mm. This detailed profile was then resampled at measurement intervals of 1.0mm* - 90.5mm, and averaged over 100mm lengths. The absolute percentage error was then calculated.

$E_{\%} = | (V - V_{Ref}) / V_{Ref} | * 100$

This was repeated for 300 different artificial profiles. The error is shown in terms of the 95th percentile of the distribution of absolute percentage error.
* Used to calculate the reference index.

Figure D5. The Influence of Measurement Interval with Constant Averaging Length on 10m Variance.

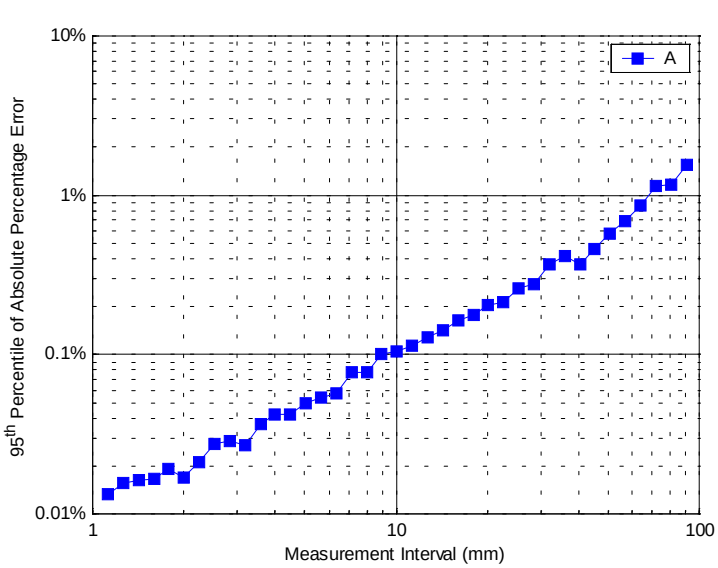

Series A is the error in 30m Variance resulting from different measurement intervals followed by a constant profile averaging length.
A realistic artificial profile, whose evenness corresponded to ISO 8608 class A, was created with a measurement interval of ~0.52mm. This detailed profile was then resampled at measurement intervals of 1.0mm* - 90.5mm, and averaged over 100mm lengths. The absolute percentage error was then calculated.

$E_{\%} = | (V - V_{Ref}) / V_{Ref} | * 100$

This was repeated for 300 different artificial profiles. The error is shown in terms of the 95th percentile of the distribution of absolute percentage error.
* Used to calculate the reference index.

Figure D6. The Influence of Measurement Interval with Constant Averaging Length on 30m Variance.

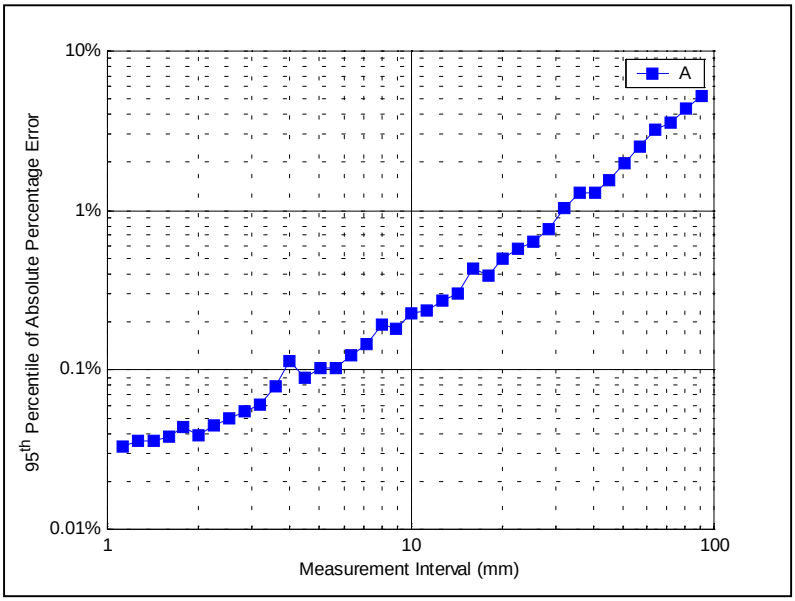

Series A is the error in CP 2.5 resulting from different measurement intervals followed by a constant profile averaging length.
A realistic artificial profile, whose evenness corresponded to ISO 8608 class A, was created with a measurement interval of ~0.52mm. This detailed profile was then resampled at measurement intervals of 1.0mm* - 90.5mm, and averaged over 100mm lengths. The absolute percentage error was then calculated.

$E_{\%} = | (V - V_{Ref}) / V_{Ref} | * 100$

This was repeated for 300 different artificial profiles. The error is shown in terms of the 95th percentile of the distribution of absolute percentage error.
* Used to calculate the reference index.

Figure D7. The Influence of Measurement Interval with Constant Averaging Length on CP 2.5.

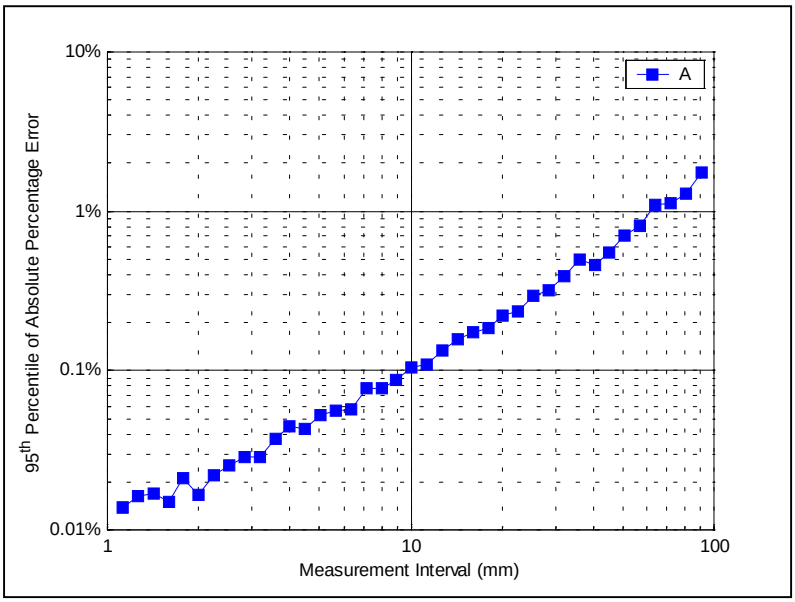

Series A is the error in CP 10 resulting from different measurement intervals followed by a constant profile averaging length.
A realistic artificial profile, whose evenness corresponded to ISO 8608 class A, was created with a measurement interval of ~0.52mm. This detailed profile was then resampled at measurement intervals of 1.0mm* - 90.5mm, and averaged over 100mm lengths. The absolute percentage error was then calculated.

$E_{\%} = | (V - V_{Ref}) / V_{Ref} | * 100$

This was repeated for 300 different artificial profiles. The error is shown in terms of the 95th percentile of the distribution of absolute percentage error.
* Used to calculate the reference index.

Figure D8. The Influence of Measurement Interval with Constant Averaging Length on CP 10.

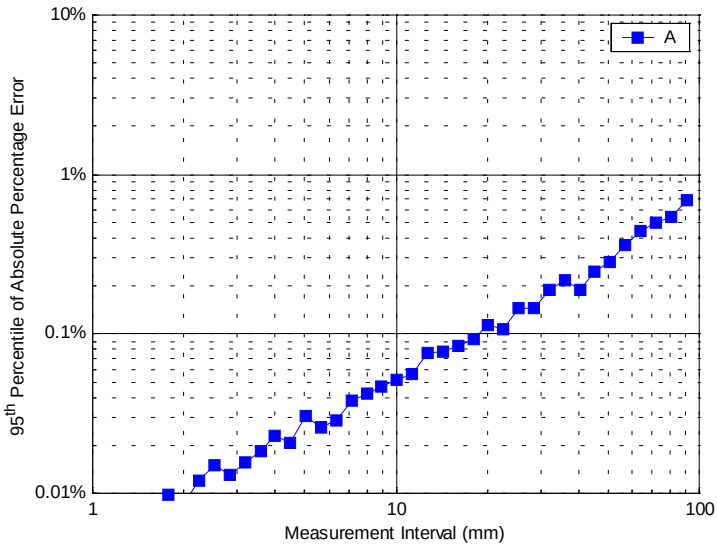

Series A is the error in CP 40 resulting from different measurement intervals followed by a constant profile averaging length.
A realistic artificial profile, whose evenness corresponded to ISO 8608 class A, was created with a measurement interval of ~0.52mm. This detailed profile was then resampled at measurement intervals of 1.0mm* - 90.5mm, and averaged over 100mm lengths. The absolute percentage error was then calculated.

$E_{\%} = | (V - V_{Ref}) / V_{Ref} | * 100$

This was repeated for 300 different artificial profiles. The error is shown in terms of the 95th percentile of the distribution of absolute percentage error.
* Used to calculate the reference index.

Figure D9. The Influence of Measurement Interval with Constant Averaging Length on CP 40.

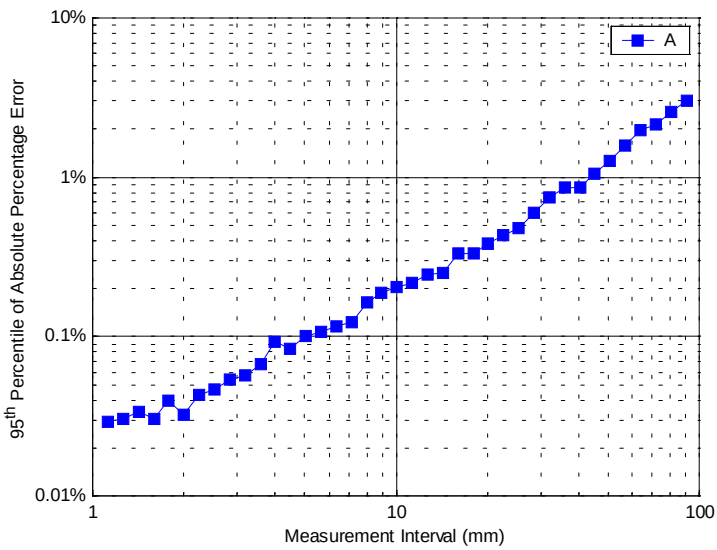

Series A is the error in $G(n_0)$ resulting from different measurement intervals followed by a constant profile averaging length.
A realistic artificial profile, whose evenness corresponded to ISO 8608 class A, was created with a measurement interval of ~0.52mm. This detailed profile was then resampled at measurement intervals of 1.0mm* - 90.5mm, and averaged over 100mm lengths. The absolute percentage error was then calculated.

$E_{\%} = | (V - V_{Ref}) / V_{Ref} | * 100$

This was repeated for 300 different artificial profiles. The error is shown in terms of the 95th percentile of the distribution of absolute percentage error.
* Used to calculate the reference index.

Figure D10. The Influence of Measurement Interval with Constant Averaging Length on $G(n_0)$.

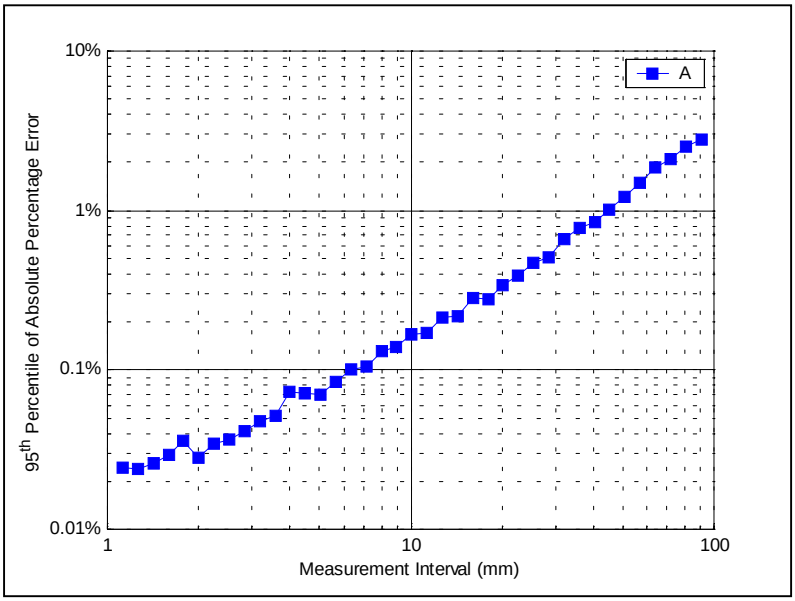

Series A is the error in w resulting from different measurement intervals followed by a constant profile averaging length.
A realistic artificial profile, whose evenness corresponded to ISO 8608 class A, was created with a measurement interval of ~0.52mm. This detailed profile was then resampled at measurement intervals of 1.0mm* - 90.5mm, and averaged over 100mm lengths. The absolute percentage error was then calculated.

$E_{\%} = | (V - V_{Ref}) / V_{Ref} | * 100$

This was repeated for 300 different artificial profiles. The error is shown in terms of the 95th percentile of the distribution of absolute percentage error.
* Used to calculate the reference index.

Figure D11. The Influence of Measurement Interval with Constant Averaging Length on w.

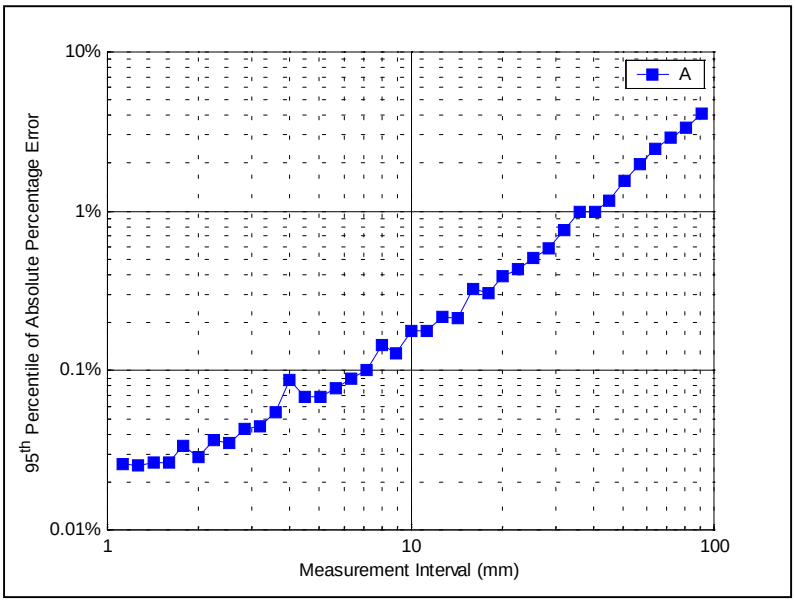

Series A is the error in Std Dev from a 3m MA resulting from different measurement intervals followed by a constant profile averaging length.
A realistic artificial profile, whose evenness corresponded to ISO 8608 class A, was created with a measurement interval of ~0.52mm. This detailed profile was then resampled at measurement intervals of 1.0mm* - 90.5mm, and averaged over 100mm lengths. The absolute percentage error was then calculated.

$E_{\%} = | (V - V_{Ref}) / V_{Ref} | * 100$

This was repeated for 300 different artificial profiles. The error is shown in terms of the 95th percentile of the distribution of absolute percentage error.
* Used to calculate the reference index.

Figure D12. The Influence of Measurement Interval with Constant Averaging Length on the Standard Deviation from a 3m Moving Average.

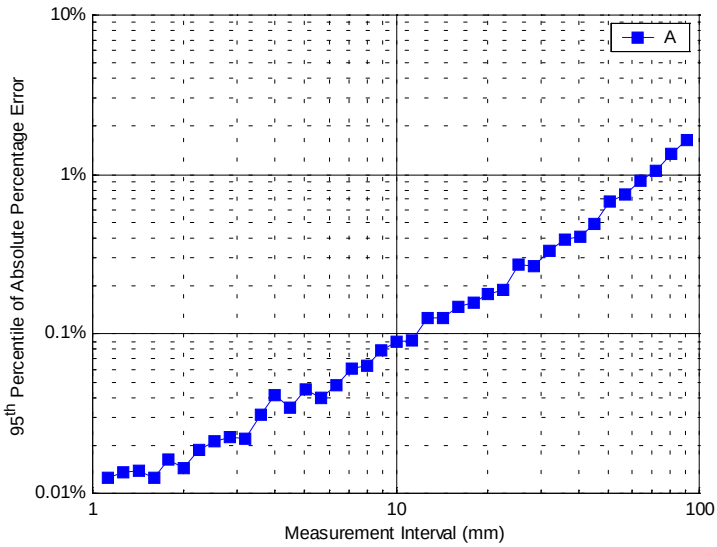

Series A is the error in Std Dev from a 10m MA resulting from different measurement intervals followed by a constant profile averaging length.
A realistic artificial profile, whose evenness corresponded to ISO 8608 class A, was created with a measurement interval of ~0.52mm. This detailed profile was then resampled at measurement intervals of 1.0mm* - 90.5mm, and averaged over 100mm lengths. The absolute percentage error was then calculated.

$E_{\%} = | (V - V_{Ref}) / V_{Ref} | * 100$

This was repeated for 300 different artificial profiles. The error is shown in terms of the 95th percentile of the distribution of absolute percentage error.
* Used to calculate the reference index.

Figure D13. The Influence of Measurement Interval with Constant Averaging Length on the Standard Deviation from a 10m Moving Average.

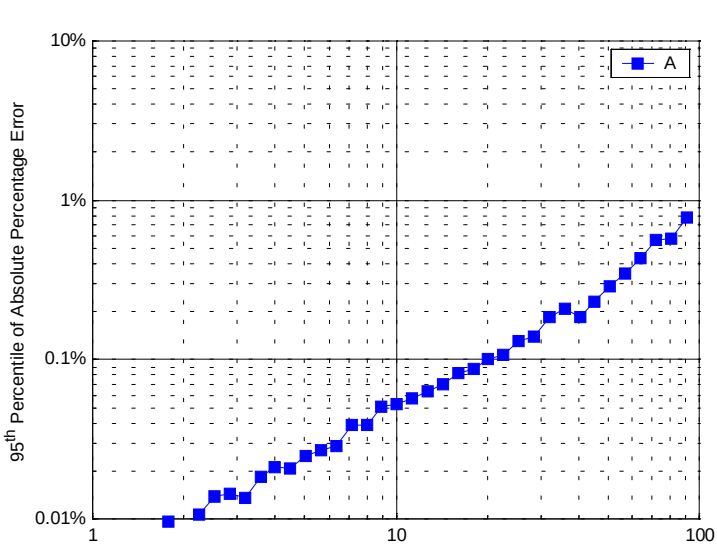

Series A is the error in Std Dev from a 30m MA resulting from different measurement intervals followed by a constant profile averaging length.
A realistic artificial profile, whose evenness corresponded to ISO 8608 class A, was created with a measurement interval of ~0.52mm. This detailed profile was then resampled at measurement intervals of 1.0mm* - 90.5mm, and averaged over 100mm lengths. The absolute percentage error was then calculated.

$E_{\%} = | (V - V_{Ref}) / V_{Ref} | * 100$

This was repeated for 300 different artificial profiles. The error is shown in terms of the 95th percentile of the distribution of absolute percentage error.
* Used to calculate the reference index.

Figure D14. The Influence of Measurement Interval with Constant Averaging Length on the Standard Deviation from a 30m Moving Average.

Annexe E: The Influence of Averaging Length with Constant Measurement Interval on Longitudinal Indices.

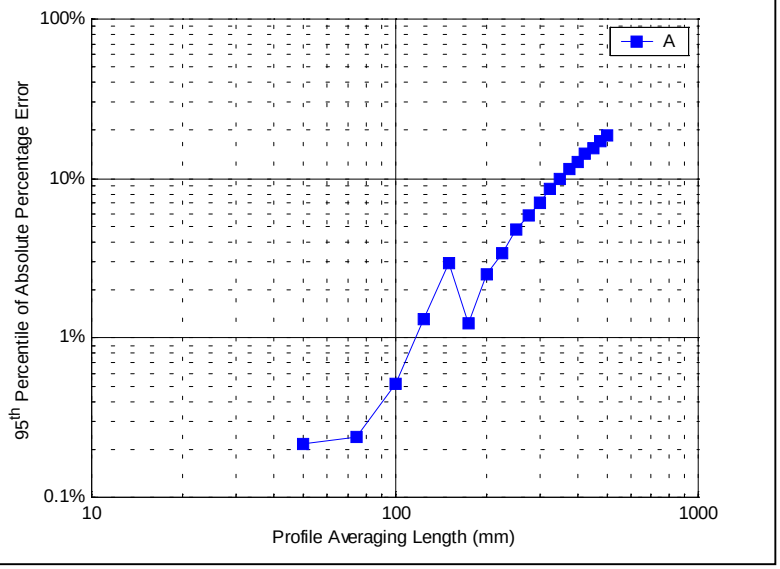

Series A is the error in IRI resulting from different averaging length.
A realistic artificial profile, whose evenness corresponded to ISO 8608 class A, was created with a measurement interval of ~0.52mm. This profile was used to calculate a reference index. This detailed profile was then resampled at a measurement interval of 1.0mm, and averaged over 25mm – 500mm. The absolute percentage error was then calculated.

$E_{\%} = | (V - V_{Ref}) / V_{Ref} | * 100$

This was repeated for 300 different artificial profiles. The error is shown in terms of the 95th percentile of the distribution of absolute percentage error.

Figure E1. The Influence of Profile Averaging Length on IRI.

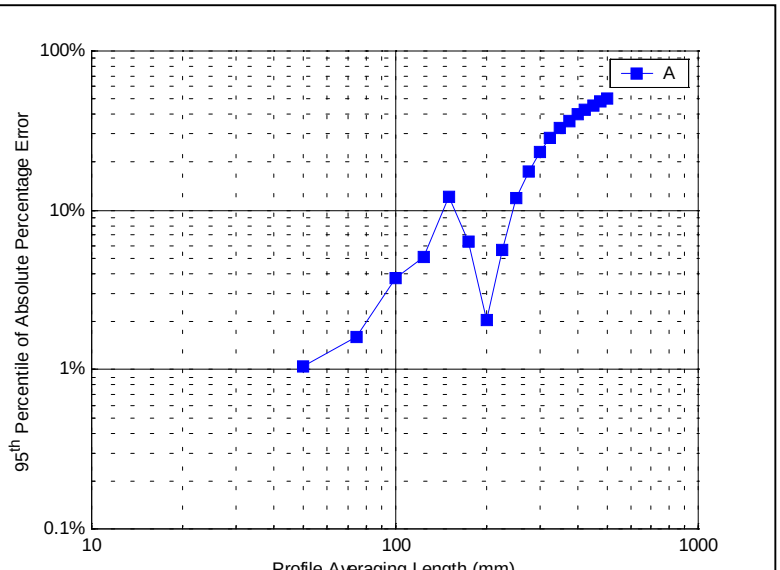

Series A is the error in PI resulting from different averaging length.
A realistic artificial profile, whose evenness corresponded to ISO 8608 class A, was created with a measurement interval of ~0.52mm. This profile was used to calculate a reference index. This detailed profile was then resampled at a measurement interval of 1.0mm, and averaged over 25mm – 500mm. The absolute percentage error was then calculated.

$E_{\%} = | (V - V_{Ref}) / V_{Ref} | * 100$

This was repeated for 300 different artificial profiles. The error is shown in terms of the 95th percentile of the distribution of absolute percentage error.

Figure E2. The Influence of Profile Averaging Length on PI.

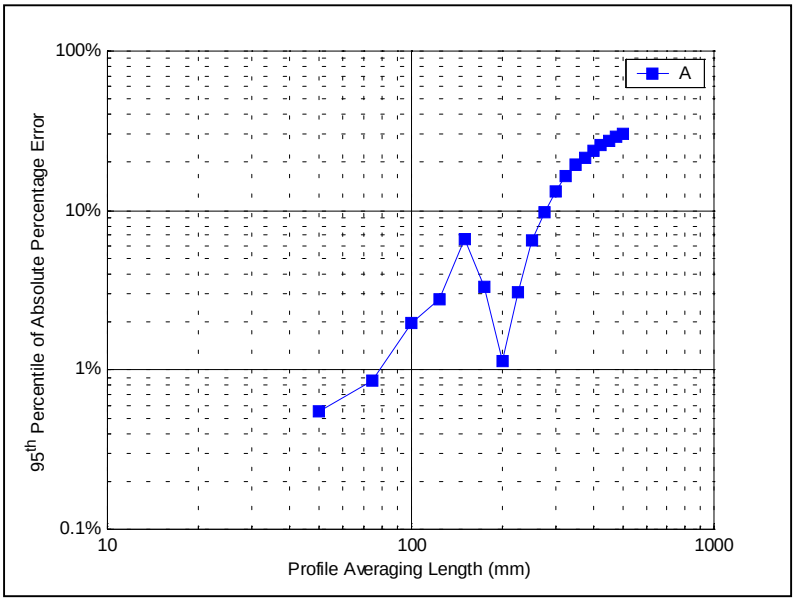

Series A is the error in RN resulting from different averaging length.
A realistic artificial profile, whose evenness corresponded to ISO 8608 class A, was created with a measurement interval of ~0.52mm. This profile was used to calculate a reference index. This detailed profile was then resampled at a measurement interval of 1.0mm, and averaged over 25mm – 500mm. The absolute percentage error was then calculated.

$E_{\%} = | (V - V_{Ref}) / V_{Ref} | * 100$

This was repeated for 300 different artificial profiles. The error is shown in terms of the 95th percentile of the distribution of absolute percentage error.

Figure E3. The Influence of Profile Averaging Length on RN.

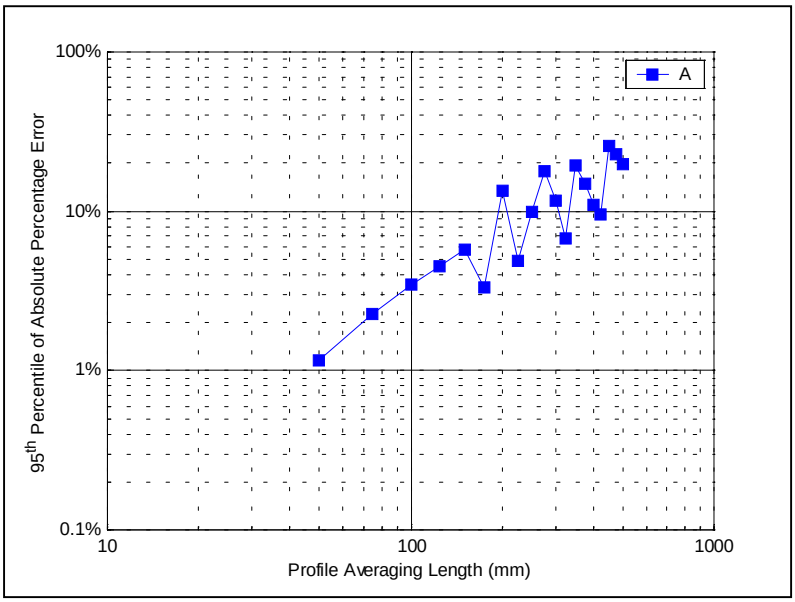

Series A is the error in 3m Variance resulting from different averaging length.
A realistic artificial profile, whose evenness corresponded to ISO 8608 class A, was created with a measurement interval of ~0.52mm. This profile was used to calculate a reference index. This detailed profile was then resampled at a measurement interval of 1.0mm, and averaged over 25mm – 500mm. The absolute percentage error was then calculated.

$E_{\%} = | (V - V_{Ref}) / V_{Ref} | * 100$

This was repeated for 300 different artificial profiles. The error is shown in terms of the 95th percentile of the distribution of absolute percentage error.

Figure E4. The Influence of Profile Averaging Length on 3m Variance.

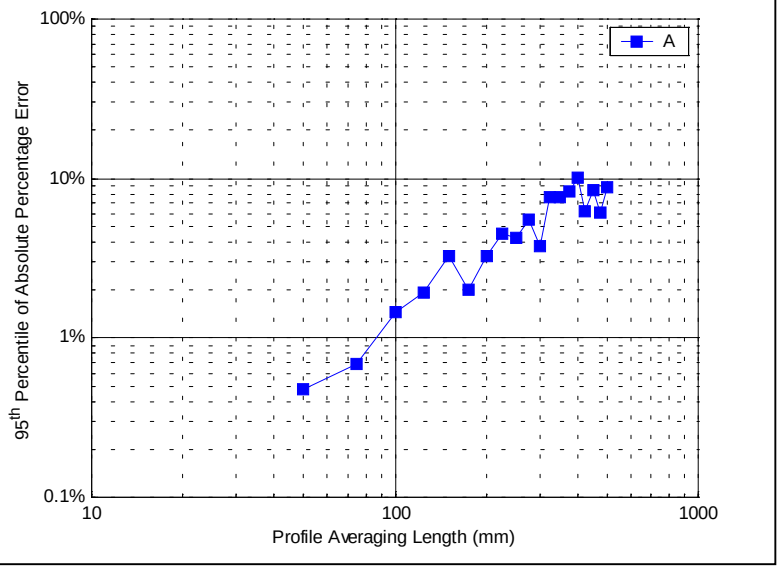

Series A is the error in 10m Variance resulting from different averaging length.
A realistic artificial profile, whose evenness corresponded to ISO 8608 class A, was created with a measurement interval of ~0.52mm. This profile was used to calculate a reference index. This detailed profile was then resampled at a measurement interval of 1.0mm, and averaged over 25mm – 500mm. The absolute percentage error was then calculated.

$E_{\%} = | (V - V_{Ref}) / V_{Ref} | * 100$

This was repeated for 300 different artificial profiles. The error is shown in terms of the 95th percentile of the distribution of absolute percentage error.

Figure E5. The Influence of Profile Averaging Length on 10m Variance.

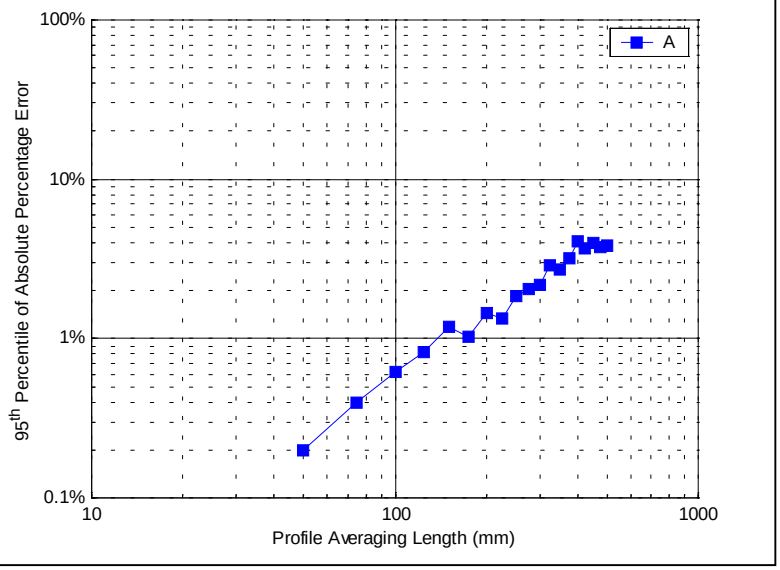

Series A is the error in 30m Variance resulting from different averaging length.
A realistic artificial profile, whose evenness corresponded to ISO 8608 class A, was created with a measurement interval of ~0.52mm. This profile was used to calculate a reference index. This detailed profile was then resampled at a measurement interval of 1.0mm, and averaged over 25mm – 500mm. The absolute percentage error was then calculated.

$E_{\%} = | (V - V_{Ref}) / V_{Ref} | * 100$

This was repeated for 300 different artificial profiles. The error is shown in terms of the 95th percentile of the distribution of absolute percentage error.

Figure E6. The Influence of Profile Averaging Length on 30m Variance.

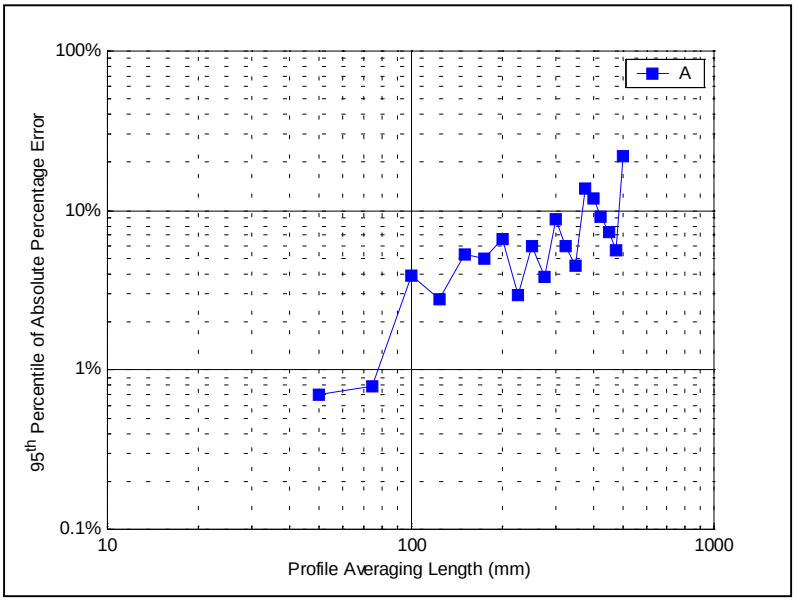

Series A is the error in CP 2.5 resulting from different averaging length.
A realistic artificial profile, whose evenness corresponded to ISO 8608 class A, was created with a measurement interval of ~0.52mm. This profile was used to calculate a reference index. This detailed profile was then resampled at a measurement interval of 1.0mm, and averaged over 25mm – 500mm. The absolute percentage error was then calculated.

$E_{\%} = | (V - V_{Ref}) / V_{Ref} | * 100$

This was repeated for 300 different artificial profiles. The error is shown in terms of the 95th percentile of the distribution of absolute percentage error.

Figure E7. The Influence of Profile Averaging Length on CP 2.5.

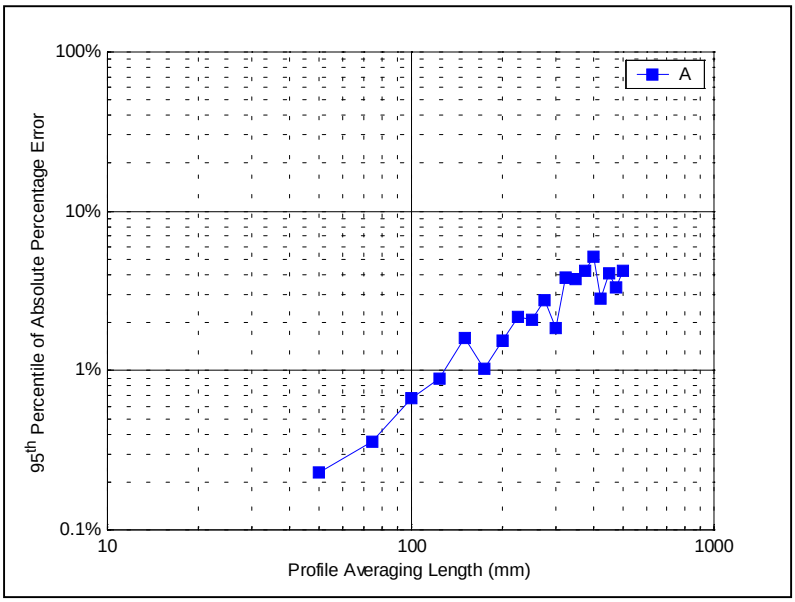

Series A is the error in CP 10 resulting from different averaging length.
A realistic artificial profile, whose evenness corresponded to ISO 8608 class A, was created with a measurement interval of ~0.52mm. This profile was used to calculate a reference index. This detailed profile was then resampled at a measurement interval of 1.0mm, and averaged over 25mm – 500mm. The absolute percentage error was then calculated.

$E_{\%} = | (V - V_{Ref}) / V_{Ref} | * 100$

This was repeated for 300 different artificial profiles. The error is shown in terms of the 95th percentile of the distribution of absolute percentage error.

Figure E8. The Influence of Profile Averaging Length on CP 10.

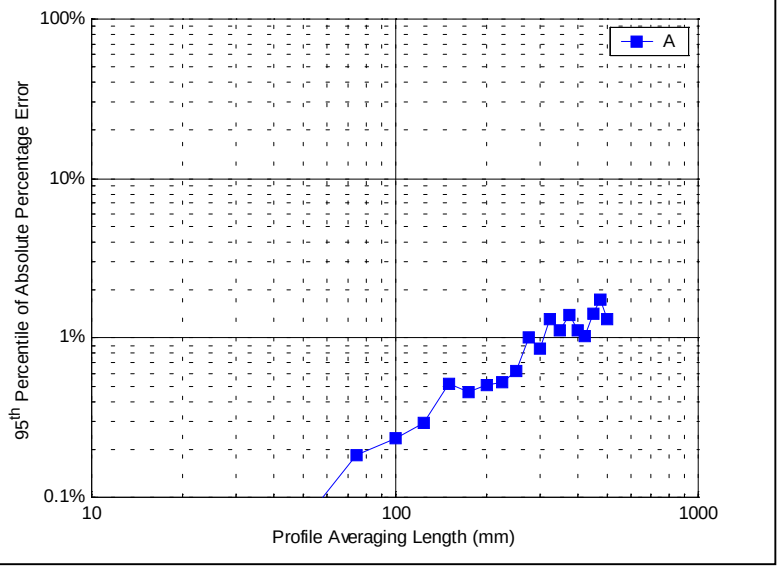

Series A is the error in CP 40 resulting from different averaging length.
A realistic artificial profile, whose evenness corresponded to ISO 8608 class A, was created with a measurement interval of ~0.52mm. This profile was used to calculate a reference index. This detailed profile was then resampled at a measurement interval of 1.0mm, and averaged over 25mm – 500mm. The absolute percentage error was then calculated.

$E_{\%} = | (V - V_{Ref}) / V_{Ref} | * 100$

This was repeated for 300 different artificial profiles. The error is shown in terms of the 95th percentile of the distribution of absolute percentage error.

Figure E9. The Influence of Profile Averaging Length on CP 40.

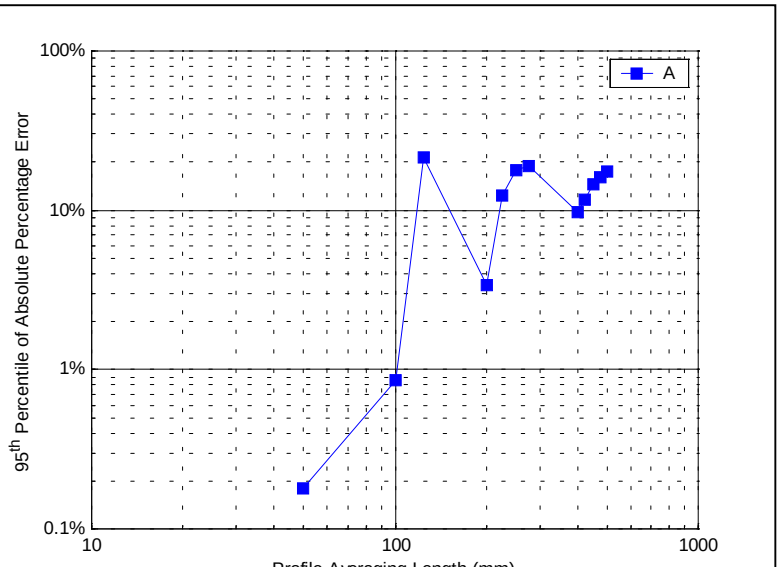

Series A is the error in $G(n_0)$ resulting from different averaging length.
A realistic artificial profile, whose evenness corresponded to ISO 8608 class A, was created with a measurement interval of ~0.52mm. This profile was used to calculate a reference index. This detailed profile was then resampled at a measurement interval of 1.0mm, and averaged over 25mm – 500mm. The absolute percentage error was then calculated.

$E_{\%} = | (V - V_{Ref}) / V_{Ref} | * 100$

This was repeated for 300 different artificial profiles. The error is shown in terms of the 95th percentile of the distribution of absolute percentage error.

Figure E10. The Influence of Profile Averaging Length on $G(n_0)$.

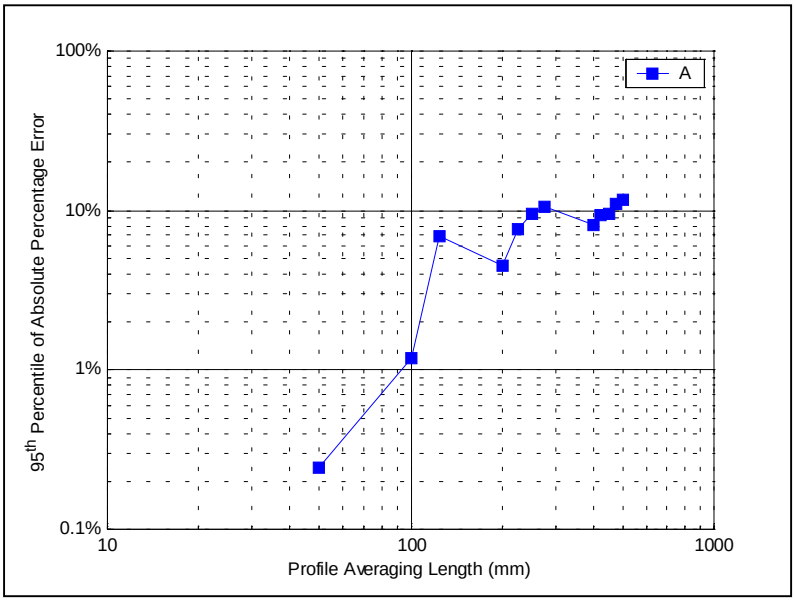

Series A is the error in w resulting from different averaging length.
A realistic artificial profile, whose evenness corresponded to ISO 8608 class A, was created with a measurement interval of ~0.52mm. This profile was used to calculate a reference index. This detailed profile was then resampled at a measurement interval of 1.0mm, and averaged over 25mm – 500mm. The absolute percentage error was then calculated.

$E_{\%} = | (V - V_{Ref}) / V_{Ref} | * 100$

This was repeated for 300 different artificial profiles. The error is shown in terms of the 95th percentile of the distribution of absolute percentage error.

Figure E11. The Influence of Profile Averaging Length on w.

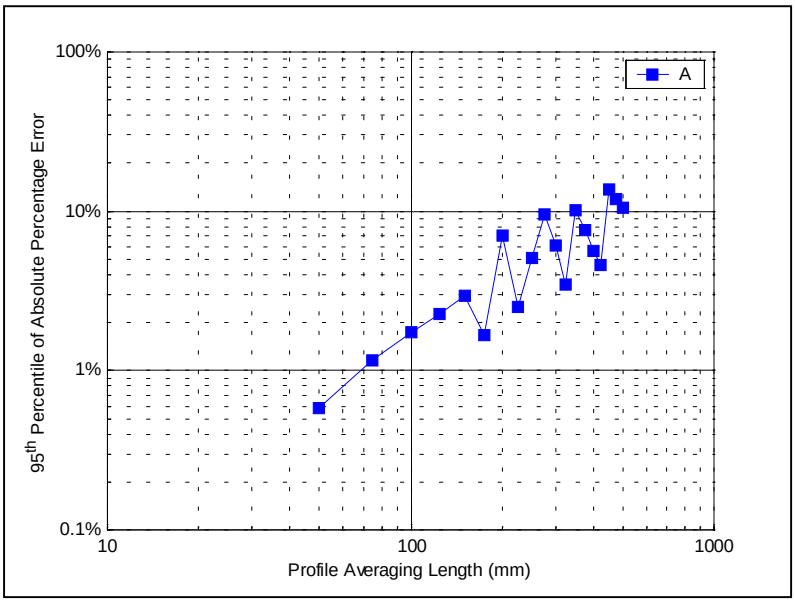

Series A is the error in the Std Dev from a 3m MA resulting from different averaging length.
A realistic artificial profile, whose evenness corresponded to ISO 8608 class A, was created with a measurement interval of ~0.52mm. This profile was used to calculate a reference index. This detailed profile was then resampled at a measurement interval of 1.0mm, and averaged over 25mm – 500mm. The absolute percentage error was then calculated.

$E_{\%} = | (V - V_{Ref}) / V_{Ref} | * 100$

This was repeated for 300 different artificial profiles. The error is shown in terms of the 95th percentile of the distribution of absolute percentage error.

Figure E12. The Influence of Profile Averaging Length on the Standard Deviation from a 3m Moving Average.

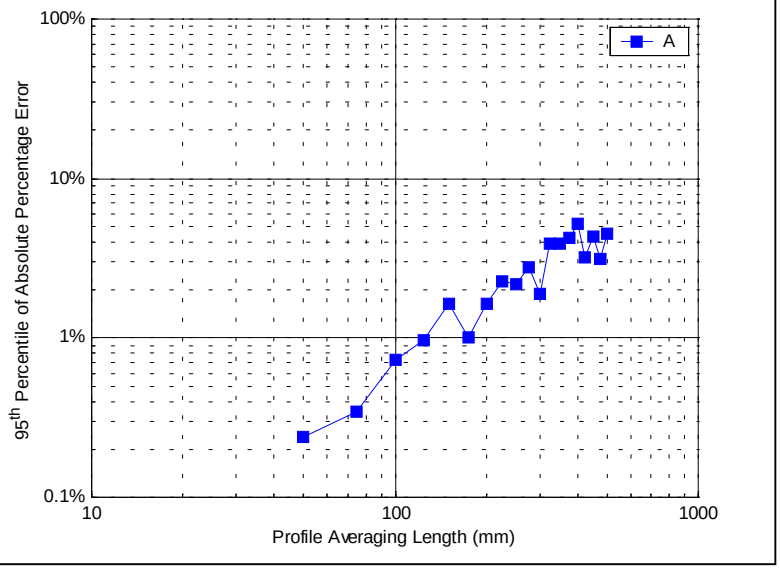

Series A is the error in Std Dev from a 10m MA resulting from different averaging length.
A realistic artificial profile, whose evenness corresponded to ISO 8608 class A, was created with a measurement interval of ~0.52mm. This profile was used to calculate a reference index. This detailed profile was then resampled at a measurement interval of 1.0mm, and averaged over 25mm – 500mm. The absolute percentage error was then calculated.

$E_{\%} = | (V - V_{Ref}) / V_{Ref} | * 100$

This was repeated for 300 different artificial profiles. The error is shown in terms of the 95th percentile of the distribution of absolute percentage error.

Figure E13. The Influence of Profile Averaging Length on the Standard Deviation from a 10m Moving Average.

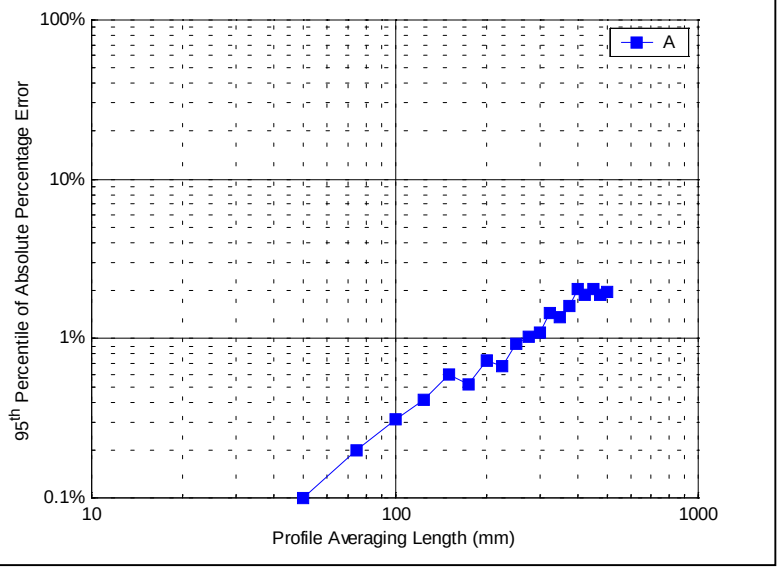

Series A is the error in Std Dev from a 30m MA resulting from different averaging length.
A realistic artificial profile, whose evenness corresponded to ISO 8608 class A, was created with a measurement interval of ~0.52mm. This profile was used to calculate a reference index. This detailed profile was then resampled at a measurement interval of 1.0mm, and averaged over 25mm – 500mm. The absolute percentage error was then calculated.

$E_{\%} = | (V - V_{Ref}) / V_{Ref} | * 100$

This was repeated for 300 different artificial profiles. The error is shown in terms of the 95th percentile of the distribution of absolute percentage error.

Figure E14. The Influence of Profile Averaging Length on the Standard Deviation from a 30m Moving Average.

Annexe F: The Influence of Random Noise on Longitudinal Indices

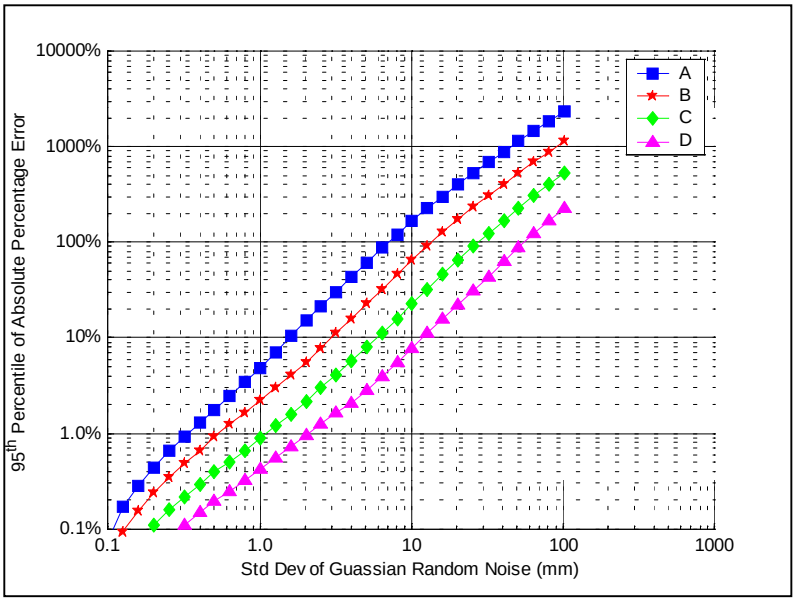

Series A is the error in IRI resulting from the addition of random noise.
A realistic artificial profile, whose evenness corresponded to ISO 8608 class A, was created with a measurement interval of ~0.52mm. This detailed profile was then resampled at a measurement interval of 1.0mm, Gaussian random noise was added, and the profile was averaged over 100mm. The absolute percentage error was then calculated.
$E_{\%} = | (V - V_{Ref}) / V_{Ref} | * 100$
The error free profile was used to calculate the reference index.
This was repeated for 300 different artificial profiles. The error is shown in terms of the 95th percentile of the distribution of absolute percentage error.
Series B, C, and D are identical to Series A except for the use of profiles of ISO 8608 class B, C, and D.

Figure F1. The Influence of Guassian Random Noise on IRI.

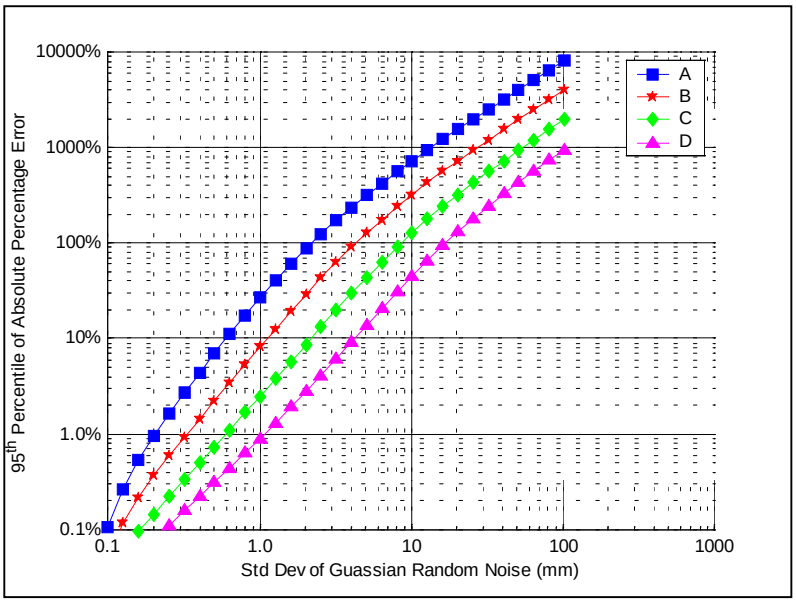

Series A is the error in PI resulting from the addition of random noise.
A realistic artificial profile, whose evenness corresponded to ISO 8608 class A, was created with a measurement interval of ~0.52mm. This detailed profile was then resampled at a measurement interval of 1.0mm, Gaussian random noise was added, and the profile was averaged over 100mm. The absolute percentage error was then calculated.
$E_{\%} = | (V - V_{Ref}) / V_{Ref} | * 100$
The error free profile was used to calculate the reference index.
This was repeated for 300 different artificial profiles. The error is shown in terms of the 95th percentile of the distribution of absolute percentage error.
Series B, C, and D are identical to Series A except for the use of profiles of ISO 8608 class B, C, and D.

Figure F2. The Influence of Gaussian Random Noise on PI.

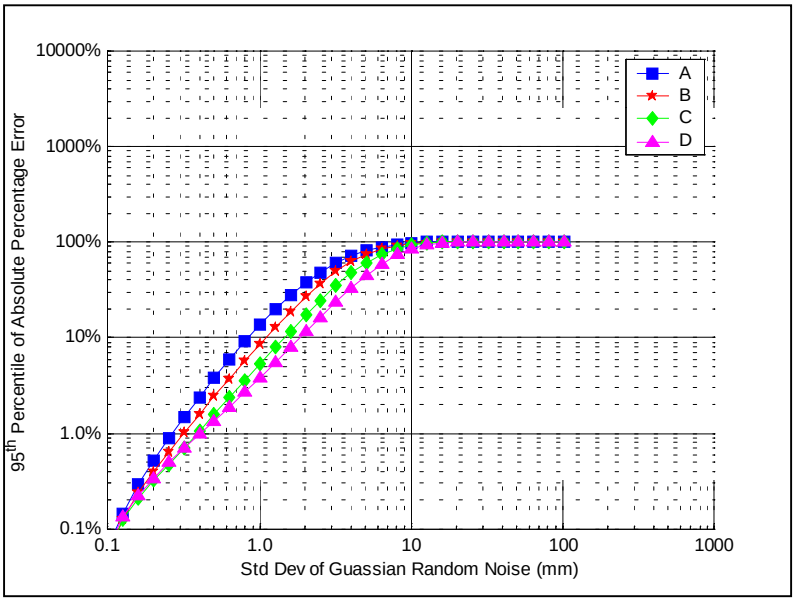

Series A is the error in RN resulting from the addition of random noise.
A realistic artificial profile, whose evenness corresponded to ISO 8608 class A, was created with a measurement interval of ~0.52mm. This detailed profile was then resampled at a measurement interval of 1.0mm, Gaussian random noise was added, and the profile was averaged over 100mm. The absolute percentage error was then calculated.
$E_{\%} = | (V - V_{Ref}) / V_{Ref} | * 100$
The error free profile was used to calculate the reference index.
This was repeated for 300 different artificial profiles. The error is shown in terms of the 95th percentile of the distribution of absolute percentage error.
Series B, C, and D are identical to Series A except for the use of profiles of ISO 8608 class B, C, and D.

Figure F3. The Influence of Gaussian Random Noise on RN.

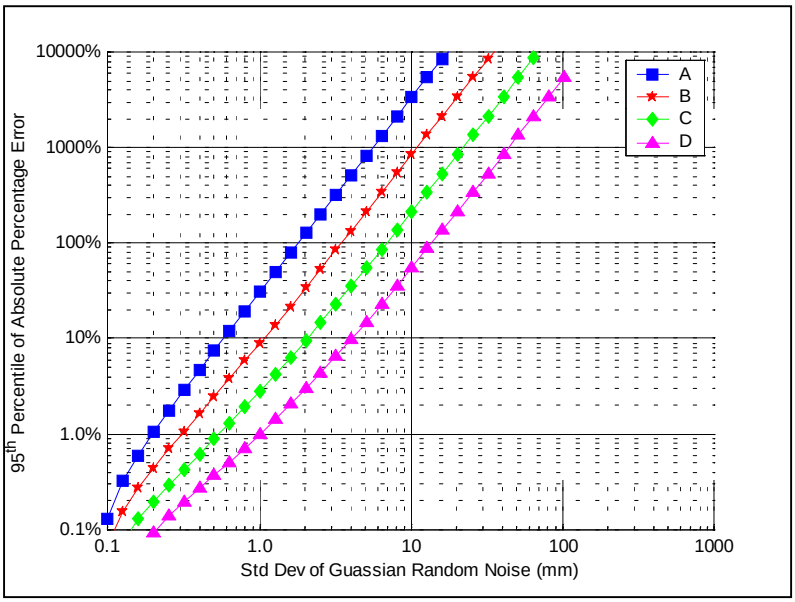

Series A is the error in 3m Variance resulting from the addition of random noise.
A realistic artificial profile, whose evenness corresponded to ISO 8608 class A, was created with a measurement interval of ~0.52mm. This detailed profile was then resampled at a measurement interval of 1.0mm, Gaussian random noise was added, and the profile was averaged over 100mm. The absolute percentage error was then calculated.
$E_{\%} = | (V - V_{Ref}) / V_{Ref} | * 100$
The error free profile was used to calculate the reference index.
This was repeated for 300 different artificial profiles. The error is shown in terms of the 95th percentile of the distribution of absolute percentage error.
Series B, C, and D are identical to Series A except for the use of profiles of ISO 8608 class B, C, and D.

Figure F4. The Influence of Gaussian Random Noise on 3m Variance.

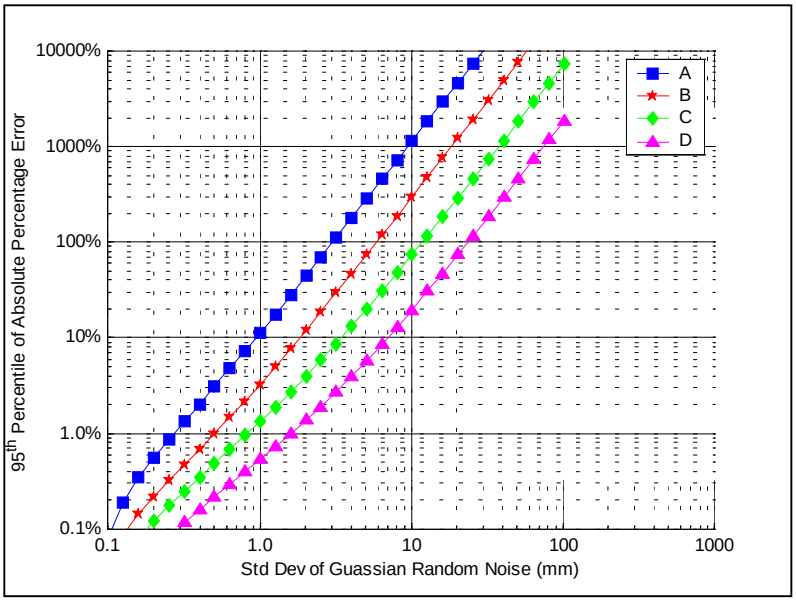

Series A is the error in 10m Variance resulting from the addition of random noise.
A realistic artificial profile, whose evenness corresponded to ISO 8608 class A, was created with a measurement interval of ~0.52mm. This detailed profile was then resampled at a measurement interval of 1.0mm, Gaussian random noise was added, and the profile was averaged over 100mm. The absolute percentage error was then calculated.
$E_{\%} = | (V - V_{Ref}) / V_{Ref} | * 100$
The error free profile was used to calculate the reference index.
This was repeated for 300 different artificial profiles. The error is shown in terms of the 95th percentile of the distribution of absolute percentage error.
Series B, C, and D are identical to Series A except for the use of profiles of ISO 8608 class B, C, and D.

Figure F5. The Influence of Gaussian Random Noise on 10m Variance.

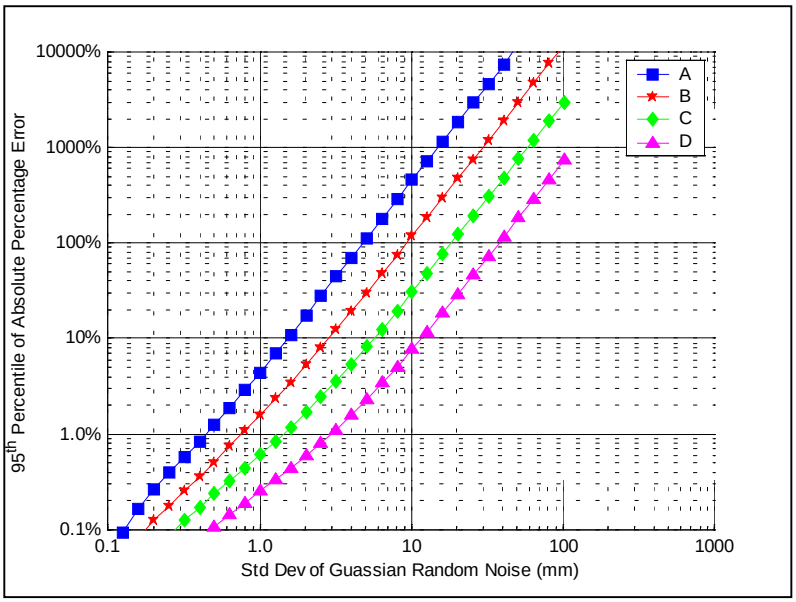

Series A is the error in 30m Variance resulting from the addition of random noise.
A realistic artificial profile, whose evenness corresponded to ISO 8608 class A, was created with a measurement interval of ~0.52mm. This detailed profile was then resampled at a measurement interval of 1.0mm, Gaussian random noise was added, and the profile was averaged over 100mm. The absolute percentage error was then calculated.
$E_{\%} = | (V - V_{Ref}) / V_{Ref} | * 100$
The error free profile was used to calculate the reference index.
This was repeated for 300 different artificial profiles. The error is shown in terms of the 95th percentile of the distribution of absolute percentage error.
Series B, C, and D are identical to Series A except for the use of profiles of ISO 8608 class B, C, and D.

Figure F6. The Influence of Gaussian Random Noise on 30m Variance.

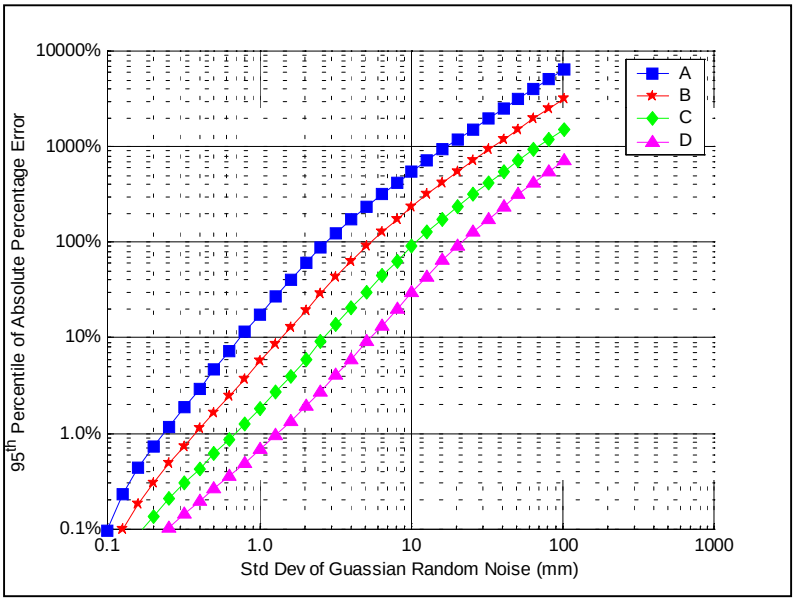

Series A is the error in CP 2.5 resulting from the addition of random noise.
A realistic artificial profile, whose evenness corresponded to ISO 8608 class A, was created with a measurement interval of ~0.52mm. This detailed profile was then resampled at a measurement interval of 1.0mm, Gaussian random noise was added, and the profile was averaged over 100mm. The absolute percentage error was then calculated.
$E_{\%} = | (V - V_{Ref}) / V_{Ref} | * 100$
The error free profile was used to calculate the reference index.
This was repeated for 300 different artificial profiles. The error is shown in terms of the 95th percentile of the distribution of absolute percentage error.
Series B, C, and D are identical to Series A except for the use of profiles of ISO 8608 class B, C, and D.

Figure F7. The Influence of Gaussian Random Noise on CP 2.5.

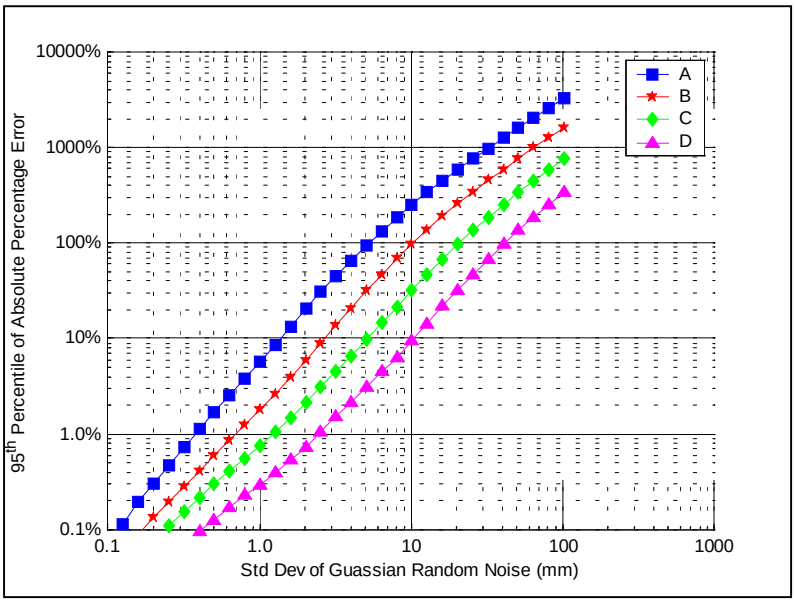

Series A is the error in CP 10 resulting from the addition of random noise.
A realistic artificial profile, whose evenness corresponded to ISO 8608 class A, was created with a measurement interval of ~0.52mm. This detailed profile was then resampled at a measurement interval of 1.0mm, Gaussian random noise was added, and the profile was averaged over 100mm. The absolute percentage error was then calculated.
$E_{\%} = | (V - V_{Ref}) / V_{Ref} | * 100$
The error free profile was used to calculate the reference index.
This was repeated for 300 different artificial profiles. The error is shown in terms of the 95th percentile of the distribution of absolute percentage error.
Series B, C, and D are identical to Series A except for the use of profiles of ISO 8608 class B, C, and D.

Figure F8. The Influence of Gaussian Random Noise on CP 10.

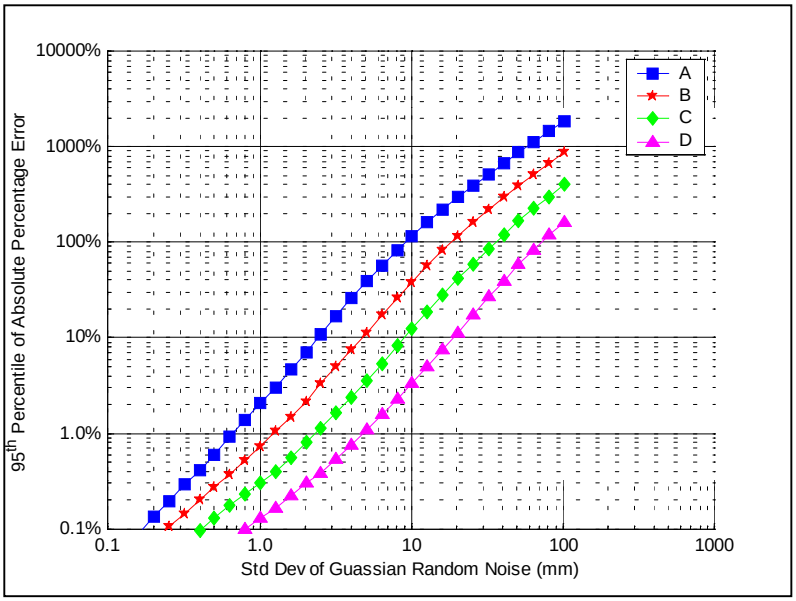

Series A is the error in CP 40 resulting from the addition of random noise.
A realistic artificial profile, whose evenness corresponded to ISO 8608 class A, was created with a measurement interval of ~0.52mm. This detailed profile was then resampled at a measurement interval of 1.0mm, Gaussian random noise was added, and the profile was averaged over 100mm. The absolute percentage error was then calculated.
$E_{\%} = | (V - V_{Ref}) / V_{Ref} | * 100$
The error free profile was used to calculate the reference index.
This was repeated for 300 different artificial profiles. The error is shown in terms of the 95th percentile of the distribution of absolute percentage error.
Series B, C, and D are identical to Series A except for the use of profiles of ISO 8608 class B, C, and D.

Figure F9. The Influence of Gaussian Random Noise on CP 40.

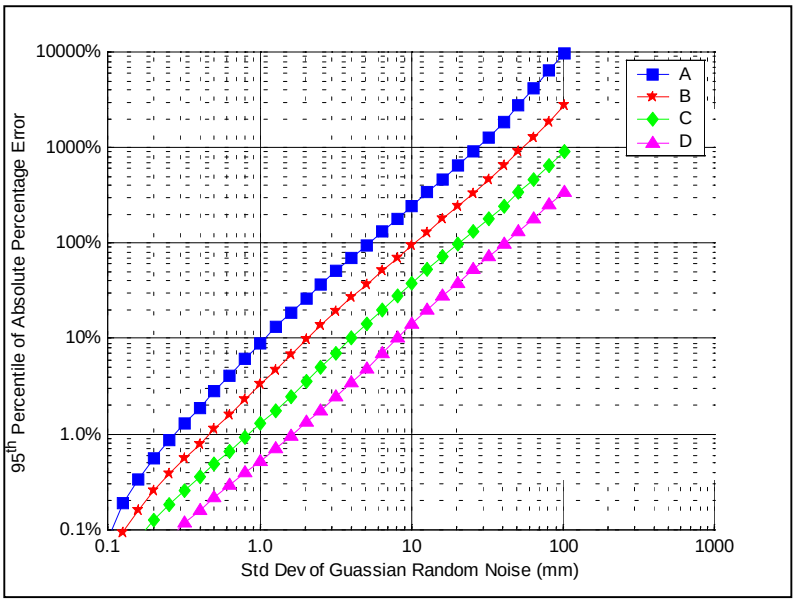

Series A is the error in $G(n_0)$ resulting from the addition of random noise.
A realistic artificial profile, whose evenness corresponded to ISO 8608 class A, was created with a measurement interval of ~0.52mm. This detailed profile was then resampled at a measurement interval of 1.0mm, Gaussian random noise was added, and the profile was averaged over 100mm. The absolute percentage error was then calculated.
$E_{\%} = | (V - V_{Ref}) / V_{Ref} | * 100$
The error free profile was used to calculate the reference index.
This was repeated for 300 different artificial profiles. The error is shown in terms of the 95th percentile of the distribution of absolute percentage error.
Series B, C, and D are identical to Series A except for the use of profiles of ISO 8608 class B, C, and D.

Figure F10. The Influence of Gaussian Random Noise on $G(n_0)$.

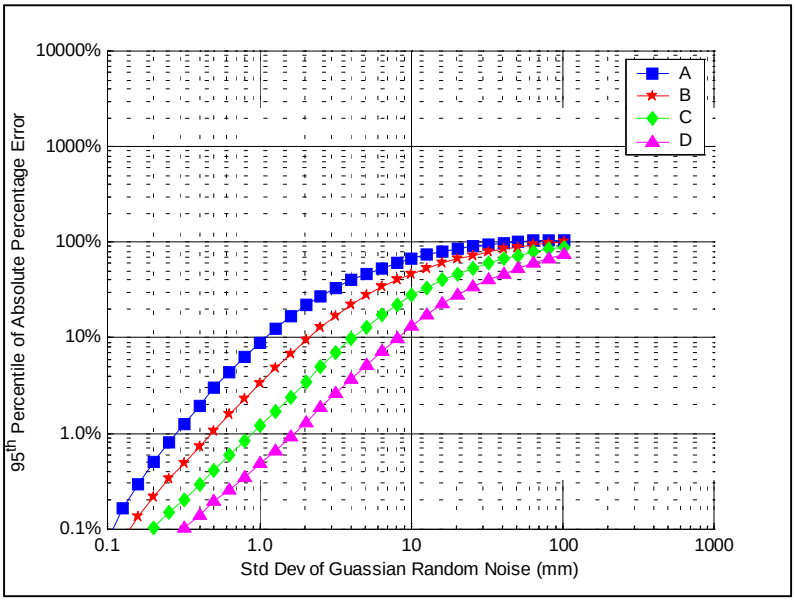

Series A is the error in w resulting from the addition of random noise.
A realistic artificial profile, whose evenness corresponded to ISO 8608 class A, was created with a measurement interval of ~0.52mm. This detailed profile was then resampled at a measurement interval of 1.0mm, Gaussian random noise was added, and the profile was averaged over 100mm. The absolute percentage error was then calculated.
$E_{\%} = | (V - V_{Ref}) / V_{Ref} | * 100$
The error free profile was used to calculate the reference index.
This was repeated for 300 different artificial profiles. The error is shown in terms of the 95th percentile of the distribution of absolute percentage error.
Series B, C, and D are identical to Series A except for the use of profiles of ISO 8608 class B, C, and D.

Figure F11. The Influence of Gaussian Random Noise on w.

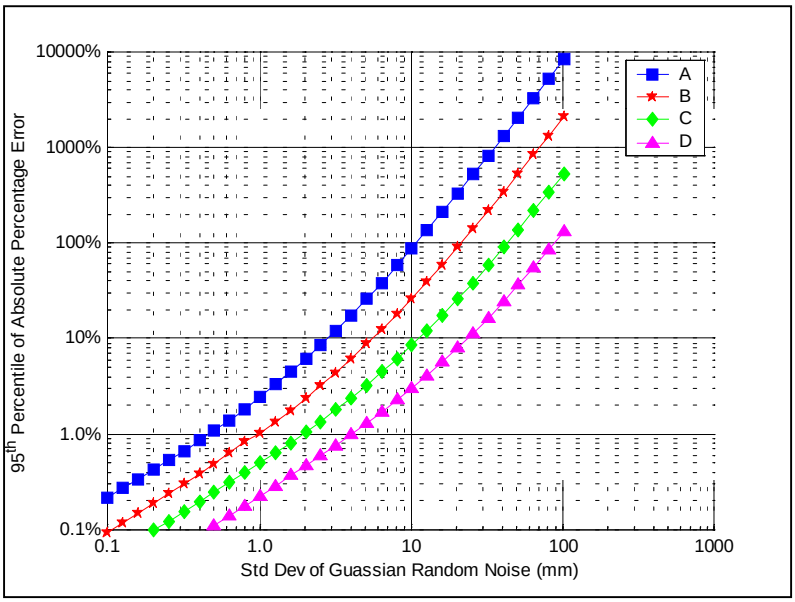

Series A is the error in SWE resulting from the addition of random noise.
A realistic artificial profile, whose evenness corresponded to ISO 8608 class A, was created with a measurement interval of ~0.52mm. This detailed profile was then resampled at a measurement interval of 1.0mm, Gaussian random noise was added, and the profile was averaged over 100mm. The absolute percentage error was then calculated.
$E_{\%} = | (V - V_{Ref}) / V_{Ref} | * 100$
The error free profile was used to calculate the reference index.
This was repeated for 300 different artificial profiles. The error is shown in terms of the 95th percentile of the distribution of absolute percentage error.
Series B, C, and D are identical to Series A except for the use of profiles of ISO 8608 class B, C, and D.

Figure F12. The Influence of Guassian Random Noise on Short Wavelength Energy.

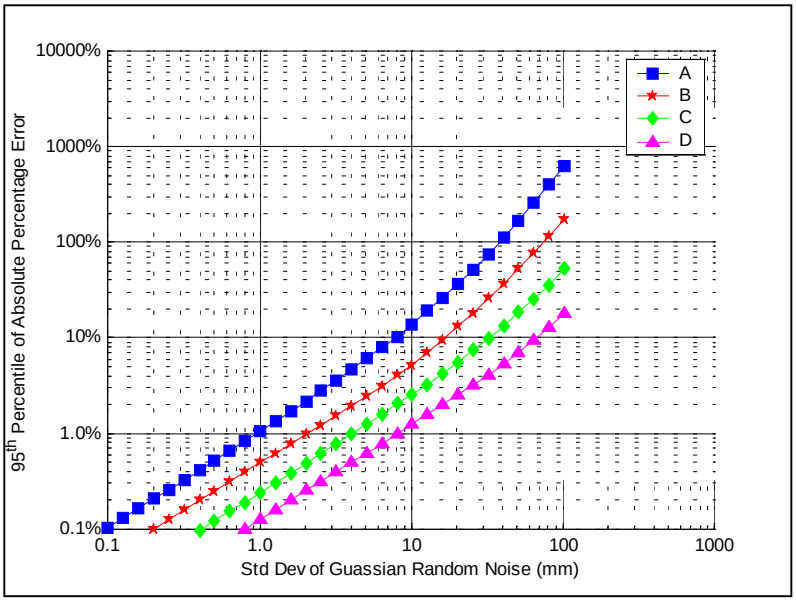

Series A is the error in MWE resulting from the addition of random noise.
A realistic artificial profile, whose evenness corresponded to ISO 8608 class A, was created with a measurement interval of ~0.52mm. This detailed profile was then resampled at a measurement interval of 1.0mm, Gaussian random noise was added, and the profile was averaged over 100mm. The absolute percentage error was then calculated.
$E_{\%} = | (V - V_{Ref}) / V_{Ref} | * 100$
The error free profile was used to calculate the reference index.
This was repeated for 300 different artificial profiles. The error is shown in terms of the 95th percentile of the distribution of absolute percentage error.
Series B, C, and D are identical to Series A except for the use of profiles of ISO 8608 class B, C, and D.

Figure F13. The Influence of Gaussian Random Noise on Medium Wavelength Energy.

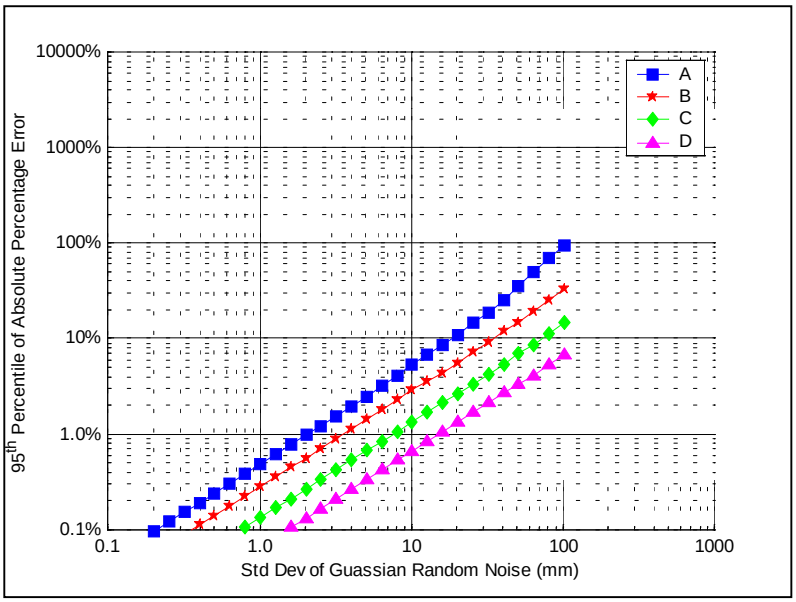

Series A is the error in LWE resulting from the addition of random noise.
A realistic artificial profile, whose evenness corresponded to ISO 8608 class A, was created with a measurement interval of ~0.52mm. This detailed profile was then resampled at a measurement interval of 1.0mm, Gaussian random noise was added, and the profile was averaged over 100mm. The absolute percentage error was then calculated.
$E_{\%} = | (V - V_{Ref}) / V_{Ref} | * 100$
The error free profile was used to calculate the reference index.
This was repeated for 300 different artificial profiles. The error is shown in terms of the 95th percentile of the distribution of absolute percentage error.
Series B, C, and D are identical to Series A except for the use of profiles of ISO 8608 class B, C, and D.

Figure F14.The Influence of Gaussian Random Noise on Long Wavelength Energy.

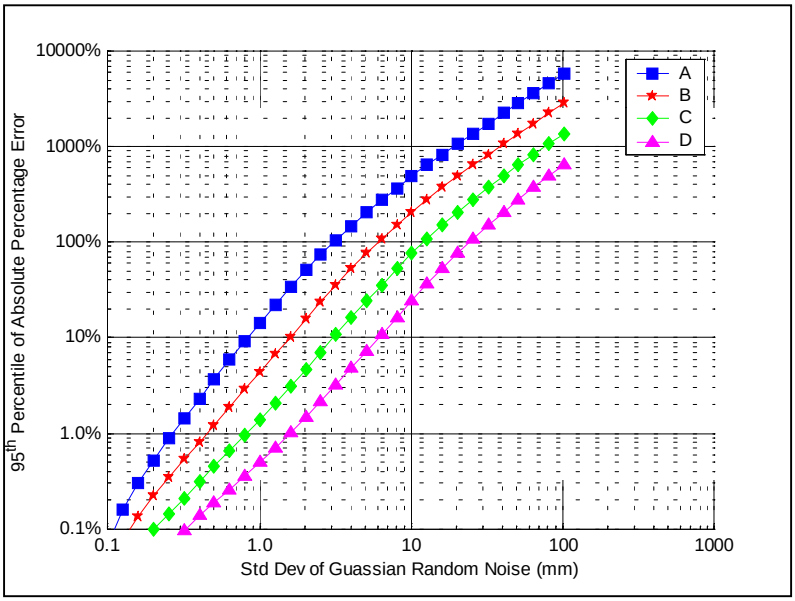

Series A is the error in the Std Dev from a 3m MA resulting from the addition of random noise.
A realistic artificial profile, whose evenness corresponded to ISO 8608 class A, was created with a measurement interval of ~0.52mm. This detailed profile was then resampled at a measurement interval of 1.0mm, Gaussian random noise was added, and the profile was averaged over 100mm. The absolute percentage error was then calculated.
$E_{\%} = | (V - V_{Ref}) / V_{Ref} | * 100$
The error free profile was used to calculate the reference index.
This was repeated for 300 different artificial profiles. The error is shown in terms of the 95th percentile of the distribution of absolute percentage error.
Series B, C, and D are identical to Series A except for the use of profiles of ISO 8608 class B, C, and D.

Figure F15. The Influence of Gaussian Random Noise on Standard Deviation from a 3m Moving Average.

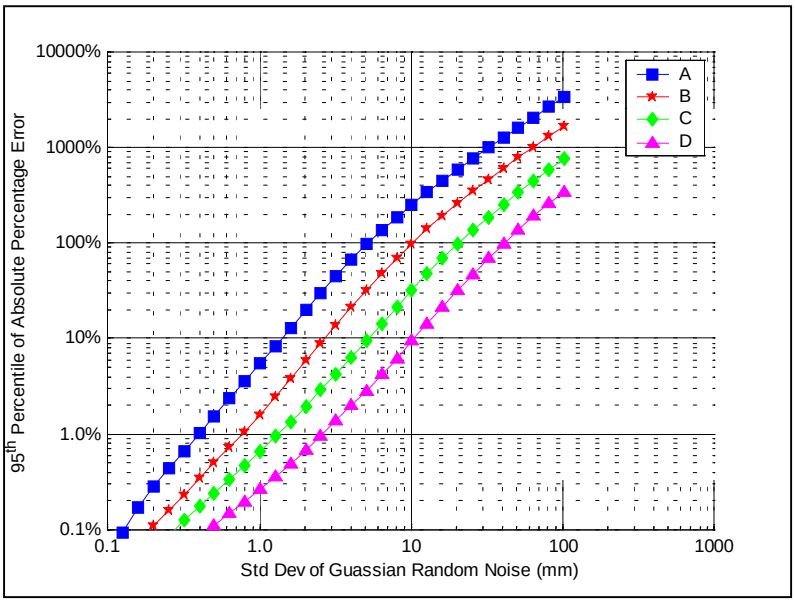

Series A is the error in Std Dev from a 10m MA resulting from the addition of random noise.
A realistic artificial profile, whose evenness corresponded to ISO 8608 class A, was created with a measurement interval of ~0.52mm. This detailed profile was then resampled at a measurement interval of 1.0mm, Gaussian random noise was added, and the profile was averaged over 100mm. The absolute percentage error was then calculated.
$E_{\%} = | (V - V_{Ref}) / V_{Ref} | * 100$
The error free profile was used to calculate the reference index.
This was repeated for 300 different artificial profiles. The error is shown in terms of the 95th percentile of the distribution of absolute percentage error.
Series B, C, and D are identical to Series A except for the use of profiles of ISO 8608 class B, C, and D.

Figure F16. The Influence of Guassian Random Noise on the Standard Deviation from a 10m Moving Average.

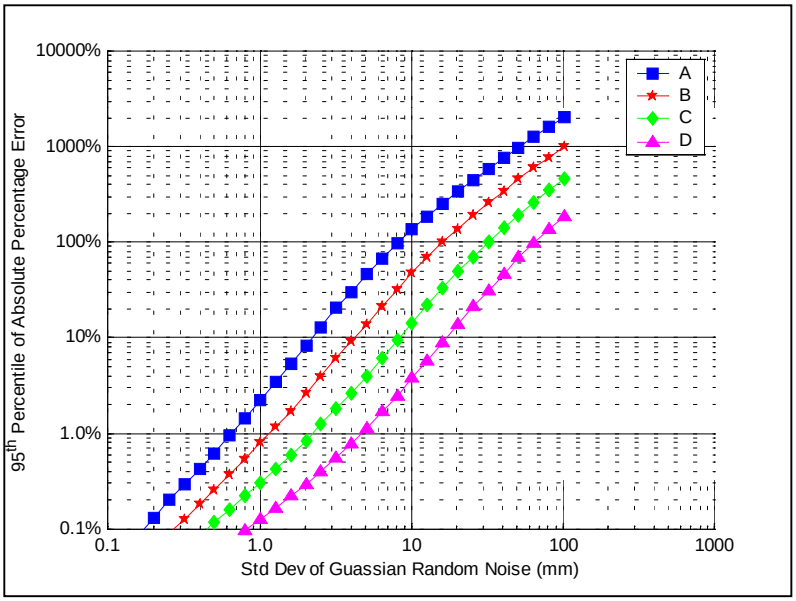

Series A is the error in Std Dev from a 30m MA resulting from the addition of random noise.
A realistic artificial profile, whose evenness corresponded to ISO 8608 class A, was created with a measurement interval of ~0.52mm. This detailed profile was then resampled at a measurement interval of 1.0mm, Gaussian random noise was added, and the profile was averaged over 100mm. The absolute percentage error was then calculated.
$E_{\%} = | (V - V_{Ref}) / V_{Ref} | * 100$
The error free profile was used to calculate the reference index.
This was repeated for 300 different artificial profiles. The error is shown in terms of the 95th percentile of the distribution of absolute percentage error.
Series B, C, and D are identical to Series A except for the use of profiles of ISO 8608 class B, C, and D.

Figure F17. The Influence of Gaussian Random Noise on the Standard Deviation from a 30m Moving Average.

Annexe G: Transverse Profiles

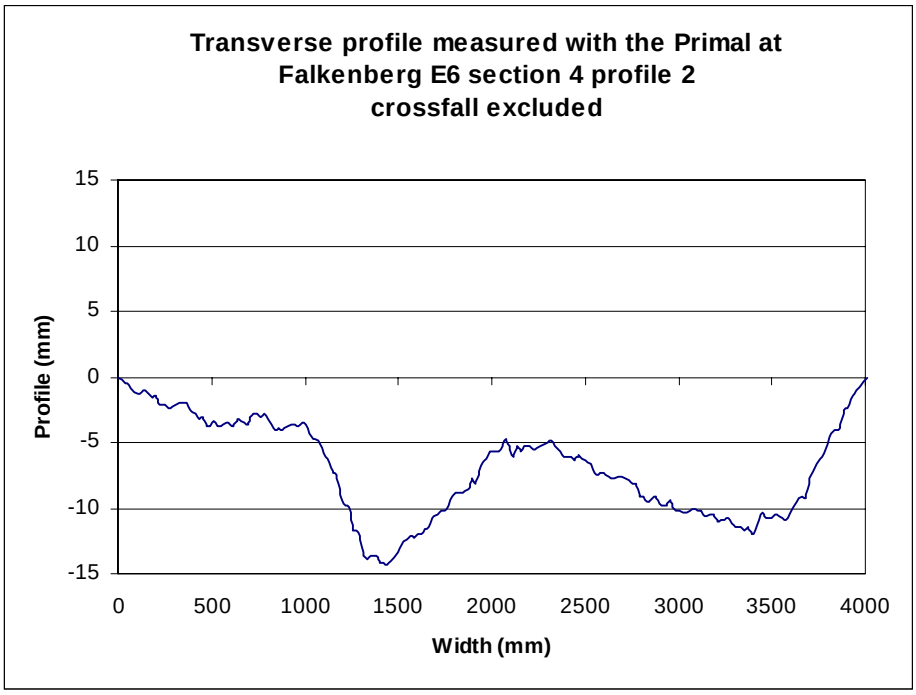

Figure G1. Transverse Profile A.

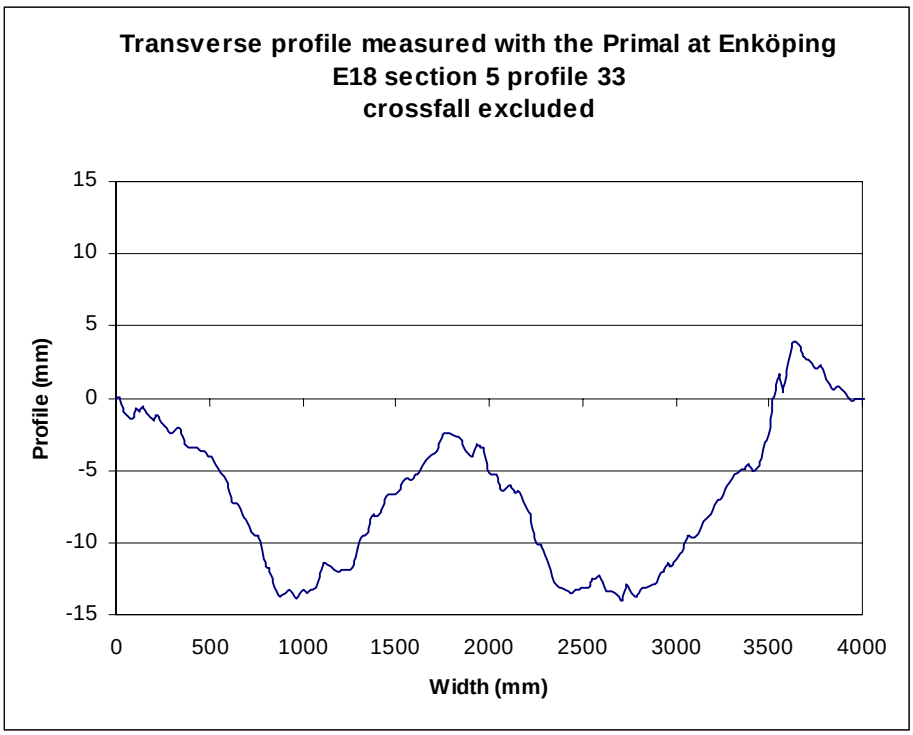

Figure G2. Transverse Profile B.

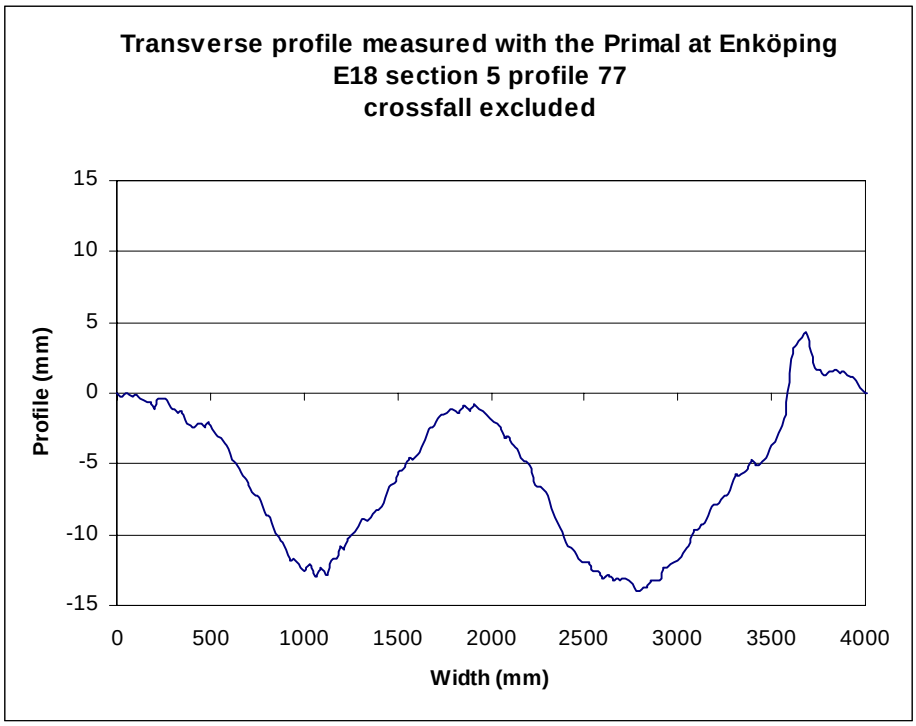

Figure G3. Transverse Profile C.

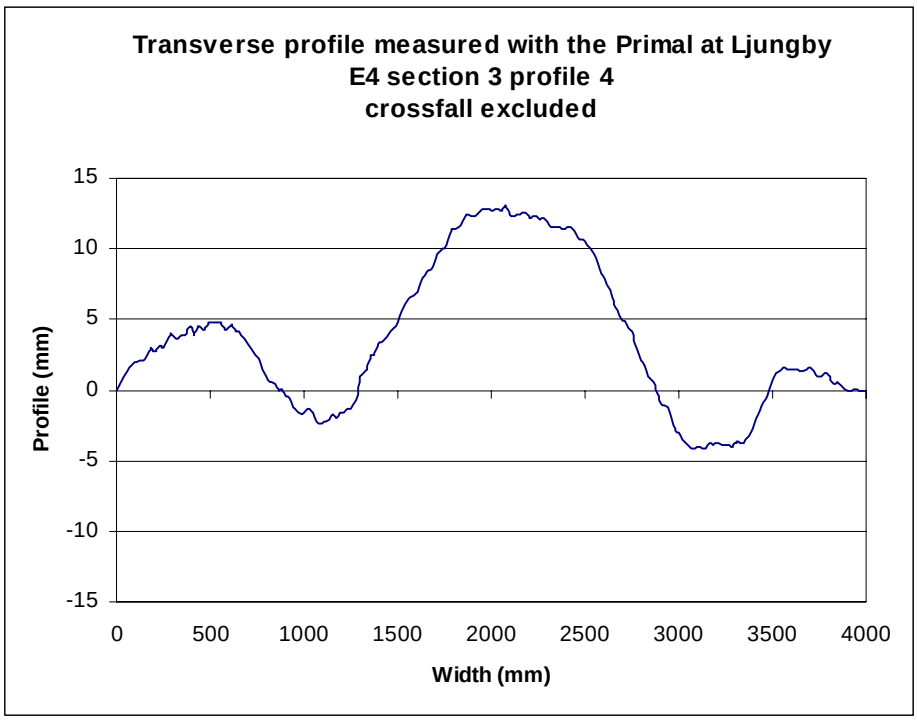

Figure G4. Transverse Profile D.

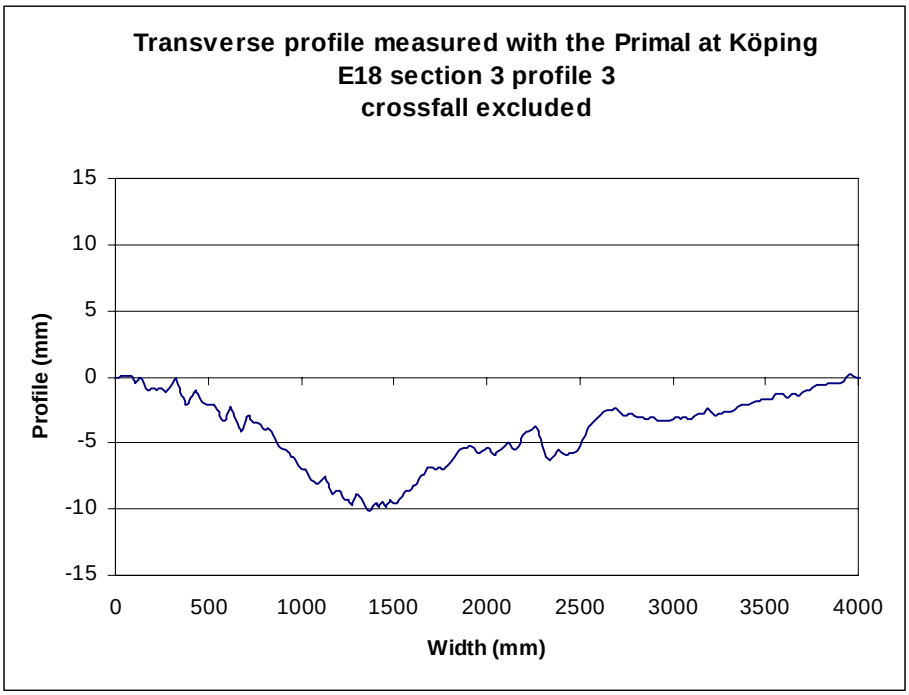

Fig G5. Transverse Profile E.

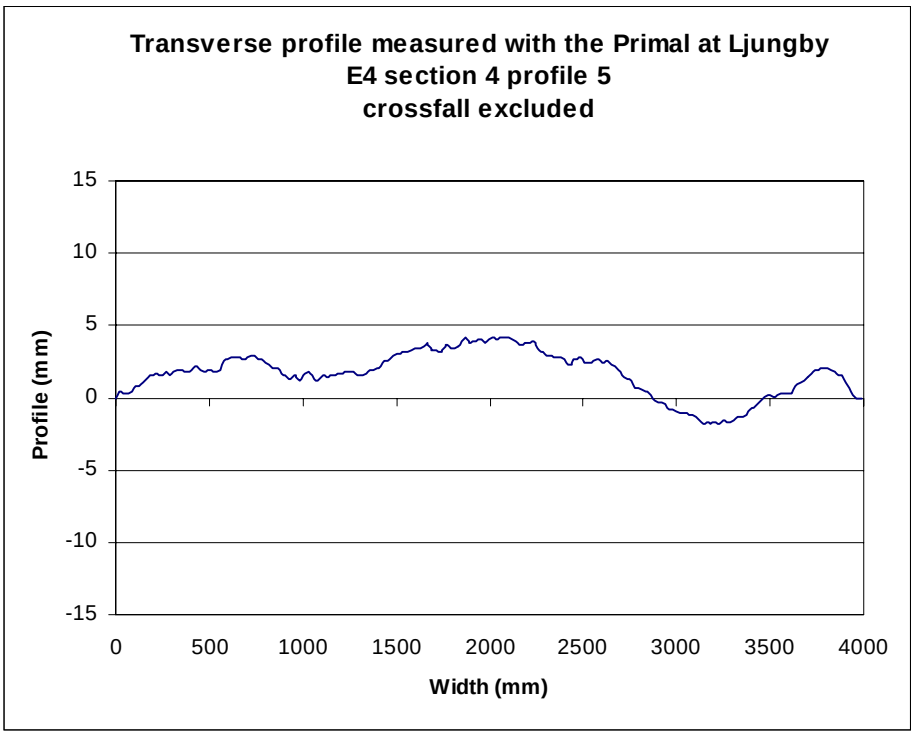

Fig G6. Transverse Profile F.

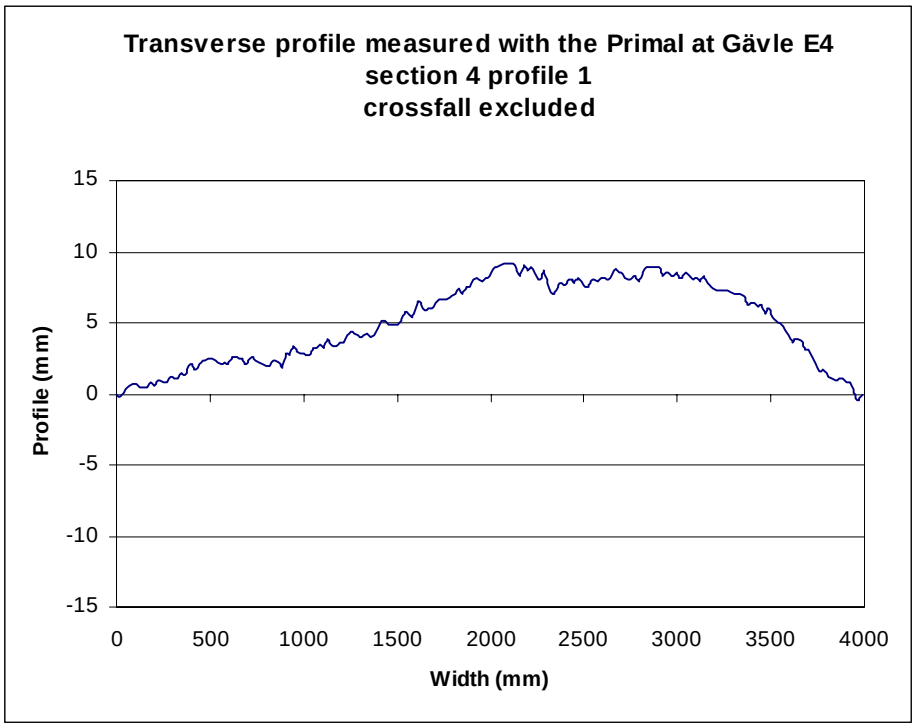

Fig G7. Transverse Profile G.

Annexe H: Terms and Acronyms

Terms defined by FILTER.

NB This list is not exhaustive – some terms are defined within the text.

Accuracy	Closeness of the agreement between the result of a measurement and a true value of the measurand.
Acquisition repetition interval	Travelled distance between two consecutive transverse profile measurements
Acquisition sampling interval	Distance between two consecutive data points in a discrete profile measurement. It is undefined for an analogue acquisition method.
Averaging distance	Length of the sub-sections under consideration (examples : 50, 100, 200, 300 or 400 m)
Canonical index	Index for which there exists a public algorithm and a widely agreed upon way to compute the index.
Crossfall	Transverse gradient across a section or full width of a pavement measured perpendicular to the centre line. Crossfall can be expressed as a percentage, a ratio (e.g. 1 in 30) or as an angle to the horizontal and can be defined in three different ways as below. By convention, it is positive when the right end of the profile is lower than its left end. Crossfall may be the design crossfall which represents the desired transverse profile, the constructed transverse profile represented by the best straight line through the new constructed transverse profile or the actual crossfall at any given time.
Crossfall, regression line definition	The angle between the horizontal and the regression straight line through the transverse road profile defined by at least seven measurement points.
Crossfall, rut bottom line definition	The angle between the horizontal and a line touching the bottoms of the left and the right wheel paths.
Crossfall, surface line definition	The angle between the horizontal and a line touching the road surface in a point to the left of the left wheel path and in a point to the right of the right wheel path.
Energy	Variance i.e. the sum of the squares of a profile curve in a given wavelength band
Frequency response function	Ratio of the Power Spectral Density of the measured profile to the Power Spectral Density of the true profile
Horizontal resolution	Smallest horizontal distance over which a change in elevation can be detected

Index	See « Summary index »
Index algorithm	Mathematical process that converts the measured profile into a summary index
International Roughness Index	Evenness number obtained by mathematical simulation of a one-wheeled vehicle running at 80 km/h on a mathematical description of a road profile.
Longitudinal profile	The intersection between the road surface and a reference plane perpendicular to the road surface and parallel to the lane direction.
Measured profile	Description of the road profile by a set of discrete values consisting of longitudinal co-ordinates and the associated vertical displacement co-ordinates
Megatexture	Deviation of a pavement surface from a true planar surface in a wavelength range of 50-500 mm
Power Spectral Density	Limiting mean-square value (e.g. of displacement) per unit bandwidth, i.e. the limit of the mean-square value in a rectangular bandwidth divided by the bandwidth, as the bandwidth approaches zero.
Profile spectrum	Power spectral density of a profile curve
Profilometer	Device that measures a pavement surface profile and records it for subsequent analysis.
Reference profile	Digitised geometric description of a longitudinal or transversal road profile obtained by means of a profiling method with known accuracy better than the one requested for the highest class of high-speed [1] profilers
Repeatability	Closeness of the agreement between the results of successive measurements of the same measurand carried out under the same conditions of measurements.
Reproducibility	Closeness of the agreement between the results of measurements of the same measurand under changed conditions of measurement.
Roughness	Unevenness in American English
Storage repetition interval	Distance corresponding to the longitudinal interval between two consecutive recordings of the transverse profile signal.
Storage sampling interval	Storage sampling interval is the distance corresponding to the interval between two consecutive data points in a digitally recorded profile signal.
Sub-section	One of the smaller sections into which the full test sections have been divided, identified by

[1] *The term « high-speed » is preferred to « dynamic ».*

	Section_label.Averaging_distance.Sequence number (example : sub-section P.100.3 is the third 100 m sub-section on test section P)
Summary index	Quantifier consisting of one number summarising the unevenness/evenness of a measured profile over a certain averaging distance ($G(n_o)$ and w shall be considered two separate indices) (PSD is not an index)
Test section	Road section or special track where the tests were carried out, identified by a code (example : section P)
Test site	Place where the test section was located (examples : Motorway E34 area B, DAF testing facility)
Transfer function	Ratio of the measured profile to the true profile versus wavelength
Transverse profile	The intersection between the road surface and a reference plane perpendicular to the road surface and to the lane direction.
True profile	Continuous function in the form of a set of curvilenear longitudinal co-ordinates and the associated vertical displacement co-ordinates that describe the road profile
Unevenness	Deviation of a pavement surface from a true planar surface in a wavelength range of 0,5-50 m
Vertical resolution	Smallest difference in elevation that can be detected
Wavelength	Minimum distance between periodically repeated parts of a profile curve

Acronyms defined by FILTER.

BASt	Bundesanstalt für Strassenwesen
BRRC	Belgian Road Research Centre
CAPL25	Coefficient APL25
CEDEX	Centro de Estudios y Experimentacion de obras Publicas (ES)
CEN	Comité Européen de Normalisation
CP	Coefficient de Planéité
DRI	Danish Road Institute
DWW	Dienst Weg- en Waterbouwkunde (NL)
ETH	Eidgenössische Technische Hochschule (CH)
EVEN	Acronym for the PIARC project on evenness measurement comparison
FEHRL	Forum of European national Highway Research Laboratories
FILTER	FEHRL Investigation on Longitudinal and Transverse Evenness of Roads
HRI	Half-car Roughness Index
IRI	International Roughness Index
ISO	International Standardization Organization
KEDE	Central Public Roads Laboratory (GR)
LCPC	Laboratoire Central des Ponts et Chaussées (FR)
NBO	Note par Bande d'Onde
NRRL	Norwegian Road Research Laboratory
PIARC	World Road Association
PSD	Power Spectral Density
RN	Ride Number
TRL	TRL Limited (GB)
UMTRI	University of Michigan Transport Research Institute
VTI	Swedish National Road and Transport Research Institute
ZAG	Zavod za gradbenistvo Slovenije